Wright State University
CORE Scholar

Browse all Theses and Dissertations | Theses and Dissertations

2022

Mercury Concentrations and Mercury Methylation Along the Freshwater to Marine Continuum

Lindsay D. Starr
Wright State University

Follow this and additional works at: https://corescholar.libraries.wright.edu/etd_all

 Part of the Environmental Sciences Commons

Repository Citation

Starr, Lindsay D., "Mercury Concentrations and Mercury Methylation Along the Freshwater to Marine Continuum" (2022). *Browse all Theses and Dissertations*. 2603.
https://corescholar.libraries.wright.edu/etd_all/2603

This Dissertation is brought to you for free and open access by the Theses and Dissertations at CORE Scholar. It has been accepted for inclusion in Browse all Theses and Dissertations by an authorized administrator of CORE Scholar. For more information, please contact library-corescholar@wright.edu.

MERCURY CONCENTRATIONS AND MERCURY METHYLATION ALONG THE FRESHWATER TO MARINE CONTINUUM

A dissertation submitted in partial fulfillment of the
requirements for the degree of
Doctor of Philosophy

By

LINDSAY D. STARR
M.S. University of Akron, 2017
B.S. Wittenberg University, 2014

2022
Wright State University

WRIGHT STATE UNIVERSITY
GRADUATE SCHOOL

April 29, 2022

I HEREBY RECOMMEND THAT THE DISSERTATION PREPARED UNDER MY SUPERVISION BY Lindsay D. Starr ENTITLED Mercury concentrations and mercury methylation along the freshwater to marine continuum BE ACCEPTED IN PARTIAL FULFILLMENT OF THE REQUIREMENTS FOR THE DEGREE OF Doctor of Philosophy.

_____
Silvia Newell, Ph.D.
Dissertation Director

_____
Donald Cipollini, Ph.D.
Director, ES Ph.D. Program

_____
Barry Milligan, Ph.D.
Vice Provost for Academic Affairs
Dean of the Graduate School

Committee on Final Examination:

_____
Carl Lamborg, Ph.D.

_____
Mark J. McCarthy, Ph.D.

_____
Sarah Tebbens, Ph.D.

_____
Alison Agather, Ph.D.

ABSTRACT

Starr, Lindsay D. Ph.D. Environmental Sciences Ph.D. Program, Wright State University, 2022. Mercury concentrations and mercury methylation along the freshwater to marine continuum.

Mercury (Hg) is a neurotoxin that can have detrimental impacts on the human nervous system and on brain development in infants. Methylmercury (MeHg) is the most toxic form of Hg and can concentrate to potentially harmful levels in higher levels of marine food webs. Production of MeHg in oxic water columns is poorly understood due to lack of knowledge of the mechanisms of formation and distribution. Recent work has reported widespread, putative Hg methylation genes in nitrite oxidizers, but any relationship with nitrifiers is unknown. This work focuses on Hg water column distribution, speciation, and methylation. The aims of this dissertation are to quantify: (1) rates and distribution of HgT and MeHg in the western basin of Lake Erie; (2) Hg methylation and nitrification rates in the Tropical North Atlantic Ocean; and (3) Hg species distribution in the Central Pacific Ocean.

In Lake Erie, a Laurentian Great Lake, the mean fraction of total Hg as MeHg in water column measurements from lake areas near three Lake Erie river inputs (summers of 2018, 2019, and 2021) were comparable (~5%), suggesting similar biogeochemical cycling for rivers feeding Lake Erie. Estimated river fluxes of MeHg were an order of magnitude greater than *in situ* production, and greater from the Detroit River (9.5 kg yr^{-1}) than from either the Maumee River (0.78 kg yr^{-1}) or Sandusky

Bay (0.03 kg yr^{-1}), as expected since the Detroit River accounts for about 95% of total water discharge into Lake Erie. These results suggest that the Detroit River is a major source of MeHg from the upper Great Lakes basin to western Lake Erie. Overall, Hg concentrations and fluxes observed in this study were up to orders of magnitude less than those reported in previous decades, which may be a positive result of the Ohio Clean Air and Water Act of 2004.

In a marine system, potential Hg methylation and nitrification rates were measured in Western Tropical North Atlantic Ocean surface waters (June and July 2019), within and near the Amazon River plume. The Hg methylation rates in this study were correlated positively and strongly to nitrification rates and *Nitrospina*-specific 16S gene expression. Potential Hg methylation and nitrification rates were highest at the most saline and least turbid stations, indicating that sediment particles and nutrient-rich, Amazon riverine discharges were not the primary factors promoting either process. These novel results in oxic seawater provide further evidence that Hg methylation may be linked to abundant, nitrifying microbes and may help explain marine MeHg distributions.

In the open Pacific Ocean, to better understand Hg partitioning and distributions, multiple Hg species were measured during a meridional section from Alaska to Tahiti in 2018. We quantified filtered total Hg (HgT) and MeHg, as well as HgT and MeHg associated with suspended particles, in high-resolution vertical profiles along the meridional transect at 152° W, which included the Alaskan shelf, North Pacific gyre, and the Loihi seamount. All measured Hg species had greater concentrations in the northern than southern Pacific Ocean, consistent with prior measurements, and the Loihi seamount was identified as a major source. Results from this expedition provide useful information

regarding potential sources and sinks of HgT and MeHg in the North Pacific Ocean, but additional Hg speciation data is needed for water masses south of Tahiti and the Southern Ocean. The overarching theme of this dissertation was to address knowledge gaps in Hg methylation in oxic waters, such as Lake Erie and the Tropical North Pacific Ocean, as well as distribution of total Hg and MeHg in Lake Erie and the Pacific Ocean.

TABLE OF CONTENTS

LIST OF FIGURES

LIST OF TABLES

ACKNOWLEDGMENTS

Thank you to my advisor, Silvia Newell, who stepped in when I needed her most three years ago. We come from different fields, and did not choose each other, but I think everything worked out just fine (smile). Thank you for believing in me and helping me to see the light at the end of the tunnel.

Thank you to Chad Hammerschmidt, who accepted me into the WSU Hg Lab.

Thank you to Alison Agather, who guided me through the Hg Lab. I appreciate your patience, problem solving, and listening abilities. Thank you for your advice, mentor and friendship.

Thank you to my committee, Carl Lamborg, Mark McCarthy, Sarah Tebbens, for all the help and support along the way, especially in the last year. I have appreciated the time each of you spent reading and rereading drafts and for your diverse feedback.

Thank you to past and present students in the WSU Hg and N lab. Thank you to past and present EES students and ES Ph.D. students. I have enjoyed meeting up, getting food, and talking with each of you. Thank you to the staff in the Earth & Environmental Sciences Department and the Environmental Sciences Ph.D. Department.

Thank you to friends and family, who have supported me through my academic career. Thank you for laughing and crying with me when times were tough, and I wanted to quit. I especially would like to thank Tom Lipp for the support over the last five years – making sure I had a balanced dinner every night after crossfit.

Lastly, I acknowledge my funding sources: Wright State Graduate School's Wright Fellowship, the EES and ES Ph.D. Departments.

Chapter 1: INTRODUCTION

1.1 Importance

Mercury (Hg) is a neurotoxin that can have detrimental impacts on the human nervous system and on brain development in infants (Grandjean and Herz, 2011; Rice et al., 2014; Tan et al., 2009). From the 17th to mid-20th centuries, the phrase "mad as a hatter" was coined to describe someone who had suffered Hg poisoning, as many hat makers were poisoned by inhaling mercuric nitrate vapor, leading to neurological problems (Farina et al., 2013). Poorly ventilated spaces in industries using Hg caused nervous system toxicity from elemental Hg concentrations as low as 20 μg m^{-3} (Lilis et al., 1985). One of the largest Hg disasters occurred in Minamata, Japan, when a local chemical plant released Hg into Minamata Bay (Kessler, 2013). The Hg in the bay contaminated fish, a main source of protein in the community's diet, which poisoned the people of Minamata (Kessler, 2013). Incidents involving Hg demonstrate its neurotoxic effects, especially in infants, and enhance the need for further Hg research in our environment (Nogara et al., 2020; Tan et al., 2009).

The most sensitive human target for Hg exposure is the nervous system and can result in neurological and behavioral disorders, such as tremors, insomnia, memory loss, neuromuscular changes, and impaired cognitive and motor functions (Pohl et al., 2011). The kidneys are also a target for Hg toxicity from inhalation, and can cause changes to urinary excretion, hematuria, and acute renal failure (Pohl et al., 2011). Increased blood

pressure, palpitations, and increased heart rate are known cardiovascular effects, as well as an increase in heart attacks after exposure (Kobal et al., 2004).

Methylmercury (MeHg) enters the human blood stream by consumption of Hg in food, particularly fish. Hg^{2+} that is converted to MeHg can be biomagnified into higher trophic level marine organisms in the food web, whereas bioaccumulation is the buildup of Hg in each organism. MeHg can bioaccumulate in marine organisms over time because it is not efficiently excreted by organisms, thus allowing Hg to biomagnify in higher trophic level fish (Tan et al., 2009). The ratio of Hg vs. ^{15}N in food webs shows that most Hg is retained going up each trophic level (Kidd et al., 2012). Seafood is the main source of protein for 1 billion people worldwide, and some populations have accumulated unhealthy levels of MeHg in their tissues (Choi & Grandjean, 2008). Populations most at risk are island and indigenous communities who consume tuna, swordfish, grouper, and mackerel, all higher trophic fish (Choi and Grandjean, 2008). Most populations are exposed to Hg by consumption of seafood and mammals that have bioaccumulated Hg in their tissues.

The World Health Organization suggests a maximum weekly intake of 1.6 μg kg^{-1}, which is about 0.10 ppm of MeHg for an average human (Poulin et al., 2008). A study from Burger and Gochfeld (2004) found an average can of tuna contains 0.41 ppm of Hg, exceeding the 0.17 ppm mean concentration for canned tuna reported by the Food and Drug Administration. The International Commission on Occupational Health (ICOH) and International Union of Pure and Applied Chemistry (IUPAC) reported that the average Hg concentration in blood is 2 μg L^{-1}, and concentrations above that may have detrimental health effects (Ye et al., 2016).

Human health risks from Hg exposure are more concerning as global Hg concentrations rise. Streets et al. (2019) modeled Hg emission trends from 2010 to 2015 and found that Hg emissions increased by 1.8% yr^{-1}. From 2010 to 2015, the largest source of Hg was from artisanal and small scale gold mining (ASGM), and the burning of coal (Streets et al., 2019). Decreases occurred in North America and Europe from the phase-out of commercially used Hg, whereas developing countries around the world have increased Hg-related activities (Streets et al., 2019). In the United States, the Great Lakes region experienced a decrease in Hg emissions from reduced industrial activities, which is reflected in recent sedimentary records (Lepak et al., 2015).

1.2 Mercury biogeochemistry

Naturally occurring Hg can originate from volcanic emissions and Hg containing minerals (Evers et al., 2007), while anthropogenic sources include fossil fuel combustion and gold production (Pirrone et al., 2010). Ice and sediment cores provide records of Hg deposition, and trends from the past 250 years have been reported from ice cores from the Fremont Glacier in Montana (Schuster et al., 2002). The Fremont record highlights several events and changes in the global cycle of atmospheric Hg deposition, such as volcanic eruptions, the North American gold rush, and gradual increases in atmospheric Hg loading from anthropogenic fossil fuel combustion. Currently, global anthropogenic emissions to air are estimated at ~2.5 kt yr^{-1} (Outridge et al., 2018). In the northeastern United States, the onset of fossil fuel combustion was recorded in a sediment core from a coastal New England estuary and showed a clear shift in Hg deposition rates during industrialization (Fitzgerald et al., 2018).

Atmospheric transport of elemental Hg (Hg^0) is the predominant pathway for movement on the Earth's surface, with a mean concentration of 1600 pg m^{-3} in the atmosphere (Mason et al., 1994). Hg^0 has a residence time in the atmosphere of six months to one year; thus, Hg^0 can travel long distances with atmospheric circulation (Horowitz et al., 2017). Hg^0 is a direct link from the atmosphere to Earth's surface by photochemical oxidation of Hg^0 to Hg^{2+}. Particles containing Hg^{2+} may be flushed out of the atmosphere by precipitation and deposited onto Earth's surface, with a mean deposition rate of 1 to 100 pg m^{-3} (Mason et al., 2012). Particle-associated Hg^{2+} can be converted back to Hg^0 after deposition via reduction. Hg^0 can then return to the atmosphere, or the deposited Hg^{2+} can bind with a methyl group (CH_3) to form MeHg through biotic or abiotic pathways (Lamborg et al., 2002; Mason et al., 1994). Methylmercury can be demethylated to Hg^{2+} from abiotic and biotic processes (Hintelmann et al., 2000).

The conversion of Hg^{2+} to MeHg can be mediated by microbial metabolism (biotic) and chemical methylation (abiotic). Abiotic reactions are thought to be a small fraction of MeHg formation and depend on pH, temperature, and inorganic and organic complexing (Celo et al., 2006). Biotic methylation may require the presence of *hgcA* and *hgcB* genes. These genes are present in anaerobic bacteria and archaea, such as *Deltaproteobacteria*, *Firmicutes*, *Chloroflexi*, and *Nitrospirae* (Capo et al., 2020). The *hgcA* gene encodes for a corrinoid-using protein. The conserved region looks like a region of protein that folds up to hold a corrinoid, like B12. The corrinoid protein, which assists the transfer of a methyl group to Hg (Parks et al., 2013). *hgcB* encodes the ferredoxin-using protein, which reduces the corrinoid protein (Parks et al., 2013). While

all Hg methylating microbes contain *hgcA, hgcB* is not always needed (Gionfriddo et al., 2016).

The Hg methylation process is also associated with reductive acetyl-coenzyme A (CoA). The acetyl-CoA pathway is also known as the Wood-Ljungdahl pathway, which involves acetogenesis (a carbon metabolism pathway that converts acetate into carbon dioxide) in anaerobic bacteria (Choi et al., 1994; Ekstrom et al., 2003). Many bacteria possess the Wood-Ljungdahl pathway, but only a small number are known to be Hg methylators, which are identified as potentially having the corrinoid protein HgcA and/or ferredoxin protein HgcB.

A putative Hg methylation gene (*hgcA*) homologue was recently identified in the microaerophilic, nitrite-oxidizing bacteria *Nitrospina* in Antarctic Sea ice (Gionfriddo et al., 2016). *Nitrospina* performs the second step of nitrification (oxidation of nitrite to nitrate, which follows oxidation of ammonium to nitrite; Santoro et al., 2010). *Nitrospina* expression of *hgc* is widespread in the surface ocean (Villar et al., 2020). *Nitrospina hgc* was detected in the mesopelagic layer of the South China Sea (Tada et al., 2020), while sequences associated with anaerobic *Deltaproteobacteria*, *Firmicutes*, *Spirochaetes*, sulfate-reducing bacteria (SRB), and methanogen *hgcAB* were not detected. Despite these advances, no aerobic pathway for MeHg production has been determined, and no clear link has been shown between nitrification and Hg methylation.

1.3 Freshwater Hg

Water column Hg methylation is often overlooked compared to Hg methylation in freshwater sediments (Eckley and Hintelmann, 2006) because sediment Hg methylation

rates are often an order of magnitude higher (0.5 to 5.0 % day^{-1}) than those in the water column (Achá et al., 2012; Avramescu et al., 2011; Hintelmann et al., 2000). Hg methylation rates may be higher in sediment, but work in the Experimental Lakes Area of Ontario showed that the larger volume of water compared to surface sediment results in more MeHg produced (Achá et al., 2012; Eckley and Hintelmann, 2006). Atmospheric deposition of Hg^0 and Hg^{2+} may be an important source of MeHg in lakes, directly impacting water column entry into the freshwater food chain. For example, Lepak et al. (2015) found that Hg signatures in fish from the Great Lakes are more isotopically similar to atmospherically derived Hg than lake sediment, highlighting the current knowledge gap in water column Hg methylation.

Mercury is often delivered to aquatic environments from wet and dry deposition, with 60% of atmospheric Hg deposition potentially attributed to anthropogenic sources (Mason al., 1994; Sunderland & Mason, 2007). Hg deposition increased with the industrial revolution but has decreased in recent decades. In developing countries, Hg concentrations have increased from local anthropogenic sources, mostly from coal-burning and waste incineration (Cohen et al., 2004; Fitzgerald et al., 1997). Local anthropogenic sources of emitted Hg can have higher Hg deposition rates because of the short residence time of Hg^{2+} and particulate Hg (Hg_{Part}; Cohen et al., 2004), disproportionately impacting areas with active coal plants, for example. Additionally, organomercury compounds were used as herbicides, fungicides, and insecticides in agriculture before 1970 (Ogorek et al., 2021; Smart, 1968).

Most known freshwater Hg methylators are anaerobic and found in anoxic sediments, but water column Hg methylation may play a key role in MeHg production in

lakes. Similarly to large lakes like the Great Lakes, most marine Hg methylation occurs in oxic surface water (Mason et al., 2012), and Hg levels in fish in Lake Erie are more closely related to atmospheric than sediment Hg (Lepak et al., 2015); thus, focusing on water column Hg methylation will address a key knowledge gap. Concentrations of total mercury (HgT) and MeHg provide a snapshot in time, but methylation and demethylation rates are needed to understand and model MeHg availability to food webs.

1.4 Marine Hg cycling

Bioaccumulation of MeHg by marine fish likely occurs in the upper 200 m of the ocean water column (Hammerschmidt & Bowman, 2012; Mason et al., 2012), which is oxygenated in most locations. Methylmercury is ubiquitous in the ocean, and most MeHg production is thought to be microbially mediated and occurs in the oxic, upper (< 1000 m) intermediate waters in the ocean (Mason et al., 2012). A generalized MeHg profile for the ocean exhibits lower concentrations in the surface ocean, increase in intermediate waters, and a general decrease in deep and bottom waters (Lamborg et al., 2014). The production and distribution of MeHg in oxic seawater contrasts with a long-standing paradigm that MeHg is produced only by anaerobic microbes, particularly those that reduce sulfur and iron (Gilmour et al., 1992; Kerin et al., 2006), as the only known microbes in culture that methylate Hg are anaerobic (Gilmour et al., 2011; Mason et al., 2012; Parks et al., 2013). Methylmercury production in the upper, oxic water column of the ocean (Lehnherr et al., 2011; Monperrus et al., 2007; Whalin et al., 2007) is hypothesized to occur within anoxic microzones associated with particles (Sunderland et

al., 2009). However, a mechanism for MeHg production in oxic seawater remains elusive.

1.5 Research Questions and Hypotheses

This dissertation addresses critical open questions about Hg methylation and distribution in aquatic environments. The focus of this work was to fill knowledge gaps as mentioned above, including Hg methylation in oxic waters, such as Lake Erie and the Tropical North Atlantic Ocean, as well as distribution of HgT and MeHg in Lake Erie and the Pacific Ocean. To better constrain MeHg distribution and production in marine and freshwater systems, I focused on three overarching questions in this research, as stated below.

Question 1: In the western basin of Lake Erie, how are Hg methylation rates influenced by HgT and MeHg concentrations at three major river inputs?

This question was addressed by quantifying both HgT and MeHg concentrations from three major river inputs: the Detroit and Maumee Rivers, and Sandusky Bay, as well as seven other stations in the western basin. *In situ* Hg methylation rates were also measured from the three river input sites to measure MeHg fluxes into the western basin of Lake Erie. As a comparison to the river inputs into the western basin, a site in the central basin was also selected. At the central basin site, which experiences hypoxia in the summer, HgT, MeHg, and Hg methylation rates were measured. The measurements at the river inputs into the western basin of Lake Erie and the comparison to the central basin help to give a clearer picture of Hg cycling in the western basin.

Expected results were that water column MeHg will flux out of the sediment at the three river input sites because of higher MeHg concentrations in the sediment. Previous work by Lepak et al. (2015) and Ogorek et al. (2021) showed that the western basin of Lake Erie has experienced Hg pollution from watershed and industrial activities, and Hg is preserved in the sediment. Hg can flux into or out of sediments depending on dissolved oxygen concentrations, temperature, and Hg concentrations in overlying water. Detroit River sediments had the highest HgT concentrations, indicating a legacy of Hg pollution (Lepak et al., 2015). This legacy pollution suggests that HgT and MeHg concentrations, and Hg methylation rates, will be highest from sites near the Detroit River discharge into western Lake Erie.

Question 2: In the Tropical North Atlantic Ocean, are Hg methylation rates associated with nitrification?

This question was addressed by quantifying potential Hg methylation and nitrification rates in the Tropical North Atlantic Ocean within and near the Amazon River plume during June and July 2019. Nitrification and Hg methylation dynamics were explored in an area of the North Atlantic Ocean, where impacts from a major river were expected. This objective was based on previous work showing that nitrifiers have the Hg methylation gene (*hgcA*; Tada et al., 2020, Villar et al., 2020).

Expected results include a potential relationship between Hg methylation and nitrification rates. Anaerobic microzones are found on suspended particles and are thought to support Hg methylation in otherwise oxic waters (Charkaborty et al., 2021). The Amazon River plume supplies large amounts of the suspended sediments and nutrients into the Tropical North Atlantic Ocean, which may promote Hg methylation and

nitrification. Potential Hg methylation and nitrification rates also were expected to be highest at the chlorophyll maximum depth, where primary productivity and microbial activity are highest.

Question 3: In the central Pacific Ocean, how do different water masses and major features impact the distribution of dissolved and particulate total Hg and MeHg species?

This question was addressed by measuring dissolved and particulate HgT and MeHg concentrations in the water column along the 152°W meridional Pacific Ocean transect and comparisons with other water column constituents. The Pacific Ocean contains different water masses; at the surface, there are gyres with depleted nutrients concentrations in the North and South Pacific, as well as areas of upwelling near the equator. In the subsurface Pacific Ocean, water masses are defined by their salinity and temperature. Such water masses as the North Pacific Intermediate Water (NPIW) defined by low salinity and oxygen (Talley, 1992), Circumpolar Deep Waters (CDW) from Antarctica that form a benthic front in the southern Pacific Ocean, and the Pacific Deep Water (PDW) defined by deep silica maximum in the northern Pacific, which is the oldest deep water in the world (Talley, 2003).

Dissolved and particulate Hg species concentrations below the surface ocean were expected to decrease from the equator to CDW in the South Pacific Ocean. CDW water is "newer" water compared to PDW, which does not contain as many dissolved constituents.

1.6 References

Achá, D., Pabón, C. A., & Hintelmann, H. (2012). Mercury methylation and hydrogen sulfide production among unexpected strains isolated from periphyton of two macrophytes of the Amazon. *FEMS Microbiology Ecology*, *80*(3), 637–645. https://doi.org/10.1111/j.1574-6941.2012.01333.x

Avramescu, M. L., Yumvihoze, E., Hintelmann, H., Ridal, J., Fortin, D., & R.S. Lean, D. (2011). Biogeochemical factors influencing net mercury methylation in contaminated freshwater sediments from the St. Lawrence River in Cornwall, Ontario, Canada. *Science of the Total Environment*, *409*(5), 968–978. https://doi.org/10.1016/j.scitotenv.2010.11.016

Burger, J., & Gochfeld, M. (2004). Mercury in canned tuna: White versus light and temporal variation. *Environmental Research*, *96*(3), 239–249. https://doi.org/10.1016/j.envres.2003.12.001

Celo, V., Lean, D. R. S., & Scott, S. L. (2006). Abiotic methylation of mercury in the aquatic environment. *Science of the Total Environment*, *368*(1), 126–137. https://doi.org/10.1016/j.scitotenv.2005.09.043

Choi, A. L., & Grandjean, P. (2008). Methylmercury exposure and health effects in humans. *Environmental Chemistry*, *5*(2), 112–120. https://doi.org/10.1071/EN08014

Cohen, M., Artz, R., Draxler, R., Miller, P., Poissant, L., Niemi, D., et al. (2004). Modeling the atmospheric transport and deposition of mercury to the Great Lakes. In *Environmental Research* (Vol. 95, pp. 247–265). https://doi.org/10.1016/j.envres.2003.11.007

Eckley, C. S., & Hintelmann, H. (2006). Determination of mercury methylation potentials in the water column of lakes across Canada. *Science of the Total Environment*, *368*(1), 111–125. https://doi.org/10.1016/j.scitotenv.2005.09.042

Evers, D. C., Han, Y.-J., Driscoll, C. T., Kamman, N. C., Goodale, W., Fallon Lambert, K., et al. (2007). Biological mercury hotspots in the Northeastern United States and Southeastern Canada. *BioScience*, *57*, 29–43.

Farina, M., Avila, D. S., da Rocha, J. B. T., & Aschner, M. (2013). Metals, oxidative stress and neurodegeneration: A focus on iron, manganese and mercury. *Neurochemistry International*. Elsevier Ltd. https://doi.org/10.1016/j.neuint.2012.12.006

Fitzgerald, W. F., Engstrom, D. R., Mason, R. P., & Nater, E. A. (1997). The Case for Atmospheric Mercury Contamination in Remote Areas. *Environmental Science and Technology*, *32*, 1–7. Retrieved from https://pubs.acs.org/sharingguidelines

Fitzgerald, W. F., Engstrom, D. R., Hammerschmidt, C. R., Lamborg, C. H., Balcom, P. H., Lima-Braun, A. L., et al. (2018). Global and Local Sources of Mercury Deposition in Coastal New England Reconstructed from a Multiproxy, High-Resolution, Estuarine Sediment Record. *Environmental Science and Technology*, *52*(14), 7614–7620. https://doi.org/10.1021/acs.est.7b06122

Gilmour, C. C., Henry, E. A., & Mitchell, R. (1992). Sulfate stimulation of mercury methylation in freshwater sediments. *Environmental Science & Technology*, *26*(11), 2281–2287. https://doi.org/10.1021/es00035a029

Gilmour, C. C., Elias, D. A., Kucken, A. M., Brown, S. D., Palumbo, A. v., Schadt, C. W., & Wall, J. D. (2011). Sulfate-reducing bacterium Desulfovibrio desulfuricans

ND132 as a model for understanding bacterial mercury methylation. *Applied and Environmental Microbiology*, *77*(12), 3938–3951. https://doi.org/10.1128/AEM.02993-10

Gionfriddo, C. M., Tate, M. T., Wick, R. R., Schultz, M. B., Zemla, A., Thelen, M. P., et al. (2016). Microbial mercury methylation in Antarctic sea ice. *Nature Microbiology*, *1*. https://doi.org/10.1038/nmicrobiol.2016.127

Graham, A. M., Aiken, G. R., & Gilmour, C. C. (2012). Dissolved organic matter enhances microbial mercury methylation under sulfidic conditions. *Environmental Science and Technology*, *46*(5), 2715–2723. https://doi.org/10.1021/es203658f

Grandjean, P., & Herz, K. T. (2011). Methylmercury and brain development: Imprecision and underestimation of developmental neurotoxicity in humans. *Mount Sinai Journal of Medicine*, *78*(1), 107–118. https://doi.org/10.1002/msj.20228

Hammerschmidt, C. R., & Bowman, K. L. (2012). Vertical methylmercury distribution in the subtropical North Pacific Ocean. *Marine Chemistry*, *132–133*, 77–82. https://doi.org/10.1016/j.marchem.2012.02.005

Hintelmann, H., Keppel-jones, K., & Douglas Evans, R. (2000). *Constants of mercury methylation and demethylation rates in sediments and comparison of tracer and ambient mercury availability*. *Environmental Toxicology and Chemistry* (Vol. 19).

Horowitz, H. M., Jacob, D. J., Zhang, Y., DIbble, T. S., Slemr, F., Amos, H. M., et al. (2017). A new mechanism for atmospheric mercury redox chemistry: Implications for the global mercury budget. *Atmospheric Chemistry and Physics*, *17*(10), 6353–6371. https://doi.org/10.5194/acp-17-6353-2017

Kerin, E. J., Gilmour, C. C., Roden, E., Suzuki, M. T., Coates, J. D., & Mason, R. P. (2006). Mercury methylation by dissimilatory iron-reducing bacteria. *Applied and Environmental Microbiology*, *72*(12), 7919–7921. https://doi.org/10.1128/AEM.01602-06

Kessler, R. (2013). The Minamata convention on mercury: A first step toward protecting future generations. *Environmental Health Perspectives*. https://doi.org/10.1289/ehp.121-A304

Kidd, K., Clayden, M., & Jardine, T. (2012). Bioaccumulation and biomagnification of mercury through food webs. *Environmental chemistry and toxicology of mercury*, 455-500.

Kobal, A. B., Horvat, M., Preze, M., Enka, A., Briki, S., Aden Krsnik, M., et al. (2004). The impact of long-term past exposure to elemental mercury on antioxidative capacity and lipid peroxidation in mercury miners. *Journal of Trace Elements*, *17*(4), 261–274. Retrieved f

Lamborg, C. H., Fitzgerald, W. F., O'donnell, J., & Torgersen, T. (2002). A non-steady-state compartmental model of global-scale mercury biogeochemistry with interhemispheric atmospheric gradients. *Geochimica et Cosmochimica Acta*, *66*, 1105–1118.

Lamborg, C. H., Hammerschmidt, C. R., Bowman, K. L., Swarr, G. J., Munson, K. M., Ohnemus, D. C., et al. (2014). A global ocean inventory of anthropogenic mercury based on water column measurements. *Nature*, *512*(1), 65–68. https://doi.org/10.1038/nature13563

Lehnherr, I., st. Louis, V. L., Hintelmann, H., & Kirk, J. L. (2011). Methylation of inorganic mercury in polar marine waters. *Nature Geoscience*, *4*(5), 298–302. https://doi.org/10.1038/ngeo1134

Lepak, R. F., Yin, R., Krabbenhoft, D. P., Ogorek, J. M., DeWild, J. F., Holsen, T. M., & Hurley, J. P. (2015). Use of Stable Isotope Signatures to Determine Mercury Sources in the Great Lakes. *Environmental Science and Technology Letters*, *2*(12), 335–341. https://doi.org/10.1021/acs.estlett.5b00277

Lilis, R., Miller, A., & Lerman, Y. (1985). Acute mercury poisoning with severe chronic pulmonary manifestations. *Chest*, *88*(2), 306–309.

Mason, R. P., Fitzgerald, W. F., & Morel, F. M. M. (1994). *Geochimica et Cosmochimica Acta* (Vol. 58).

Mason, R. P., Choi, A. L., Fitzgerald, W. F., Hammerschmidt, C. R., Lamborg, C. H., Soerensen, A. L., & Sunderland, E. M. (2012a). Mercury biogeochemical cycling in the ocean and policy implications. *Environmental Research*, *119*, 101–117. https://doi.org/10.1016/j.envres.2012.03.013

Mason, R. P., Choi, A. L., Fitzgerald, W. F., Hammerschmidt, C. R., Lamborg, C. H., Soerensen, A. L., & Sunderland, E. M. (2012b). Mercury biogeochemical cycling in the ocean and policy implications. *Environmental Research*, *119*, 101–117. https://doi.org/10.1016/j.envres.2012.03.013

Monperrus, M., Tessier, E., Amouroux, D., Leynaert, A., Huonnic, P., & Donard, O. F. X. (2007). Mercury methylation, demethylation and reduction rates in coastal and marine surface waters of the Mediterranean Sea. *Marine Chemistry*, *107*(1), 49–63. https://doi.org/10.1016/j.marchem.2007.01.018

Nogara, P. A., Schmitz, G. L., Costa, N. de S., Kamdem, J. P., Rocha, J. B., & Oliveira, C. S. (2020). The evolution of Selenium and Mercury research from 1700 to 2017 based on bibliometric analysis. *Research, Society and Development*, *9*(2), e150922177. https://doi.org/10.33448/rsd-v9i2.2177

Ogorek, J. M., Lepak, R. F., Hoffman, J. C., DeWild, J. F., Rosera, T. J., Tate, M. T., et al. (2021). Enhanced Susceptibility of Methylmercury Bioaccumulation into Seston of the Laurentian Great Lakes. *Environmental Science and Technology*, *55*(18), 12714–12723. https://doi.org/10.1021/acs.est.1c02319

Outridge, P. M., Mason, R. P., Wang, F., Guerrero, S., & Heimbürger-Boavida, L. E. (2018, October 16). Updated Global and Oceanic Mercury Budgets for the United Nations Global Mercury Assessment 2018. *Environmental Science and Technology*. American Chemical Society. https://doi.org/10.1021/acs.est.8b01246

Parks, J. M., & Smith, J. C. (2016). Modeling Mercury in Proteins. In *Methods in Enzymology* (Vol. 578, pp. 103–122). Academic Press Inc. https://doi.org/10.1016/bs.mie.2016.05.041

Parks, Jerry M, Johs, A., Podar, M., Bridou, R., Hurt, R. A., Smith, S. D., et al. (2013). The Genetic Basis for Bacterial Mercury Methylation. *Science*, *339*(6125), 1332–1335.

Pirrone, N., Cinnirella, S., Feng, X., Finkelman, R. B., Friedli, H. R., Leaner, J., et al. (2010). Global mercury emissions to the atmosphere from anthropogenic and natural sources. *Atmospheric Chemistry and Physics*, *10*(13), 5951–5964. https://doi.org/10.5194/acp-10-5951-2010

Pohl, H. R., Roney, N., & Abadin, H. G. (n.d.). *Metal Ions Affecting the Neurological System*.

Poulin, J., Gibb, H., & Prüss-Üstün, A. (2008). *Mercury Assessing the environmental burden of disease at national and local levels Public Health and the Environment Geneva 2008*.

Rice, K. M., Walker, E. M., Wu, M., Gillette, C., & Blough, E. R. (2014). Environmental mercury and its toxic effects. *Journal of Preventive Medicine and Public Health*. Korean Society for Preventive Medicine. https://doi.org/10.3961/jpmph.2014.47.2.74

Santoro, A. E., Casciotti, K. L., & Francis, C. A. (2010). Activity, abundance and diversity of nitrifying archaea and bacteria in the central California Current. *Environmental Microbiology*, *12*(7), 1989–2006. https://doi.org/10.1111/j.1462-2920.2010.02205.x

Schuster, P. F., Krabbenhoft, D. P., Naftz, D. L., Cecil, L. D., Olson, M. L., Dewild, J. F., et al. (2002). Atmospheric mercury deposition during the last 270 years: A glacial ice core record of natural and anthropogenic sources. *Environmental Science and Technology*, *36*(11), 2303–2310. https://doi.org/10.1021/es0157503

Smart, N. A. (1968). Use and residues of mercury compounds in agriculture. *Residue Reviews*, *23*, 1–36. https://doi.org/10.1007/978-1-4615-8437-7_1

Streets, D. G., Horowitz, H. M., Lu, Z., Levin, L., Thackray, C. P., & Sunderland, E. M. (2019). Global and regional trends in mercury emissions and concentrations, 2010–2015. *Atmospheric Environment*, *201*, 417–427.

Sunderland, E. M., & Mason, R. P. (2007). Human impacts on open ocean mercury concentrations. *Global Biogeochemical Cycles*, *21*(4). https://doi.org/10.1029/2006GB002876

Sunderland, E. M., Krabbenhoft, D. P., Moreau, J. W., Strode, S. A., & Landing, W. M. (2009). Mercury sources, distribution, and bioavailability in the North Pacific Ocean: Insights from data and models. *Global Biogeochemical Cycles*, *23*(2). https://doi.org/10.1029/2008GB003425

Tada, Y., Marumoto, K., & Takeuchi, A. (2020). Nitrospina-Like Bacteria Are Potential Mercury Methylators in the Mesopelagic Zone in the East China Sea. *Frontiers in Microbiology*, *11*. https://doi.org/10.3389/fmicb.2020.01369

Tan, S. W., Meiller, J. C., & Mahaffey, K. R. (2009). The endocrine effects of mercury in humans and wildlife. *Critical Reviews in Toxicology*.

Villar, E., Cabrol, L., & Heimbürger-Boavida, L. E. (2020). Widespread microbial mercury methylation genes in the global ocean. *Environmental Microbiology Reports*, *12*(3), 277–287. https://doi.org/10.1111/1758-2229.12829

Whalin, L., Kim, E. H., & Mason, R. (2007). Factors influencing the oxidation, reduction, methylation and demethylation of mercury species in coastal waters. *Marine Chemistry*, *107*(3), 278–294. https://doi.org/10.1016/j.marchem.2007.04.002

Ye, B. J., Kim, B. G., Jeon, M. J., Kim, S. Y., Kim, H. C., Jang, T. W., et al. (2016). Evaluation of mercury exposure level, clinical diagnosis and treatment for mercury intoxication. *Annals of Occupational and Environmental Medicine*. BioMed Central Ltd.

Chapter 2: MERCURY METHYLATION AND POTENTIAL RATES IN THE WESTERN BASIN OF LAKE ERIE

Lindsay D. Starr, Mark M. McCarthy, Chad R. Hammerschmidt, Arthur Zastepa, Silvia E. Newell

2.1 Abstract

Little is known about the sources and cycling of bioaccumulative methylmercury (MeHg) in Lake Erie, despite the lake having a world-renowned sport fishery. During the summers of 2018 to 2021, concentrations and fluxes of total mercury (HgT) and methylmercury (MeHg) were examined near the Detroit and Maumee River mouths, as well as the junction with Sandusky Bay, which all discharge into the western and central basins of Lake Erie. Average HgT concentrations were similar at the Detroit (5.4 ± 0.8 pM) and Sandusky Bay inputs (5.3 ± 0.9 pM), which were less than the Maumee River mouth (11.6 ± 2.8 pM). Similarly, MeHg concentrations were lower at the Detroit River (0.38 ± 0.25 pM) and Sandusky Bay inputs (0.24 ± 0.13 pM) than at the Maumee River mouth (0.63 ± 0.46 pM; $p = 0.03$). The mean fraction of HgT as MeHg in water was comparable among the sites (~5%), suggesting similar biogeochemical cycling. Estimated river discharge fluxes of MeHg were much greater from the Detroit River (9.5 kg yr^{-1}) than from either the Maumee River (0.78 kg yr^{-1}) or Sandusky Bay (0.03 kg yr^{-1}), as expected, since the Detroit River accounts for about 95% of total river water discharge into Lake Erie. The highest potential for Hg methylation was measured at the Sandusky Bay input (0.045 ± 0.012 day^{-1}), followed by the Detroit River (0.031 ± 0.006

day^{-1}) and Maumee River (0.005 ± 0.003 day^{-1}), while the rate in the Central Basin was 0.062 ± 0.027 day^{-1}. Annual river supply was an order of magnitude greater than *in situ* production in the western and central basins of Lake Erie. These results suggest that the Detroit River is the major source of MeHg to western Lake Erie, and much of the MeHg produced in river water may be derived from *in situ* transformations, especially for the Maumee River and Sandusky Bay. Overall, Hg concentrations and fluxes observed in this study were orders of magnitude less than those reported in previous decades, which may be a positive result of the Ohio Clean Air and Water Act passed in 2004.

2.2 Introduction

Lake Erie is the most biologically productive of the Laurentian Great Lakes and supports fisheries, recreational boating, tourism, and shipping industries, with an estimated value greater than USD$50 million annually (Watson et al., 2016). Unfortunately, it also has a long history of Hg pollution. The western basin of Lake Erie has higher surface sediment HgT concentrations than the other two basins (central and eastern), mainly attributed to industrial activities in the Detroit River watershed. Detroit was the epicenter for machinery production in the 1800s because of its proximity to iron ore deposits in the northern Great Lakes region and access to transportation waterways (Painter et al., 2001; Jia et al., 2010). Additionally, in the mid-1900s, the BASF Wyandotte Chemical Corporation (Wyandotte, Michigan), Dow Chemical Corporation (Sarnia, Ontario), and the Detrex Chemical Corporation (Ashtabula, Ohio) all used Hg cells in the electrolytic production of chlorine and caustic soda and are reported to have discharged 4.5 to 88 kg Hg day^{-1} from 1939 to 1970 (Walters et al., 1974). This past

pollution of the Detroit and Maumee Rivers has placed them on the Area of Concern (AOC) list for high levels of bacteria, metals, and greases. The Maumee River sediments contain unregulated waste from industrial sources, heavy metal contamination, and combined sewer overflow. All of these materials are included in sediments dredged to maintain the shipping channel, bringing all these materials back to the surface.

MeHg is a harmful neurotoxin that bioaccumulates up the aquatic food web, ultimately accumulating in large fish. Bioaccumulated MeHg can cause neurological birth defects in humans (Rice et al., 2014). Hg methylation pathways have been best studied in anoxic sediments and linked to pathways such as sulfate and iron reduction (Kerin et al., 2006; Pak & Bartha, 1998). Thus, most Hg research in Lake Erie has focused on Hg concentrations in higher trophic level fish and surficial lake sediments (Marvin et al., 2004; Zhou et al., 2017). In the United States, there are currently 3,900 fish consumption advisories for Hg, including 12 sport fish from Lake Erie (*Ohio Sport Fish Consumption Advisory*, 2021). Hg in the western basin of Lake Erie is a problem due to consumption of higher trophic level fish, such as bass and walleye. A major knowledge gap, however, involves MeHg water column concentrations and Hg methylation rates in the western basin of Lake Erie, where watershed-derived total Hg loading is predominant (Lepak et al., 2015).

Mercury is naturally delivered to aquatic environments from wet and dry deposition, with as much as 60% of atmospheric Hg deposition attributed to anthropogenic sources (Mason et al., 1994; Sunderland & Mason, 2007). Mercury concentrations have increased from local anthropogenic sources over the last 150 years, mostly from coal-burning and waste incineration (Cohen et al., 2004; Streets et al., 2019).

Additionally, organomercury compounds were used as herbicides, fungicides, and insecticides in agriculture before 1970. After 1970, the main sources of Hg emissions to the environment were from coal combustion and industrial activities (Smart, 1968; Ogorek et al., 2021). Mercury is released into the atmosphere as elemental Hg (Hg^0) and oxidized and deposited as Hg^{2+}. Once deposited, Hg^{2+} can be transformed to MeHg by biotic and abiotic processes attaching a methyl group to Hg^{2+}. Production of MeHg has been linked to anaerobic microbial pathways (Choi et al., 1994; Ekstrom et al., 2003) by heterotrophic and/or chemolithoautotrophic microbes, such as sulfate reduction and acetogenesis in lake sediments (Benoit et al., 1999; Eckley & Hintelmann, 2006). Methylmercury is often incorporated at the base of the food web by unicellular organisms that are consumed by zooplankton (Mason et al., 1996). Slow rates of elimination of MeHg relative to dietary intake results in bioaccumulation of MeHg up trophic levels (Hammerschmidt and Fitzgerald, 2006).

Water column Hg methylation is often overlooked compared to Hg methylation in freshwater sediments (Eckley and Hintelmann, 2006). Sediment Hg methylation rates are often an order of magnitude higher (0.5 to 5.0 day^{-1}) than those in the water column of freshwater lakes (Hintelmann et al., 2000; Achá et al., 2012; Avramescu et al., 2011). While Hg methylation rates may be higher in sediment, work in the Experimental Lakes Area of Ontario showed that Hg methylation from the water column is overall higher, as the water has a larger mass of MeHg than surface sediment (Achá et al., 2012; Eckley and Hintelmann, 2006). Methylmercury formed in the water column may have a more direct pathway into the base of the aquatic food web since it does not have to diffuse into the water column (Eckley and Hintelmann, 2006). Additionally, atmospheric deposition

of Hg^0 and Hg^{2+} may be an important source of Hg to the Great Lakes, contributing to water column methylation. For example, Lepak et al. (2015) found that isotopic Hg signatures in fish from the Great Lakes were more similar to atmospherically derived Hg than sediment-derived Hg. These findings highlight a current knowledge gap in Hg, suggesting that water column production of MeHg dominates food web bioaccumulation. However, this hypothesis has yet to be tested through direct observation.

The western Lake Erie watershed is primarily agricultural, with urban and industrial influences as well. Together, the Maumee and Detroit Rivers contribute 97.5% of the water load into the western basin of Lake Erie. The drainage basins of the three rivers range in size and have varied land use from agriculture to industrial. The Detroit River watershed is dominated by an urban landscape and comprises ~90% of the total water discharge into Lake Erie (Scavia et al., 2016). Water in the Detroit River drains from Lake St. Clair and the Upper Great Lakes (Lakes Superior, Michigan, and Huron) and contributes ~94% of the water discharged to the western basin of Lake Erie. Detroit River water also receives wastewater from chemical manufacturing and local coal combustion (Marvin et al., 2004). In contrast, the Maumee River contributes only ~5% of the water discharge but 30 to 50% of the annual nutrient load due to agricultural land use dominating the river drainage basin (Richards et al., 2010; Boedecker et al., 2020). The Sandusky River, draining into the central basin, has a watershed size of 4.7×10^2 km^2 (compared to 2.2×10^4 km^2 for the Maumee River; Scavia et al., 2016) and is also primarily agricultural (Calhoun et al., 2002). Agriculture can be a Hg source, as Hg binds with soils, and soil tilling can mobilize Hg and allow it to discharge into rivers and surface waters (Lyons et al., 2006).

HgT loading from 12 rivers flowing into the western basin (not including the Detroit River) ranged from 0.7 to 36 kg yr^{-1} (Fitzgibbon et al., 2008). Of these 12 rivers, the Maumee River contributed the highest HgT flux to Lake Erie (36 kg yr^{-1}), and the Sandusky River load was 9.8 kg yr^{-1} (Fitzgibbon et al., 2008). In contrast, water column flux measurements for the Detroit River were orders of magnitude higher (1,595 kg yr^{-1}; Kelly et al., 1991). Hg concentrations in surficial sediments have been reported for western Lake Erie (Lepak et al., 2015), but there are few Hg concentrations reported from the water column and no published record of Hg methylation rates. Painter et al. (2001) found spatial trends of Hg and other heavy metal contamination in sediments increasing from the eastern to western basin, and north to south in the central basin, which all exceeded Canadian Federal and Provincial sediment quality guidelines. Marvin et al. (2002) found a similar trend, with higher sediment Hg concentrations in the western versus eastern basin. Using an isotope mixing model, Lepak et al. (2015) found that Hg sources in western basin sediments were dominated by industrial sources in the watershed.

Methylmercury concentrations in Lake Erie fish have increased since the 1990s (Sadraddini et al., 2011; Lepak et al., 2015), and understanding the sources of this increased MeHg is increasingly critical. While all known Hg methylators are anaerobic and found in anoxic sediments, most marine Hg methylation appears to occur in the oxic surface water (Ullrich et al., 2001), and Hg in Lake Erie fish was more closely related to atmospheric than sediment Hg sources (Lepak et al., 2015); thus, water column Hg methylation may be a key location for Hg methylation. Concentrations of HgT and MeHg provide a snapshot in time, but methylation and demethylation rates are needed to

understand and model MeHg contamination in food webs. Therefore, the objective of this study was to quantify water column HgT and MeHg concentrations, as well as potential Hg methylation rates, near the mouths of three rivers discharging into the western and central basins of Lake Erie. A station experiencing bottom-water hypoxia in the central basin was also examined to determine whether water column Hg concentrations and methylation rates would increase under hypoxic conditions. We hypothesized that fluxes and methylation rate would be highest from the Detroit River, as it has a history of Hg pollution in the watershed.

2.3 Methods

2.3.1 Sample collection

Sampling was conducted in September 2018 and October 2019 aboard the *R/V Limnos* with Environment and Climate Change Canada (ECCC) and from the Ohio State University Stone Lab Gibraltar III in July 2021. In September 2018, ten sampling sites were selected from ECCC monitoring locations (Figure 2.1; Table 2.1). Depth, temperature, dissolved oxygen, and transmittance were measured using a SBE25plus CTD. Water column samples were collected for unfiltered HgT and MeHg at the ten stations, including the Detroit and Maumee River mouths and Sandusky Bay inputs. The Maumee River mouth was sampled from within the shipping channel, thus had a sampling depth of 8 m, which is much deeper than other areas near the Maumee River mouth (~1-2 m). Three sites visited in 2018 were sampled again in October 2019 from 1 m below the water surface and 1 m above the sediment-water interface for potential Hg

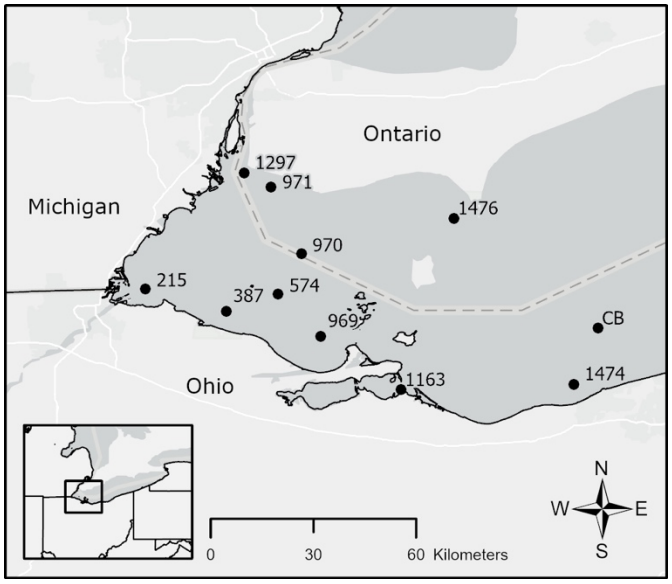

Figure 2.1. Map of western and central basins of Lake Erie showing sampling sites from 2018 and 2019 near inputs of the Detroit and Maumee Rivers and Sandusky Bay, and 2021 from the central basin. All stations, except CB were sampled in 2018 for HgT and MeHg, in 2019 stations 1297, 215, and 1163 were analyzed for Hg methylation rates, and in 2021 CB was sampled for HgT, MeHg, and Hg methylation rates.

Table 2.1. Site locations for Lake Erie sampling with maximum depth sampled and analyses conducted.

Site	Latitude	Longitude	Maximum depth (m)	Year Sampled	
215	41.73401	83.38515	7.8	2018 (HgT, MeHg)	2019 (Hg rate)
387	41.67402	83.17344	5.0	2018 (HgT, MeHg)	
574	41.71948	83.03668	7.6	2018 (HgT, MeHg)	
969	41.60871	82.92489	5.5	2018 (HgT, MeHg)	
970	41.8252	82.97607	8.0	2018 (HgT, MeHg)	
971	41.99923	83.05622	6.5	2018 (HgT, MeHg)	
1163	41.46978	82.71348	6.3	2018 (HgT, MeHg)	2019 (Hg rate)
1297	42.03638	83.13541	7.0	2018 (HgT, MeHg)	2019 (Hg rate)
1474	41.48467	82.26113	11.5	2018 (HgT, MeHg)	
1476	41.91747	82.57524	9.0	2018 (HgT, MeHg)	
Central Basin	41.70000	82.86666	7.0	2021 (HgT, MeHg, Hg rate)	

methylation rates. These sites (stations 215, 1297, and 1163; Table 2.1) were located near the inputs of the Maumee and Detroit Rivers and Sandusky Bay (Figure 2.1). Potential Hg methylation rate experiments were conducted again in July 2021 from the central basin of Lake Erie (Figure 2.1; Table 2.1).

2.3.2 HgT

HgT was measured at Wright State University by the addition of bromine monochloride (BrCl; 1% by volume; Bloom & Crecelius, 1983). After 12-72 hours, samples were neutralized with NH_2OH prior to reduction with $SnCl_2$. Samples were purged with Hg-free N_2 and quantified by dual Au-amalgamation cold vapor atomic fluorescence spectrometry (CVAFS; Bloom & Fitzgerald, 1988; Fitzgerald & Gill, 1979). The HgT method detection limit was 0.01 pM.

2.3.3 MeHg

1.5 L Samples were acidified 1% by volume with trace metal grade H_2SO_4 after sampling and brought back to Wright State University for analysis. Before analysis, samples were neutralized with 12 M KOH, adjusted to pH = 4.9 with 4 M acetate buffer, and then derivatized with sodium tetraethylborate (Bowman and Hammerschmidt, 2011). Samples were purged with Hg-free N_2 (30 L total at 0.8 L min^{-1}) to transfer volatile methylethylmercury (MeHg derivative) from solution onto Tenax resin after the effluent gas stream passed through reagent grade soda lime. Methylethylmercury was quantified by GC-CVAFS (Tseng et al., 2005). Standards were calibrated with TORT-3 reference material (lobster hepatopancreas, National Research Council of Canada).

2.3.4 Potential Hg Methylation Rates

Four 2-L replicates of surface and bottom water (1 m above sediment-water interface) were collected at each station for analysis of potential Hg methylation rates. Water was amended to 9–11 pM $^{200}Hg^{2+}$ (final concentration; 96.41% $^{200}Hg(NO_3)_2$), which was about 2× greater than ambient HgT concentrations in Lake Erie as measured in 2018. After Hg isotope amendment, water samples were incubated in an on-deck incubator or off the dock at Stone Lab (2021). After incubation, water was amended with $CH_3{}^{199}Hg$ (for isotope dilution analysis, described below) within 30 min of being removed from the incubator and promptly acidified to 1% by volume with H_2SO_4 to stop biological Hg transformations. Acidified water was analyzed for MeHg isotopes at Wright State University within three months of collection.

Before analysis, samples were neutralized with 12 M KOH, adjusted to pH = 4.9 with 4 M acetate buffer, and then derivatized with sodium tetraethylborate (Bowman and Hammerschmidt, 2011). Samples were then purged with N_2, and methylethylmercury was concentrated on Tenax. Mercury isotope composition of purged MeHg was quantified with isotope-dilution gas chromatography inductively coupled plasma mass spectrometry (GC-IPMS; Perkin Elmer Elan 9000; Hintelmann & Evans, 1997; Hintelmann et al., 1995). Mercury methylation potentials were calculated from the amount of added $^{200}Hg^{2+}$ that was transformed to $CH_3{}^{200}Hg$ during incubation (Eckley and Hintelmann, 2006). The detection limit for Hg methylation is dependent on ambient MeHg concentration, estimated from $CH_3{}^{202}Hg$ isotope; average ambient with standard error MeHg

concentrations were 0.43 ± 0.07 pM (n = 14) in 2019 and 0.24 ± 0.10 pM (n = 8) in 2021, which were comparable to average MeHg concentrations in 2018 (0.34 ± 0.04; n = 35).

2.4 Results

Ambient environmental measurements, including temperature, dissolved oxygen (DO), and percent transmittance are shown in Figures 2.2, 2.3, and 2.4 for sampling years 2018, 2019, and 2021, respectively. Environmental parameters from CTD water column profiles in 2018 for Sandusky Bay and the Maumee and Detroit River inputs had average (with standard error) temperatures of 24 ± 0.02, 23 ± 0.06, and 22 ± 0.01 °C; average DO concentrations were 6.7 ± 0.7, 5.8 ± 0.9, and 5.6 ± 0.4 mg l^{-1}; and average percent transmittance was 11.9 ± 1.5, 1.3 ± 0.6, and 59.8 ± 0.4%, respectively (Figure 2.2). Average water column values in 2018 were different between sites for temperature (Tukey, $p < 0.001$) and percent transmittance (Tukey, $p < 0.001$), but not for DO. Water column CTD values in 2019 for Sandusky Bay and the Maumee and Detroit River inputs had average temperatures of 22.0 ± 0.1, 17.5 ± 0.01, and 15.9 ± 0.01 °C; average DO concentrations were 5.4 ± 0.2, 6.5 ± 0.6, and 6.5 ± 0.6 mg l^{-1}; and average percent transmittance values were 6.7 ± 0.1, 0.2 ± 0.1, and 64.2 ± 0.5 %, respectively (Figure 2.4). Average water column values in 2019 were different for average temperature and percent transmittance between all sites (Tukey, $p < 0.04$), and the Sandusky Bay input was different from the Maumee and Detroit River inputs for DO (Tukey, $p < 0.003$). Sampling in the central basin in 2021 occurred in July, and temperature averaged 20.3 ± 3.9 °C, and DO concentrations were 7.1 ± 2.4 mg l^{-1}; transmittance was not measured (Figure 2.5).

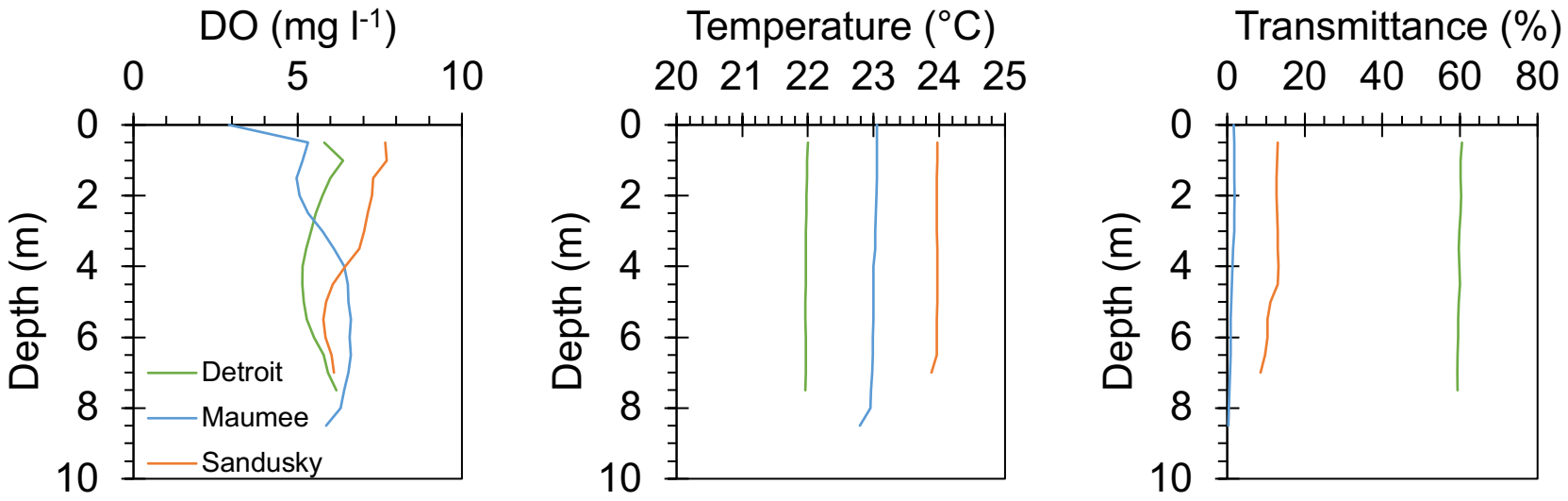

Figure 2.2. DO, temperature, and transmittance at stations near the Detroit and Maumee river mouths and Sandusky Bay connection to Lake Erie for sampling year 2018.

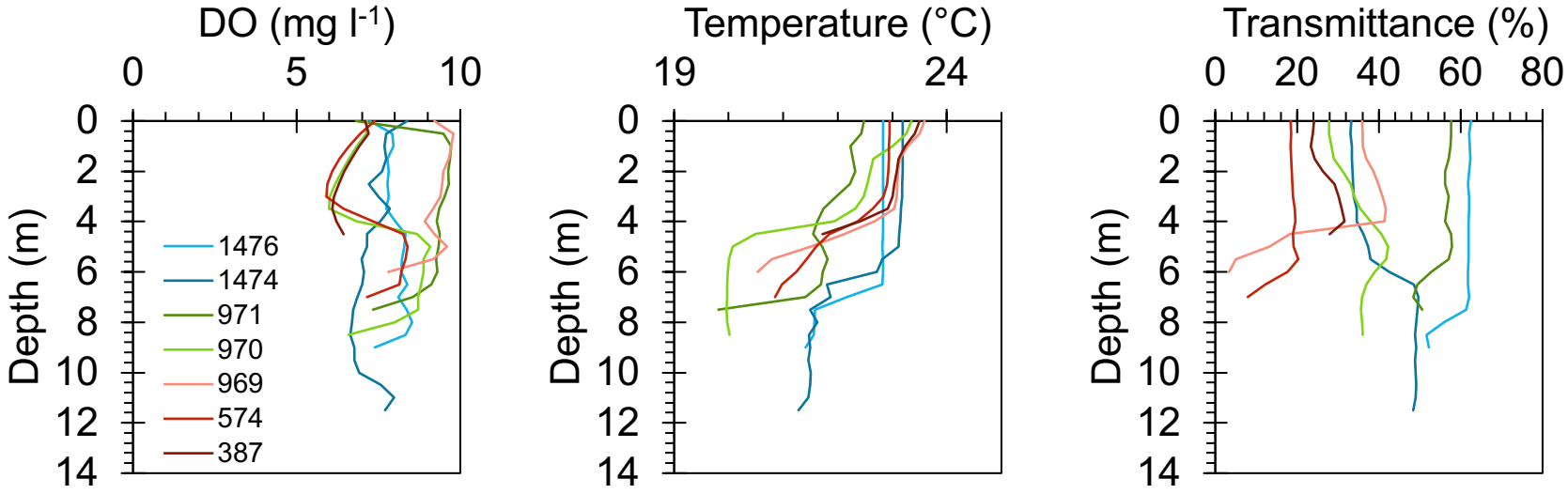

Figure 2.3. DO, temperature, and transmittance for non-river mouth stations in Lake Erie for sampling year 2018. Stations are color grouped for relation to river input stations: red Maumee River group, green Detroit River group, and blue Sandusky/central basin group.

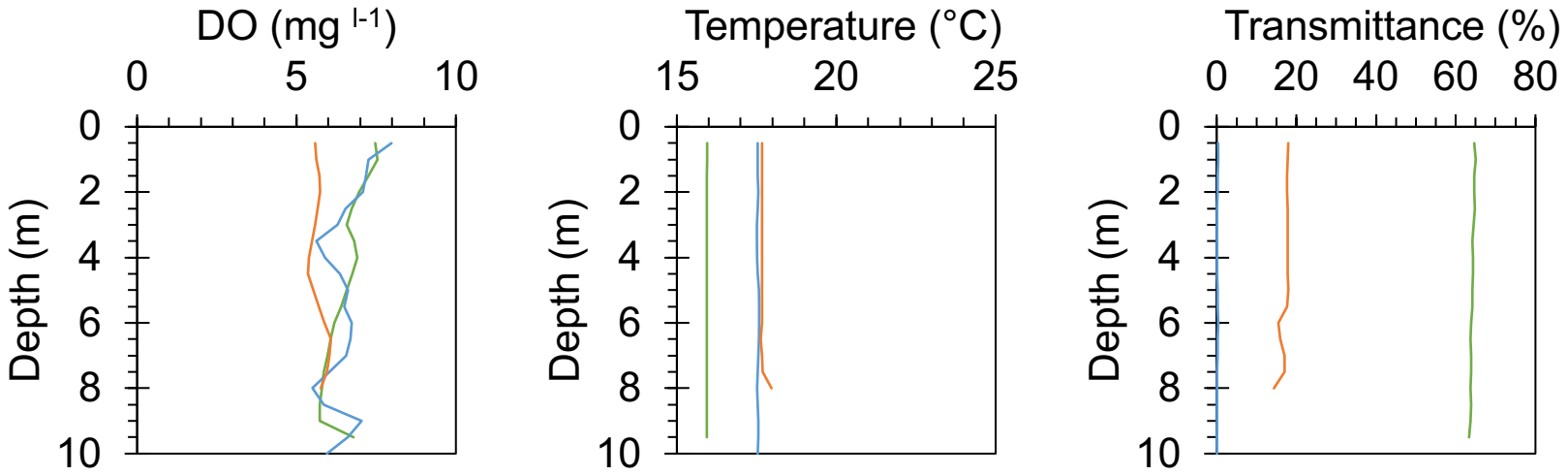

Figure 2.4. DO, temperature, and transmittance at stations near the Detroit and Maumee river mouths and Sandusky Bay connection to Lake Erie for sampling year 2019.

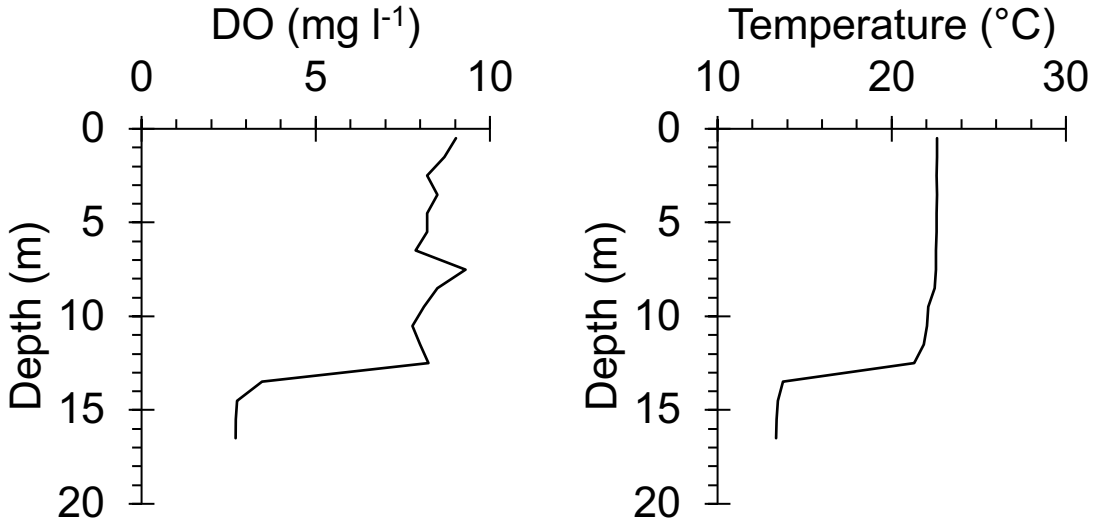

Figure 2.5. DO and temperature at the Central Basin station in 2021. Transmittance data was not collected.

2.4.1 2018 HgT and MeHg

Water column samples were collected in 2018 from ten stations around the western basin of Lake Erie. At these stations, HgT concentrations ranged from 2.6 to 15.2 pM and averaged 5.8 ± 2.7 pM (Table 2.2). The Maumee River mouth (station 215) had the highest average HgT concentration (11.6 ± 2.8, n = 6, Figure 2.6; Tukey, $p = 0.01$) compared to other sites. Moving away from the Maumee River mouth to stations 387 and 969, HgT concentrations from the water column were 5.4 ± 0.19 and 5.2 ± 0.27 pM, respectively. The Detroit River mouth (station 1297) had an average HgT concentration of 5.4 ± 0.5 pM and moving away from the river mouth to station 971, HgT had an average concentration of 3.5 ± 0.1 pM. The Sandusky Bay connection to central Lake Erie (station 1163) had an average HgT concentration of 5.7 ± 0.5 pM, and a station away from the mouth (station 1474) had an average of 3.0 ± 0.1 pM. Two stations in the middle of the western basin, stations 574 and 970, had averages of 6.7 ± 0.3 and 7.0 ± 0.6 pM, respectively.

The average MeHg concentration for all ten sites in 2018 ranged from 0.04 to 1.16 pM and averaged 0.32 ± 0.04 pM. The Maumee River mouth (station 215) had an average of 0.63 ± 0.21 pM, and station 387 had an average of 0.26 ± 0.11 pM. The Detroit River mouth station (station 1297) had an average MeHg concentration of 0.38 ± 0.11 pM, and station 1474 had an average of 0.23 ± 0.05 pM. The Sandusky Bay connection to Lake Erie (station 1163) had an average MeHg concentration of 0.24 ± 0.06 pM. The three river input stations had lower concentrations of MeHg in the surface water than near bottom water, possibly indicating a flux from sediment (Figure 2.7).

Table 2.2. Sampling sites from 2018 with maximum depth and mean HgT and MeHg concentrations with standard error from water column sampling. *denotes values without standard error.

Site	Max depth (m)	HgT (pM)			n	MeHg (pM)			n
215	7.8	11.6	±	2.8	5	0.63	±	0.21	5
387	5	5.4	±	0.4	4	0.26	±	0.11	4
574	7.6	6.7	±	0.6	5	0.30	±	0.08	5
969	5.5	5.2	±	0.6	6	0.07*			1
970	8	7	±	1.3	4	0.39	±	0.03	4
971	6.5	3.5	±	0.1	4	0.30*			1
1163	6.3	5.3	±	0.9	4	0.24	±	0.06	4
1297	7	5.4	±	0.8	4	0.29	±	0.09	5
1474	11.5	3	±	0.2	4	0.23	±	0.05	4
1476	9	2.9	±	0.3	4	0.17	±	0.09	3

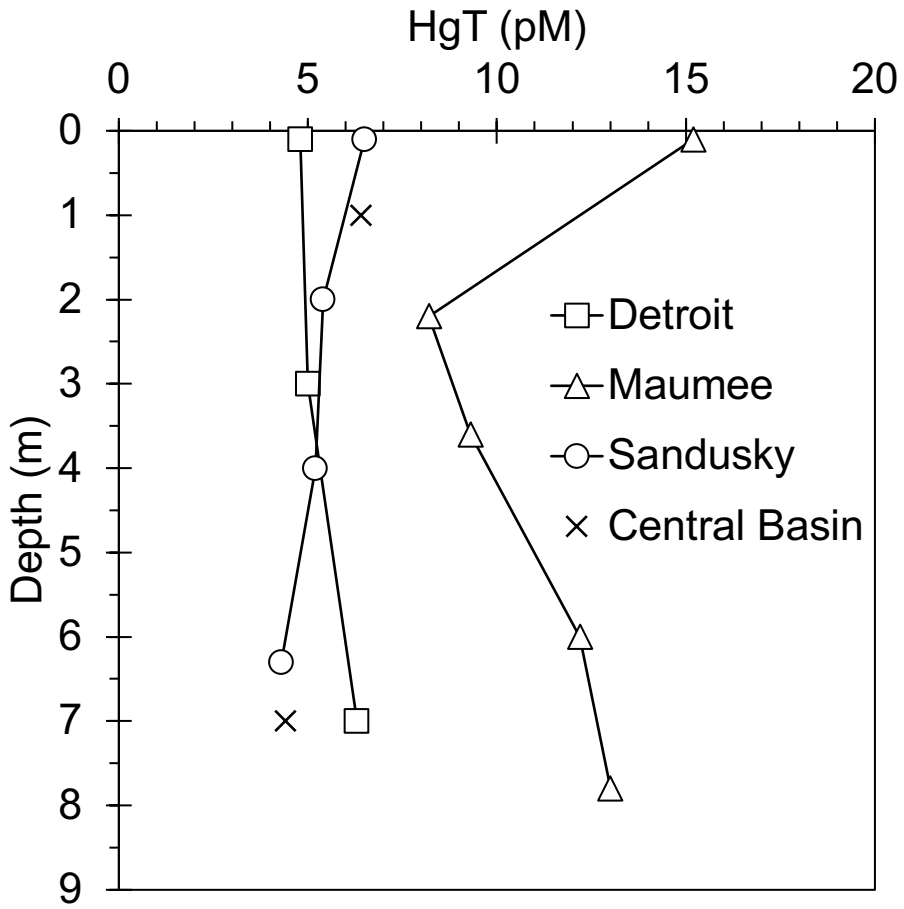

Figure 2.6. Total Hg concentrations from the three river input stations in 2018 and central basin in 2021. Sandusky and Detroit Rivers show a well-mixed water column, whereas the Maumee River mouth has a decrease in concentrations at 2 m depth, then a gradual increase.

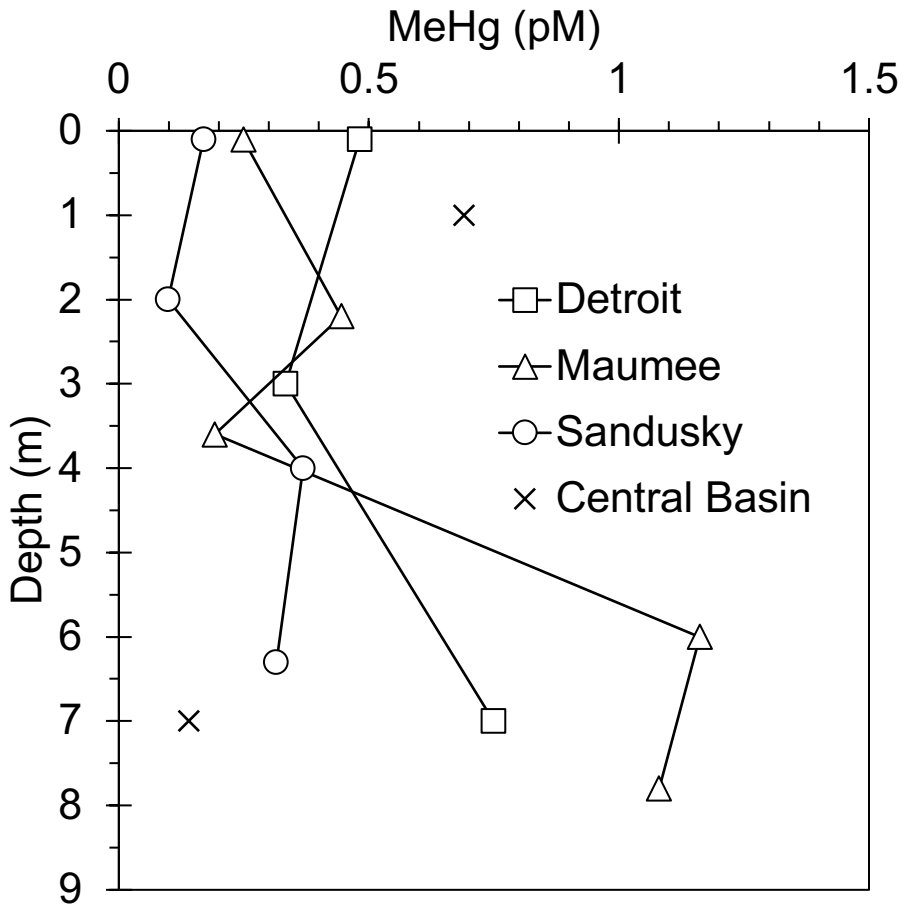

Figure 2.7. Methylmercury concentrations from the three river input stations in 2018 and central basin in 2021. Detroit and Maumee River mouths have increased bottom water concentrations from a possible flux from sediments.

2.4.2 Potential Specific Hg Methylation Rates in western Lake Erie in 2019

Highest potential Hg methylation rates were found where Sandusky Bay meets Lake Erie (0.045 ± 0.012 day^{-1}), followed by the Detroit (0.031 ± 0.006 day^{-1}) and Maumee River mouths (0.005 ± 0.003 day^{-1}; Figure 2.8). Ambient MeHg concentrations were estimated from $CH_3{}^{202}Hg$ (^{202}Hg was not used as a spike; Hintelmann & Evans, 1997) and were 0.53 ± 0.16 pM (n = 6) for the Maumee River mouth, 0.34 ± 0.12 pM (n = 6) for the Detroit River mouth, and 0.66 ± 0.09 pM (n = 4) for the Sandusky Bay input.

2.4.3 Total Hg, MeHg, and Potential Hg Methylation Rates in the central basin (2021)

Mean HgT and MeHg concentrations were 5.6 ± 0.56 pM (n = 5) and 0.50 ± 0.24 pM (n = 2), respectively (Figures 2.6 and 2.7). Surface and bottom water samples had a mean potential specific Hg methylation rate of 0.073 ± 0.051 day^{-1} (n = 4), which was indistinguishable from rates in bottom water (0.051 ± 0.035 day^{-1}; n = 4).

2.5 Discussion

HgT and MeHg concentrations and Hg methylation rates at sites across western and central Lake Erie were examined. HgT concentrations in the water column were higher in the Maumee River mouth (Tukey, $p = 0.01$) compared to the Detroit River mouth and Sandusky Bay input. Methylmercury concentrations from the three river inputs were not different from one another (Tukey, $p > 0.22$). The ratio of MeHg to HgT was highest at the Detroit River mouth, indicating a higher proportion of MeHg in total Hg concentrations compared to the Sandusky Bay and Maumee River inputs (Figure 2.9).

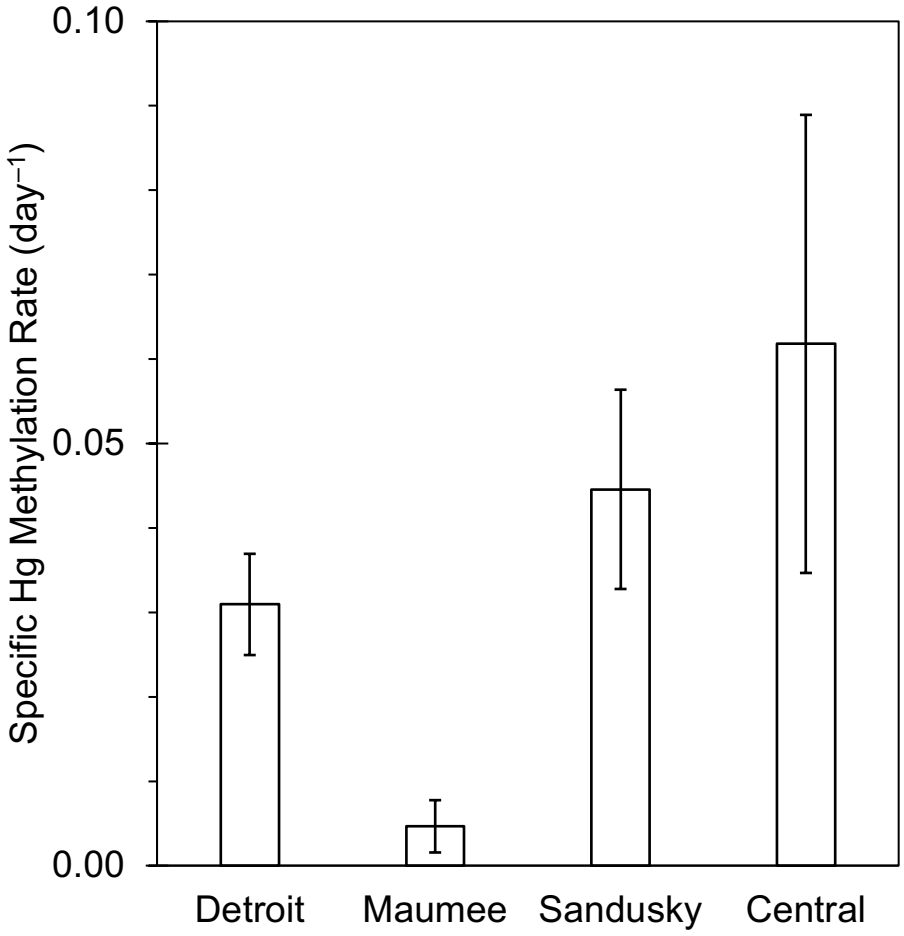

Figure 2.8. Potential specific Hg methylation rates for the three river input sites and a site in the central basin.

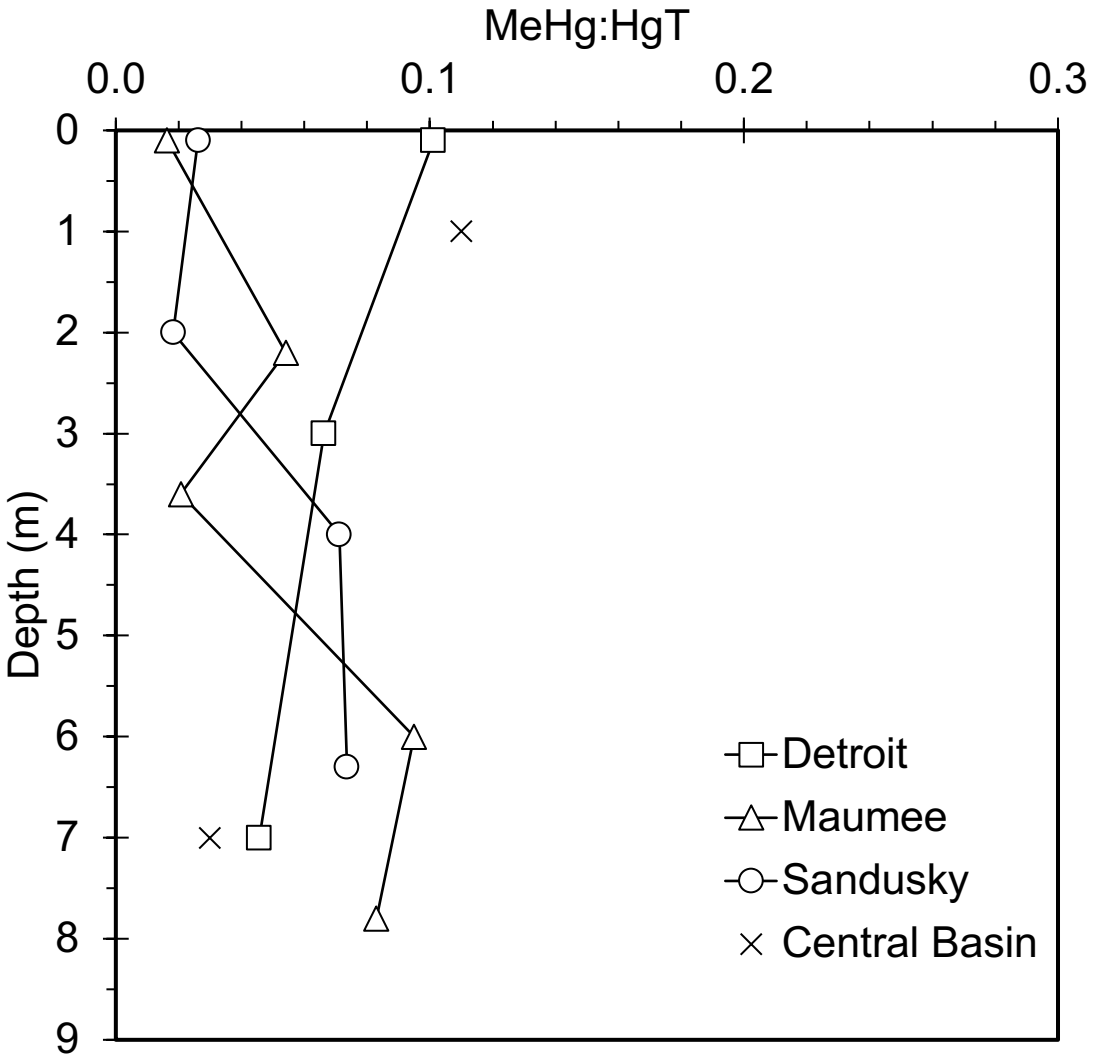

Figure 2.9. Ratio of MeHg:HgT for the three river input sites and the central basin.

Mercury specific methylation rates were highest in the central basin at the Sandusky Bay input and central basin but were not different from the Detroit and Maumee River mouths (Tukey, $p = 0.85$). The lack of difference between the sites could be explained by Lake Erie being well-mixed and the water within the lake having a short residence time (1.2 years). The residence time of water in the western basin is dependent on season and river discharges, but average residence time is estimated at 50 days (Matisoff et al., 2016). The circulation of water in the western basin leaves a gyre like area in the center and is where elevated HgT and MeHg concentrations were measured (Holocomb et al., 1993).

In this study, HgT and MeHg concentrations from all sites in the western basin had a mean of 5.6 ± 0.5 pM. In the western basin, excluding river input sites, HgT and MeHg ranged from 2.9 to 7.0 pM and ranged from 0.07 to 0.39 pM respectively. The United States Geological Survey (USGS) routinely monitors stations for HgT and MeHg, and Lepak et al. (2015) found HgT concentrations of 12.5 ± 2.08 pM (n = 25) in the western basin. Data previously collected but not published from the USGS for August 2010 ranged from 5.0 to 11.6 pM (mean 8.9 ± 0.1 pM, n = 12; Ogorek et al., 2021) for HgT and 0.12 to 0.20 pM (mean 0.5 ± 0.01 pM, n = 12) for MeHg (Ogorek et al., 2021). The lower values reported in this study compared to those reported by Lepak et al. (2015) suggest that western basin Hg concentrations decreased by about 21% yr^{-1} (newer concentrations subtracted from older concentrations, divided by total time between sampling, multiplied by 100). Atmospheric deposition for the western basin of Lake Erie has decreased from 19 μg m^{-2} yr^{-1} in 2005 to 13 μg m^{-2} yr^{-1} in 2019 (Fitzgibbons et al., 2008; NAPD, 2020). The change of 2.3% yr^{-1} decrease for atmospheric deposition does not align with the decrease in water column MeHg concentrations (21%). This could be

from analytical differences or greater changes within the lake compared to the atmosphere.

2.5.1 River Input Fluxes

Scaling up the concentrations measured in this study with the annual discharge of each river, we estimate that HgT river input loadings per year would be highest in the Detroit River (172 kg yr^{-1}), followed by the Maumee River (14.4 kg yr^{-1}) and Sandusky Bay (0.94 kg yr^{-1}). Our load estimates are lower than those previously calculated by Kelly et al. (1991) for the Detroit River and Fitzgibbon et al. (2008) for the Maumee and Sandusky Rivers. For the Detroit River, Kelly et al. (1991) reported a flux of 1,594 kg yr^{-1}, with an average HgT concentration in the river of 10 ng l^{-1} (50 pM), attributed to chemical manufacturing in the area and much greater than the water from Lake Huron. Water from Lake Huron flows into and through Lake St. Clair, and then from the Detroit River into the western basin of Lake Erie. Lepak et al. (2015) measured HgT concentrations in Lake Huron with a mean of 1.0 ± 0.2 pM (n = 15). Lake St. Clair is also known to have high Hg and trace metal concentrations in sediment from heavy historical industry (Jia et al., 2010).

Fitzgibbon et al. (2008) reported that the Maumee River had the highest flux of all Ohio rivers into Lake Erie at 36 kg yr^{-1}, which was attributed to the large watershed size and the amount of agricultural lands containing organic matter. Soil loss from erosion on agricultural lands increases Hg flux from the landscape because particles and organic matter strongly bind with Hg (Babiarz et al., 1998; Fitzgibbon et al., 2008). Measured values from Lake Erie in this study were less than those previously reported in the 1990s

and early 2000s, which could be explained in part by seasonality, as we sampled in summer when discharge is lower, but other studies also sampled in the late Summer and early Fall (Ogorek et al., 2021). Sites sampled in the present study were located near river inputs, rather than in the rivers, where there may be higher suspended sediment and organic matter. Alternatively, these reductions in Hg concentrations and loads may reflect improvements in Hg pollution due to the Clean Air and Water Act in Ohio implemented in 2004. Zhou et al. (2017) attributed the overall decline of Hg in the Great Lakes to a decrease in regional atmospheric Hg emissions. Ogorek et al. (2021) also reported much lower concentrations in Lake Erie (1.2 pM) than reported previously, supporting the explanation that legislation enacted to reduce Hg pollution has succeeded. Decreased Hg loads are promising for long-term improvements in Hg pollution. A recent study by Blanchfield et al. (2021) from the Experimental Lakes Area in Canada showed that, after additions of Hg ceased, the annual percent increase of MeHg in local fish decreased, suggesting that decreasing Hg emissions can decrease Hg in biota, lessening the human health risks from MeHg poisoning.

2.5.2 In situ Hg methylation Flux

Potential Hg methylation rates in the western basin of Lake Erie were not different between sites (Tukey, $p > 0.87$). Methylation rates have not been reported from Lake Erie previously, but they have been measured in other freshwater lakes. Eckley and Hintelmann (2006) reported water column rates of 0.006 to 0.148 day^{-1} in five lakes in Canada, but no MeHg was observed in the one eutrophic lake included in that study. Eckley et al. (2005) also measured potential Hg methylation rates in a lake

surrounded by a wetland (0.01 to 0.09 day^{-1}), similar to those measured in Lake Erie (0.005 to 0.062 day^{-1}). Gray & Hines (2009) measured methylation rate potentials in sediment in Salmon Falls Creek Reservoir, Idaho, and reported rate constants of 0.023 to 0.170 day^{-1}, with these higher rates attributed to local gold mining.

Flux calculations can also be made from the potential rates reported here. Highest methylation rates were observed in the hypoxic central basin (0.062 ± 0.027 day^{-1}), followed by the Sandusky Bay connection (0.045 ± 0.012 day^{-1}), and lower rates from the western basin near the Maumee (0.005 ± 0.003 day^{-1}) and Detroit (0.031 ± 0.006 day^{-1}) River mouths. The total volume of Lake Erie is 484 km^3, with 63% of the volume in the central basin, 5% in the western basin, and the remaining 32% in the eastern basin. The western basin has an average depth of 7.4 m and surface area of 301 km^2 (Bocaniov et al., 2016). The central basin has an average depth of 18.5 m and surface area of 16,100 km^2 (Bocaniov et al., 2016).

Lake Erie was divided into the western and central basins as in Holocomb et al. (1993) and Bocaniov et al. (2016), where samples collected from near the Detroit and Maumee River mouths were considered western basin, and samples collected in the central basin and near the Sandusky Bay connection were considered central basin. In the western Basin, the Detroit River supplies 94% of the water to the western basin, and the Maumee supplies 4% (Scavia et al. 2016). In the central basin, the Sandusky River supplies 1% of water, so it was assumed that the other sampling site in the central basin represents 99% of the water in the central basin. Using the percent volume from each river (or lake station), it was estimated that 0.0072 kg yr^{-1} of MeHg is sourced from the central basin stations, and 0.0002 kg yr^{-1} is sourced from the Detroit and Maumee River

mouths in the western basin. However, annually, *in situ* Hg methylation production is an order of magnitude lower than our calculated river loads, as well as the river loads reported by Fitzgibbons et al. (2008).

2.5.3 Flux from Lake Erie sediment

Bottom water concentrations from water column profiles in 2018 were elevated near the Detroit and Maumee River mouths for HgT and MeHg. Previous measurements in Lake Erie showed that the western basin had the highest sediment Hg concentration of all the Laurentian Great Lakes (Lepak et al., 2015). Sedimentation plays an important role in the removal of Hg from the water column, and Hg binds with organic ligands and is preserved in the sediment record (Randall and Chattopadhyay, 2013). However, many lakes also exhibit net MeHg production and diffusion from sediments into the water column (Sellers et al., 2001). Hg in sediment pore water is bound to thiols but can diffuse from sediment. Here, estimations of Hg flux from sediment pore water were based on Fick's first law. Diffusive flux of Hg in sediment pore water can be modeled by:

$$F = -\left(\frac{\varphi D_w}{\theta^2}\right)\frac{\partial C}{\partial x}$$

Where F is the flux of Hg concentration C at depth x, φ is sediment porosity, θ is tortuosity, and D_w is the diffusion coefficient of Hg in water in the absence of a sediment matrix. Porosity values were obtained from Matisoff et al. (2016) for sites near our three sampling sites and were 0.75 for Sandusky Bay and 0.80 for both the Maumee and Detroit river mouths. Tortuosity was estimated from porosity using Boudreau (1996):

$$\theta^2 = 1 - \ln(\varphi^2)$$

D_w for inorganic Hg was obtained from Gill et al. (1999) and was 9.5 x 10^{-6} cm^2 s^{-1} at 25°C. The MeHg rate constant was obtained from Hammerschmidt et al. (2004) and was 1.20 x 10^{-5} cm^2 s^{-1} at 25°C. Porewater Hg concentrations were not measured in this study. Previously measured sediment concentrations from Lepak et al. (2015) and Ogorek et al (2021) were used to estimate porewater HgT concentrations for the three river sites using the partitioning coefficient (K_d; L kg^{-1}), which is the affinity of a particle to Hg. Porewater concentrations for MeHg were estimated using sediment concentrations from Ogorek et al. (2021) and K_d values from Bowman et al. (2021).

Estimations of diffusive flux of MeHg from Lake Erie sediments ranged from −0.18 to 0.14 pmol m^{-2} yr^{-1} (Table 2.3). The central basin and Sandusky Bay stations had negative fluxes into sediments of –0.05 and −0.06 pmol m^{-2} yr^{-1}, respectively. Only the Maumee River site had a positive efflux out of sediments (Table 2.3; Figure 2.10). This result was consistent with the MeHg:HgT ratio, where the Maumee River mouth water column samples were elevated near the bottom water (Figure 2.7). Further analyses of MeHg fluxes across the sediment-water interface in Lake Erie should be conducted in different seasonal conditions. A mass balance of MeHg for the western and central basins for river flux, potential MeHg production, and fluxes from sediments indicated that most MeHg is from river fluxes into both basins (Table 2.2).

2.6 Summary

HgT, MeHg, and Hg methylation rates were analyzed from sampling years 2018, 2019, and 2021 in the western and central basins of Lake Erie. Overall, there has been a decrease in Hg in sediment noted for the Great Lakes, and the decreases in Hg.

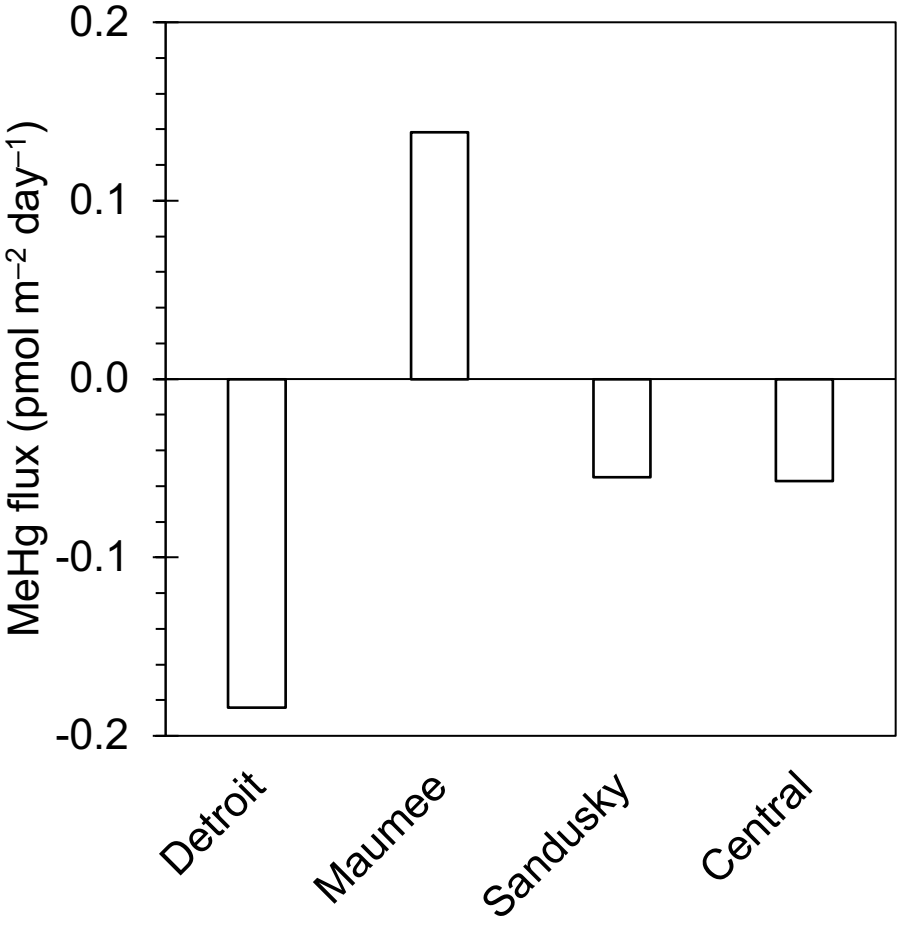

Figure 2.10. Sediment-water interface MeHg fluxes for the three river input sites.

Table 2.3. MeHg flux from water column river input measurements and sediments, units Kg yr^{-1}

Site	Watershed Size (km^2)	Discharge ($m3\ s^{-1}$)	Hg deposition*	MeHg River Flux	MeHg Production Rates (10^{-3})	MeHg Flux from sediment
Detroit	1,813	5,058	24	10	0.150	-0.004
Maumee	16,460	195	214	0.79	0.002	0.003
Sandusky	4,726	23	61	0.03	0.074	-0.001
Central Basin	n.d.	n.d.	n.d	n.d.	7.120	-0.001

*Hg deposition values calculated using USGS mean annual flow and annual deposition rate of 19 µg m^{-2}

concentrations in surface sediments over time are likely a result of the Ohio Clean Air and Water act implemented in 2004 (Lepak et al., 2015; Zhou et al., 2017). In 2018, water column samples for unfiltered HgT and MeHg were collected from 10 sites in the western basin and were highest from near the Detroit and Maumee river mouths and the Sandusky Bay connection to Lake Erie. In 2019, Hg methylation rate experiments were conducted from the Detroit and Maumee River and Sandusky Bay inputs, and the highest rates were observed near the Maumee River mouth. In 2021, Hg methylation rate experiments were conducted at one site in the central basin of Lake Erie, along with HgT and MeHg water column concentrations. All of these results were used to generate flux measurements from rivers and sediments. MeHg was released from sediments and into the water column near the Maumee River mouth (0.003 kg yr^{-1}), but net fluxes into sediments were observed near the Detroit River mouth and Sandusky Bay connection to Lake Erie.

2.7 References

Achá, D., Pabón, C. A., & Hintelmann, H. (2012). Mercury methylation and hydrogen sulfide production among unexpected strains isolated from periphyton of two macrophytes of the Amazon. *FEMS Microbiology Ecology*, *80*(3), 637–645. https://doi.org/10.1111/j.1574-6941.2012.01333.x

Avramescu, M. L., Yumvihoze, E., Hintelmann, H., Ridal, J., Fortin, D., & R.S. Lean, D. (2011). Biogeochemical factors influencing net mercury methylation in contaminated freshwater sediments from the St. Lawrence River in Cornwall, Ontario, Canada. *Science of the Total Environment*, *409*(5), 968–978. https://doi.org/10.1016/j.scitotenv.2010.11.016

Babiarz, C. L., Hurley, J. P., Benoit, J. M., Shafer, M. M., Andren, A. W., & Webb, D. A. (1998). *Seasonal influences on partitioning and transport of total and methylmercury in rivers from contrasting watersheds*. *Biogeochemistry* (Vol. 41).

Babiarz, C. L., Hurley, J. P., Hoffmann, S. R., Andren, A. W., Shafer, M. M., & Armstrong, D. E. (2001). Partitioning of total mercury and methylmercury to the colloidal phase in freshwaters. *Environmental Science and Technology*, *35*(24), 4773–4782. https://doi.org/10.1021/es010895v

Benoit, J. M., Gilmour, C. C., Mason, R. P., & Heyes, A. (1999). Sulfide controls on mercury speciation and bioavailability to methylating bacteria in sediment pore waters. *Environmental Science and Technology*, *33*(6), 951–957. https://doi.org/10.1021/es9808200

Bloom, N., & Fitzgerald, W. F. (1988). Determination of volatile mercury species at the picogram level by low-temperature gas chromatography with cold-vapor atomic fluorescence detection. *Analytica Chimica Acta*, *208*, 151–161. https://doi.org/https://doi.org/10.1016/S0003-2670(00)80743-6

Bloom, N. S., & Crecelius, E. A. (1983). Determination of mercury in seawater at sub-nanogram per liter levels. *Marine Chemistry*, *14*(1), 49–59. https://doi.org/https://doi.org/10.1016/0304-4203(83)90069-5

Bloom, N. S., Watras, C. J., & Hurley, J. P. (1991). Impact of acidification on the methylmercury cycle of remote seepage lakes. *Water, Air, and Soil Pollution*, *56*, 477–491.

Bocaniov, S. A., Leon, L. F., Rao, Y. R., Schwab, D. J., & Scavia, D. (2016). Simulating the effect of nutrient reduction on hypoxia in a large lake (Lake Erie, USA-Canada) with a three-dimensional lake model. *Journal of Great Lakes Research*, *42*(6), 1228–1240. https://doi.org/10.1016/j.jglr.2016.06.001

Boedecker, A. R., Niewinski, D. N., Newell, S. E., Chaffin, J. D., & McCarthy, M. J. (2020). Evaluating sediments as an ecosystem service in western Lake Erie via quantification of nutrient cycling pathways and selected gene abundances. *Journal of Great Lakes Research*, *46*(4), 920–932. https://doi.org/10.1016/j.jglr.2020.04.010

Boudreau, B. P. (1996). The diffusive tortuosity of fine-grained unlithified sediments. *Geochimica et Cosmochimica Acta*, *60*(16), 3139–3142. https://doi.org/https://doi.org/10.1016/0016-7037(96)00158-5

Bowman, K. L., & Hammerschmidt, C. R. (2011). Extraction of monomethylmercury from seawater for low-femtomolar determination. *Limnology and Oceanography: Methods*, *9*(APRIL), 121–128. https://doi.org/10.4319/lom.2011.9.121

Bowman, K. L., Lamborg, C. H., Agather, A. M., & Hammerschmidt, C. R. (2021). The role of plastic debris in the biogeochemical cycle of mercury in Lake Erie and San Francisco Bay. *Marine Pollution Bulletin*, *171*, 112768. https://doi.org/https://doi.org/10.1016/j.marpolbul.2021.112768

Calhoun, F. G., Baker, D. B., & Slater, B. K. (2002). Soils, Water Quality, and Watershed Size: Interactions in the Maumee and Sandusky River Basins of Northwestern Ohio. *Journal of Environmental Quality*, *31*, 47–53. https://doi.org/10.2134/jeq2002.4700a

Choi, S.-C., Chase, T., & Bartha, R. (1994). Metabolic Pathways Leading to Mercury Methylation in Desulfovibrio desulfuricans. *Applied and Environmental Microbiology*, *60*(11), 4072–4077. Retrieved from https://journals.asm.org/journal/aem

Cohen, M., Artz, R., Draxler, R., Miller, P., Poissant, L., Niemi, D., et al. (2004). Modeling the atmospheric transport and deposition of mercury to the Great Lakes. In *Environmental Research* (Vol. 95, pp. 247–265). https://doi.org/10.1016/j.envres.2003.11.007

Eckley, C. S., & Hintelmann, H. (2006). Determination of mercury methylation potentials in the water column of lakes across Canada. *Science of the Total Environment*, *368*(1), 111–125. https://doi.org/10.1016/j.scitotenv.2005.09.042

Ekstrom, E. B., Morel, F. M. M., & Benoit, J. M. (2003). Mercury methylation independent of the acetyl-coenzyme a pathway in sulfate-reducing bacteria. *Applied and Environmental Microbiology*, *69*(9), 5414–5422. https://doi.org/10.1128/AEM.69.9.5414-5422.2003

Fitzgerald, W. F., & Gill, G. A. (1979). Subnanogram Determination of Mercury by Two-Stage Gold Amalgamation and Gas Phase Detection Applied to Atmospheric Analysis. *Transform Techniques in Chemistry*, *51*(11), 59. Retrieved from https://pubs.acs.org/sharingguidelines

Fitzgerald, W. F., Engstrom, D. R., Hammerschmidt, C. R., Lamborg, C. H., Balcom, P. H., Lima-Braun, A. L., et al. (2018). Global and Local Sources of Mercury Deposition in Coastal New England Reconstructed from a Multiproxy, High-Resolution, Estuarine Sediment Record. *Environmental Science and Technology*, *52*(14), 7614–7620. https://doi.org/10.1021/acs.est.7b06122

Fitzgibbon, T. O., Berry Lyons, W., Gardner, C. B., & Carey, A. E. (2008). A preliminary study of the Hg flux from selected Ohio watersheds to Lake Erie. *Applied Geochemistry*, *23*(12), 3434–3441. https://doi.org/10.1016/j.apgeochem.2008.07.013

Gill, G. A., Bloom, N. S., Cappellino, S., Driscoll, C. T., Dobbs, C., Mcshea, L., et al. (1999, March 1). Sediment-water fluxes of mercury in Lavaca Bay, Texas. *Environmental Science and Technology*. ACS. https://doi.org/10.1021/es980380c

Gray, J. E., & Hines, M. E. (2009). Biogeochemical mercury methylation influenced by reservoir eutrophication, Salmon Falls Creek Reservoir, Idaho, USA. *Chemical Geology*, *258*(3–4), 157–167. https://doi.org/10.1016/j.chemgeo.2008.09.023

Hammerschmidt, C. R., & Fitzgerald, W. F. (2006). Methylmercury cycling in sediments on the continental shelf of southern New England. *Geochimica et Cosmochimica Acta*, *70*(4), 918–930. https://doi.org/10.1016/j.gca.2005.10.020

Hammerschmidt, C. R., Fitzgerald, W. F., Lamborg, C. H., Balcom, P. H., & Visscher, P. T. (2004). Biogeochemistry of methylmercury in sediments of Long Island Sound. In *Marine Chemistry* (Vol. 90, pp. 31–52). https://doi.org/10.1016/j.marchem.2004.02.024

Hintelmann, H., & Evans, R. D. (1997). Application of stable isotopes in environmental tracer studies - Measurement of monomethylmercury (CH3Hg+) by isotope dilution ICP-MS and detection of species transformation. *Fresenius J Anal Chem*, *358*, 378–385.

Hintelmann, Holger, Evans, R. D., & Villeneuve, J. Y. (1995). Measurement of mercury methylation in sediments by using enriched stable mercury isotopes combined with methylmercury determination by gas chromatography–inductively coupled plasma mass spectrometry. *Journal of Analytical Atomic Spectrometry*, *10*(9), 619–624. https://doi.org/10.1039/JA9951000619

Hintelmann, Holger, Keppel-jones, K., & Douglas Evans, R. (2000). *Constants of mercury methylation and demethylation rates in sediments and comparison of tracer and ambient mercury availability*. *Environmental Toxicology and Chemistry* (Vol. 19).

Holcombe, T. L., Warren, J. S., Taylor, L. A., Reid, D. F., & Herdendorf, C. E. (1997). Lake floor geomorphology of Western Lake Erie. *Journal of Great Lakes Research*, *23*, 190–201.

Jia, J., Thiessen, L., Schachtschneider, J., Waltho, J., & Marvin, C. (2010). Contaminant Trends in Suspended Sediments in the Detroit River-Lake St. Clair-St. Clair River Corridor, 2000 to 2004. *Water Quality Research Journal Canada*, *45*, 69–80. Retrieved from http://iwaponline.com/wqrj/article-pdf/45/1/69/229657/wqrjc0450069.pdf

Kelly, T. J., Czuczwa, J. M., Sticksel, P. R., Sverdrup, G. M., Koval, P. J., & Hodanbosi, R. F. (1991). Atmospheric and Tributary Inputs of Toxic Substances to Lake Erie. *Journal of Great Lakes Research*, *17*(4), 504–516. https://doi.org/10.1016/S0380-1330(91)71386-5

Kerin, E. J., Gilmour, C. C., Roden, E., Suzuki, M. T., Coates, J. D., & Mason, R. P. (2006). Mercury methylation by dissimilatory iron-reducing bacteria. *Applied and Environmental Microbiology*, *72*(12), 7919–7921. https://doi.org/10.1128/AEM.01602-06

Lepak, R. F., Yin, R., Krabbenhoft, D. P., Ogorek, J. M., Dewild, J. F., Holsen, T. M., & Hurley, J. P. (2015). Use of Stable Isotope Signatures to Determine Mercury Sources in the Great Lakes. *Environmental Science and Technology Letters*, *2*(12), 335–341. https://doi.org/10.1021/acs.estlett.5b00277

Lyons, W. B., Fitzgibbon, T. O., Welch, K. A., & Carey, A. E. (2006). Mercury geochemistry of the Scioto River, Ohio: Impact of agriculture and urbanization. *Applied Geochemistry*, *21*(11), 1880–1888. https://doi.org/10.1016/j.apgeochem.2006.08.005

Marvin, C., Painter, S., Williams, D., Richardson, V., Rossmann, R., Hoof, P. van, et al. (2004). Spatial and Temporal Trends in Surface Water and Sediment Contamination in the Laurentian Great Lakes. *Environmental Pollution*, *129*, 131–144.

Mason, R. P., Fitzgerald, W. F., & Morel, F. M. M. (1994). *Geochimica et Cosmochimica Acta* (Vol. 58).

Mason, R. P., Reinfelder, J. R., & Morel, F. M. M. (1996). Uptake, Toxicity, and Trophic Transfer of Mercury in a Coastal Diatom. *Environmental Science and Technology*, *30*, 1835–1845. Retrieved from https://pubs.acs.org/sharingguidelines

Matisoff, G., Kaltenberg, E. M., Steely, R. L., Hummel, S. K., Seo, J., Gibbons, K. J., et al. (2016). Internal loading of phosphorus in western Lake Erie. *Journal of Great Lakes Research*, *42*(4), 775–788. https://doi.org/10.1016/j.jglr.2016.04.004

Ogorek, J. M., Lepak, R. F., Hoffman, J. C., DeWild, J. F., Rosera, T. J., Tate, M. T., et al. (2021). Enhanced Susceptibility of Methylmercury Bioaccumulation into Seston of the Laurentian Great Lakes. *Environmental Science and Technology*, *55*(18), 12714–12723. https://doi.org/10.1021/acs.est.1c02319

Ohio Sport Fish Consumption Advisory. (2021). Retrieved from www.odh.ohio.gov

Painter, S., Marvin, C., Rosa, F., Reynoldson, T. B., Charlton, M. N., Fox, M., et al. (2001). Sediment contamination in Lake Erie: A 25-year retrospective analysis. *Journal of Great Lakes Research*, *27*(4), 434–448. https://doi.org/10.1016/S0380-1330(01)70658-2

Pak, K.R., & Bartha, R. (1998). Mercury Methylation and Demethylation in Anoxic Lake Sediments and by Strictly Anaerobic Bacteria*. Applied and Environmental Microbiology*. Vol. 64

Randall, P. M., & Chattopadhyay, S. (2013). Mercury contaminated sediment sites-An evaluation of remedial options. *Environmental Research*, *125*, 131–149. https://doi.org/10.1016/j.envres.2013.01.007

Rice, K. M., Walker, E. M., Wu, M., Gillette, C., & Blough, E. R. (2014). Environmental mercury and its toxic effects. *Journal of Preventive Medicine and Public Health*. Korean Society for Preventive Medicine. https://doi.org/10.3961/jpmph.2014.47.2.74

Richards, R. P., Baker, D. B., Crumrine, J. P., & Stearns, A. M. (2010). Unusually large loads in 2007 from the Maumee and Sandusky Rivers, tributaries to Lake Erie. *Journal of Soil and Water Conservation*, *65*(6), 450–462. https://doi.org/10.2489/jswc.65.6.450

Sadraddini, S., Ekram Azim, M., Shimoda, Y., Mahmood, M., Bhavsar, S. P., Backus, S. M., & Arhonditsis, G. B. (2011). Temporal PCB and mercury trends in Lake Erie fish communities: A dynamic linear modeling analysis. *Ecotoxicology and Environmental Safety*, *74*(8), 2203–2214. https://doi.org/10.1016/j.ecoenv.2011.07.031

Scavia, D., DePinto, J. v., & Bertani, I. (2016). A multi-model approach to evaluating target phosphorus loads for Lake Erie. *Journal of Great Lakes Research*, *42*(6), 1139–1150. https://doi.org/10.1016/j.jglr.2016.09.007

Sellers, P., Kelly, C. A., & Rudd, J. W. M. (2001). Fluxes of methylmercury to the water column of a drainage lake: The relative importance of internal and external sources. *Limnol. Oceanogr* (Vol. 46).

Smart, N. A. (1968). Use and residues of mercury compounds in agriculture. *Residue Reviews*, *23*, 1–36. https://doi.org/10.1007/978-1-4615-8437-7_1

Streets, D. G., Horowitz, H. M., Lu, Z., Levin, L., Thackray, C. P., & Sunderland, E. M. (2019). Global and regional trends in mercury emissions and concentrations, 2010–2015. *Atmospheric Environment*, *201*, 417–427. https://doi.org/10.1016/j.atmosenv.2018.12.031

Sunderland, E. M., & Mason, R. P. (2007). Human impacts on open ocean mercury concentrations. *Global Biogeochemical Cycles*, *21*(4).

Tseng, C. M., Hammerschmidt, C. R., & Fitzgerald, W. F. (2005). Determination of methylmercury in environmental matrixes by on-line flow injection and atomic fluorescence spectrometry. *Analytical Chemistry*, *76*(23), 7131–7136.

Ullrich, S. M., Tanton, T. W., & Abdrashitova, S. A. (2001). Mercury in the Aquatic Environment: A Review of Factors Affecting Methylation. *Critical Reviews in Environmental Science and Technology*, *31*(3), 241–293.

Walters, L., Kovacik, T. L., & Herdendorf, C. E. (1974). Mercury occurrence in sediment cores from Western Lake Erie. The Ohio Journal of Science. (Vol. 74).

Watson, S. B., Miller, C., Arhonditsis, G., Boyer, G. L., Carmichael, W., Charlton, M. N., et al. (2016, June 1). The re-eutrophication of Lake Erie: Harmful algal blooms and hypoxia. *Harmful Algae*. Elsevier B.V. https://doi.org/10.1016/j.hal.2016.04.010

Zhou, C., Cohen, M. D., Crimmins, B. A., Zhou, H., Johnson, T. A., Hopke, P. K., & Holsen, T. M. (2017a). Mercury Temporal Trends in Top Predator Fish of the Laurentian Great Lakes from 2004 to 2015: Are Concentrations Still Decreasing? *Environmental Science and Technology*, *51*(13), 7386–7394.

Chapter 3: MERCURY METHYLATION LINKED TO NITRIFICATION IN THE TROPICAL NORTH ATLANTIC OCEAN

Lindsay D. Starr, Mark J. McCarthy, Chad R. Hammerschmidt, Ajit Subramaniam, Marissa C. Despins, Joseph P. Montoya, Silvia E. Newell

3.1 Abstract

Methylmercury (MeHg) is a toxin that poses health risks to humans and wildlife, primarily through consumption of seafood (Mason et al., 2012). Most MeHg bioaccumulation by marine fish likely occurs in the upper 200 m of the ocean, which is mostly oxygenated (Mason et al., 2012). However, mechanisms of Hg methylation in oxic seawater remain unknown, since the *hgcAB* gene cluster, which encodes proteins for MeHg production, had been found exclusively in anaerobic microbes (Gilmour et al., 2011; Parks et al., 2013). Recent work, however, has shown that *hgc*-homologues are widespread in oxic seawater, including in the microaerophilic nitrifier *Nitrosp*ina (Tada et al. 2020; Gilmour et al. 1992). Here, we show that potential MeHg production rates in Western Tropical North Atlantic Ocean surface waters, within and near the Amazon River plume, were correlated positively and strongly to nitrification rates and *Nitrospina*-specific 16S gene expression. Potential Hg methylation and nitrification rates were highest at the most saline and least turbid stations, indicating that sediment particles and nutrient-rich, riverine discharges were not the primary factors promoting either process. These novel results in oxic seawater provide further evidence that Hg methylation is linked to abundant, nitrifying microbes and may help explain marine MeHg distributions.

3.2 Introduction

Methylmercury is ubiquitous in the ocean, most of which is oxygenated from surface to bottom, and most MeHg is thought to be produced microbially (Mason et al., 2012). The presence and distribution of MeHg in oxic seawater conflicts with a long-standing paradigm that MeHg is produced only by anaerobic microbes, particularly those that reduce sulfur and iron (Gilmour et al., 2011; Monperrus et al., 2007). The only known microbes in culture that methylate Hg are anaerobic (Gilmour et al., 2011; Mason et al., 2012; Parks et al., 2013). Methylmercury production has been measured in the upper, oxic water column of the ocean (Villar et al. 2020; Whalin et al. 2007; Lehnherr et al. 2011; Munson et al. 2018), where it is hypothesized to occur within anoxic microzones associated with particles (Ortiz et al. 2015). Based on these measurements, and independent flux calculations based on concentration measurements (Hammerschmidt and Bowman, 2012), *in situ* production can account for >90% of MeHg in oxic surface water of the open ocean, where most seafood is harvested. However, a mechanism for MeHg production in oxic seawater remains elusive.

A putative Hg methylation gene homologue (*hgc*) was recently described in the microaerophilic, nitrite-oxidizing bacteria *Nitrospina* in Antarctic sea ice (Gionfriddo et al., 2016); *Nitrospina* performs the second step of nitrification (oxidation of nitrite to nitrate, which follows oxidation of ammonium to nitrite; Santoro et al. 2010). *Nitrospina* expression of *hgc* is also widespread in the surface ocean (Gilmour et al. 1992). *Nitrospina hgc* was also detected in the mesopelagic layer of the South China Sea (Tada et al. 2020), while sequences associated with anaerobic *Deltaproteobacteria*, *Firmicutes*, *Spirochaetes*, sulfate-reducing bacteria (SRB), and methanogen *hgcAB,* were not

detected. Despite these advances, no aerobic pathway for MeHg production has been determined, and no clear link has been shown between nitrification and Hg methylation in the ocean.

We sampled water from the Western Tropical North Atlantic Ocean at six stations associated with the Amazon River plume (Figure 3.1) between 18 June and 6 July 2019, during a cruise exploring the impact of the plume on planktonic productivity and communities. Stations were selected to span a gradient of planktonic productivity and surface-water salinity. Water was collected with a CTD-rosette equipped with 10-L Niskin bottles for determination of potential Hg methylation and nitrification rates, dissolved inorganic nitrogen (N) and urea concentrations, and abundance of associated genes from both surface waters (~5 m) and deep chlorophyll maxima (between 27 and 100 m depth among stations; Table 3.1).

3.3 Methods

3.3.1 Sample Collection

Water was sampled from the Western Tropical North Atlantic Ocean at six stations associated with the Amazon River plume (Figure 3.1) between 18 June and 6 July 2019 aboard the *R/V Endeavor*. Stations were selected to span a gradient of planktonic productivity and surface water salinity from international waters and territorial waters of Barbados, Suriname, and French Guiana. Temperature, dissolved oxygen, salinity, photosynthetically active radiation (PAR), turbidity (beam attenuation), and chlorophyll fluorescence were profiled with a SBE 911 CTD at each station. The CTD downcast was used to identify features (e.g., deep chlorophyll maxima) in the depth.

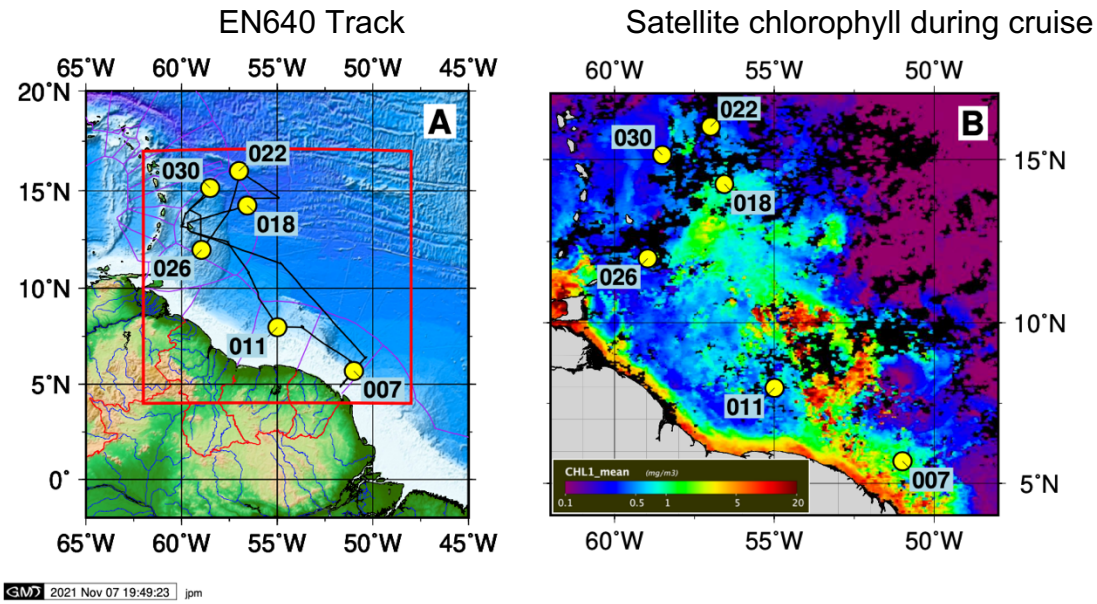

Figure 3.1 (A) Stations in the North Atlantic Ocean where surface and deep chlorophyll maximum water samples were collected. Red box shows domain of (B). Monthly composite map of surface chlorophyll derived from MODIS Aqua and VIIRS sensors for June 2019. The high chlorophyll concentration shows the influence of the Amazon River outflow spreading northward. Surface waters (~5 m) ranged in salinity from 16.1 to 33.4 (Table 3.1). Chlorophyll satellite data obtained from *GlobColour (http://globcolour.info)* used in this study was developed, validated, and distributed by ACRI-ST, France. profile and inform the choice of specific water sampling depths for the upward cast.

Water from selected depths was collected with 10-L Niskin bottles for measurement of gross potential Hg methylation and nitrification rates, as well as dissolved inorganic N and urea concentrations, from both surface water (upper 5 m) and deep chlorophyll maxima (ranging between 27 and 100 m among stations; Table 3.2). Experimental incubations for Hg and N transformations commenced within two hours of sampling. Water for ambient nutrient concentrations (NH_4^+, NO_3^-, NO_2^-, urea, and ortho-PO_4^{3-}) was filtered immediately upon CTD retrieval using a 60-mL syringe through a sample-rinsed, 0.22-µm Nylon syringe filter (Table 3.2). Filtrate was frozen promptly and stored at −20 °C until analysis.

3.3.2 Nitrification rate measurements

At each station, 1 L of seawater from each sampling depth was amended with 8 µL of 10 mM 98% $^{15}NH_4Cl$ (final concentration 0.08 µM), mixed, and distributed into three 125-mL polypropylene bottles (Nalgene). Another 125-mL bottle was filled with unamended seawater as a control. Prior to incubation, initial subsamples were filtered (0.22 µm Nylon syringe filter) from amended and unamended samples into one 15-mL polypropylene tube and two 20-mL plastic scintillation vials. Incubation bottles (unamended control plus three amended) were then placed into an on-deck, flow-through incubator for ~24 hr at ambient light and temperature. Samples collected from chlorophyll maxima were covered with neutral density screen to approximate *in situ* PAR intensity. After 24 hr, subsamples were collected and filtered as described above for initial samples. All filtered water samples were frozen until analysis at Wright State University.

Table 3.1 Amazon River plume stations, sampling date, sampling depths (m), salinity, temperature (°C), photosynthetically active radiation (PAR; W m^{-2}), and beam attenuation (Beam; m^{-1}; surface and deep chlorophyll maximum).

Station	Date	Depth	Salinity	Temperature	PAR	Beam
7	6/18/19	3.6	16.1	29.0	713	81
		100	36.1	28.2	17	88
11	6/21/19	3.7	33.4	27.9	392	86
		25	34.4	27.9	59	86
18	6/27/19	5.4	29.9	27.9	1145	86
		50	36.1	26.9	25	87
22	6/30/19	5.9	31.9	27.9	647	86
		74	37.2	25.8	17	87
26	7/2/19	5.7	33.2	27.9	368	86
		58	35.8	27.3	10	86
30	7/5/19	5.3	33.4	28.1	1317	85
		83	36.2	27.6	17	85

Total NH_4^+ concentrations were analyzed with a Lachat Quikchem 8500 FIA nutrient analyzer in samples (12.5 mL) collected in 15 mL polypropylene tubes. $^{15}NO_3^-$ produced via nitrification was reduced to $^{15}NO_2^-$ via Cd reductions (Hampel et al., 2018; Jeffrey et al., 2012; Newell et al., 2011) performed by transferring 25 mL of sample water from the two 20-mL scintillation vials into 50-mL centrifuge tubes and adding 100 mg of MgO, 6.6 g of NaCl, and 1g of acidified Cd to each sample. Samples were then incubated with constant gentle agitation for ~17 hr, followed by centrifugation at 1000 rpm for 15 min. The supernatant (~7.5 mL) was transferred into 12 mL Exetainers (Labco) without air bubbles. $^{15}NO_2^-$ was subsequently reduced to $^{15}N_2O$ by injecting each sample with 0.25 mL of 2 M NaN_3:20 % CH_3COOH solution and incubating for 1 hr at 30 °C prior to pH neutralization with 0.15 mL of 10 M NaOH (McIlvin and Altabet, 2005).

Samples were stored in the dark until analysis of $^{45}N_2O$ with a ThermoFinnigan GasBench + PreCon trace gas concentration system connected to a ThermoScientific Delta V Plus isotope-ratio mass spectrometer (Bremen, Germany) at the University of California-Davis Stable Isotope Laboratory. Nitrification rates were calculated and corrected for NaN_3 reduction efficiency based on concurrent standard reduction and the fraction of the NH_4^+ pool labeled (Hampel et al., 2020).

3.3.3 Hg methylation rate measurements

Four 2-L replicates of seawater were collected at each station and depth for analysis of potential Hg methylation rates. Water was amended to 10 pM Hg (final concentration; 96.41% $^{200}Hg(NO_3)_2$), which is about 10× greater than ambient total Hg

Table 3.2. Nutrient concentrations (μM) for each station and depth (mean ± standard error of three replicate injections from a single sample, except for n = 1 for ortho-PO_4^{3-} at station 18). ND = not detected (detection limit for urea = 0.27 μM).

Station	Depth (m)	NH_4^+	ortho-PO_4^{3-}	NO_2^-	NO_3^-	Urea
7	3.6	0.520 ± 0.005	0.167 ± 0.007	0.064 ± 0.002	0.094 ± 0.008	0.220 ± 0.028
	100	0.930 ± 0.023	0.324 ± 0.004	0.196 ± 0.005	0.287 ± 0.004	0.433 ± 0.041
11	3.7	0.856 ± 0.016	0.312 ± 0.003	0.143 ± 0.005	0.058 ± 0.002	ND
	27	0.887 ± 0.009	0.333 ± 0.004	0.215 ± 0.008	0.152 ± 0.004	ND
18	5.4	0.682 ± 0.001	0.064	0.129 ± 0.004	0.052 ± 0.002	ND
	50	0.836 ± 0.006	0.030	0.156 ± 0.017	0.187 ± 0.002	ND
22	5.9	0.745 ± 0.013	0.284 ± 0.007	0.134 ± 0.014	0.061 ± 0.003	ND
	75	0.853 ± 0.009	0.357 ± 0.002	0.163 ± 0.011	0.051 ± 0.001	0.352 ± 0.022
26	5.7	0.781 ± 0.005	0.279 ± 0.008	0.155 ± 0.003	0.102 ± 0.008	ND
	58	1.227 ± 0.024	0.335 ± 0.014	0.265 ± 0.011	0.691 ± 0.005	ND
30	5.3	0.757 ± 0.011	0.313 ± 0.003	0.152 ± 0.003	0.066 ± 0.002	ND
	83	2.271 ± 0.010	0.219 ± 0.009	0.180 ± 0.003	0.334 ± 0.009	ND

concentrations in the North Atlantic mixed layer (Bowman et al., 2015). After Hg isotope amendment, water samples were incubated in the on-deck, flow-through incubator. Water samples from deep chlorophyll maxima were covered with neutral density screen to simulate *in situ* light intensity based on PAR measurements (Table 3.1), and surface water was incubated without a light filter. All samples were incubated at ambient sea-surface temperature (Table 3.1) for ~24 hr. After incubation, water was amended with $CH_3{}^{199}Hg$ (for isotope dilution analysis, described below) within 30 min of being removed from the incubator and promptly acidified with H_2SO_4 (1% by volume) to stop biological Hg transformations. Acidified water was analyzed for MeHg isotopes at Wright State University within three months of collection.

For analysis, acidity of water samples was titrated with 12 M KOH, buffered with 4 M acetate buffer and 0.3 mM ascorbic acid to a pH of 4.9, and derivatized with sodium tetraethylborate (Bowman and Hammerschmidt, 2011; Munson et al., 2014). Samples were then purged with N_2, and methylethylmercury (MeHg derivative) was concentrated on Tenax. Mercury isotope composition of purged MeHg was quantified with isotope-dilution gas chromatography inductively coupled plasma mass spectrometry (GC-ICPMS; Perkin Elmer Elan 9000; Hintelmann et al., 1995; Hintelmann and Evans, 1997). Potential Hg methylation rates were calculated from the amount of added $^{200}Hg^{2+}$ that was transformed to $CH_3{}^{200}Hg$ during incubation (Hintelmann et al., 2000). The detection limit for Hg methylation is dependent on ambient MeHg concentration, estimated from $CH_3{}^{202}Hg$ isotope dilution to average 0.14 ± 0.01 pM (n = 48), which is comparable to other measurements in the North Atlantic Ocean (Bowman et al., 2015).

3.3.4 Phytoplankton Diagnostic Pigments

Samples were collected for estimating phytoplankton pigment concentrations from the upper 100 m of the water column. Three liters of water were collected from four different depths from the surface to the deep chlorophyll maximum, according to the CTD downcast profile, and filtered (GF/F). The filters were frozen in liquid nitrogen until analysis following the HPLC method of Van Heukelem and Thomas (2001).

3.3.5 Nucleic acid extraction and amplification

RNA samples were collected at the surface and chlorophyll maxima at the six sites. A known volume of water was pushed through a 0.22 μM Sterivex filter pack (Millipore). Nucleic acids were stabilized by filling the Sterivex filter with RNAlater (ThermoFisher) and stored at −80 ºC until extraction.

RNA was extracted from Sterivex filters using a RNeasy DNeasy PowerWater Sterivex Kit (Qiagen) according to manufacturer instructions. Nucleic acid concentrations were measured, and RNA extract quality was assessed, using 260/280 and 260/230 ratios, with a NanoDrop Microvolume Spectrophotometer (ThermoFisher). RNA extractions were synthesized to cDNA using the ProtoScript First Strand cDNA Synthesis Kit (BioLabs). The remaining RNA extractions were stored at −80 ºC for future use. cDNA was stored at −80 ºC until amplification.

A qPCR amplification assay was completed using a Mastercycler ep Realplex2 Real-Time PCR system (Eppendorf). *Nitrospina*-specific 16S sequences were amplified using primers NitSSU_130 F (5’ -GGGTGAGTAACAC GTGAATAA-3’) and NitSSU_282 R (5’-TCAG GCCGGCTAAMCA-3’; Mincer et al., 2007). The uncultured

Nitrospinaceae sequence EB080L20_F04 was used as a qPCR standard. The standard underwent seven serial dilutions (10^{-4} – 10^{-10} ng μL^{-1}) to create the standard curve (R^2 > 0.99, efficiency > 85%). All samples were amplified in triplicate using the following chemical volumes: 10 µL Luna Universal qPCR Master Mix (New England BioLabs), 1 µL NitSSU_130F and NitSSU_282R, and 1 µL of standard or sample (1000-2000 ng cDNA). The total volume (20 µL) was amplified using thermal cycling parameters in Mincer et al. (2007). *Nitrospina* 16S gene copies were calculated as (ng * number mol^{-1}) / (bp * ng g^{-1} * g mol^{-1} of bp) and are reported in gene copies mL^{-1} of sample water (modified from Hampel et al. 2020). The calculated *Nitrospina*-specific 16S gene copy numbers represent relative, not absolute, values, since copy numbers were normalized to the RNA concentration (ng mL^{-1} filtered) extracted from each Sterivex due to inconsistent amplification efficiency with cDNA synthesis (Newell et al., 2016).

3.4 Results and Discussion

Potential rates of Hg methylation ranged from 0.41 to 1.29 pmol L^{-1} day^{-1} among all samples and did not differ between the upper 5 m (0.55 ± 0.15 pmol L^{-1} day^{-1}) and the chlorophyll maxima (0.69 ± 0.19 pmol L^{-1} day^{-1}; paired *t*-test, $p = 0.10$). These rates are comparable to those measured using similar techniques in the Arctic Ocean and coastal Mediterranean Sea (0.03–0.61 pmol L^{-1} day^{-1}; Villar et al. 2020; Lehnherr et al. 2011). Additionally, given that the added Hg substrate was 10 times higher than ambient concentrations in this study, we estimate that *in situ* rates would be about 10 times lower than the potential rates estimated here, suggesting *in situ,* gross Hg methylation rates of 0.04 to 0.13 pmol L^{-1} day^{-1}. Globally, net MeHg production in the ocean is estimated at

1−10 Mmol year^{-1} or 0.005 to 0.05 pmol L^{-1} day^{-1} for net methylation rates (Hammerschmidt and Bowman, 2012; Mason et al., 2012), which include demethylation rates. Ambient MeHg concentrations were estimated from $CH_3{}^{202}Hg$ isotope dilution measurements (mean = 0.14 ± 0.01 pM; n = 48) and fall within the range of previous MeHg measurements (0.03–0.20 pM) in the equatorial Atlantic Ocean (Mason and Sullivan, 1999). Estimated *in situ* rates imply turnover rates of 0.3–0.9 day^{-1} for MeHg in the upper water column of the Amazon River plume region, which are 5- to 15-fold higher than the highest turnover rates estimated for the Mediterranean Sea (Villar et al. 2020).

Nitrification rates in this study (0 to 292 nmol L^{-1} day^{-1}) at sites as much as 1800 km from the Amazon River mouth are up to an order of magnitude greater than rates from other studies in the oligotrophic Atlantic Ocean (0 to 12 nmol L^{-1} day^{-1}; Clark et al. 2008; Newell et al. 2013) and are more comparable to the range of rates measured at coastal shelf sites, particularly those influenced by large rivers (Bristow et al., 2015; Heiss and Fulweiler, 2016). Nitrification rates from the California Current ranged from 9 to 210 nmol L^{-1} day^{-1}, similar to those from the North Atlantic equatorial current in this study (Santoro et al. 2010). Potential nitrification rates reported here are similar in magnitude to those from an Atlantic Ocean site near the coast of Georgia (USA; 382 ± 35 nmol L^{-1} day^{-1}; Tolar et al. 2017), the Northern Gulf of Mexico coastal shelf near the Mississippi River plume (9 to 494 nmol L^{-1} day^{-1}; Bristow et al. 2015), and a coastal shelf region impacted by the Narragansett River in the northwestern Atlantic Ocean (up to 99 nmol L^{-1} day^{-1}; Heiss and Fulweiler 2016). The consistently large range of nitrification rates across these studies suggests that coastal ocean nitrification (and nitrite

oxidizers) may play a key role in global marine Hg methylation if nitrifiers are ubiquitously related to Hg methylation.

Potential Hg methylation and nitrification rates in seawater were correlated positively (Spearman's rho = 0.92; $p = 0.03$; Figure 3.2), suggesting that nitrifying microbes may be an important source of MeHg in surface waters of the study area. Potential rates of Hg methylation and nitrification were highest at the most saline and least turbid stations (Stations 26 and 30 Figure 3.1; Table 3.1; Table 3.3), implying that sediment particles (hotspots for anoxic microzones; Chakraborty et al. 2021) and nutrient-rich, riverine discharges were not the primary factors promoting either process. Accordingly, correlating rates of Hg methylation and nitrification observed in this study may be representative of ocean surface water globally.

Recent work linked the *hgcAB* Hg methylation gene cluster and the nitrite oxidizer, *Nitrospina,* to potential MeHg production in the ocean (Tada et al. 2020; Gilmour et al.1992). The *Nitrospina*-16S gene (Hou et al., 2018) was expressed at our sampling stations (Figure 3.3). There was a strong, positive correlation between expression of *Nitrospina*-16S normalized gene copies and Hg methylation rates ($R^2 = 0.70$, $p = 0.001$), as well as *Nitrospina*-16S and nitrification rates ($R^2 = 0.80$, $p = 0.0004$). However, the relationship with Hg methylation rates deteriorates if results from station 30 (the station with the highest rates) are excluded. Across all stations, there was no difference in *Nitrospina*-16S expression between surface and chlorophyll maximum depths ($p > 0.05$). The observation that potential nitrification and Hg methylation rates were strongly related (Spearman's rho = 0.92, $p = 0.03$; Figure 3.2) suggests that *Nitrospina* is involved in both methylating Hg and oxidizing nitrite in the oxic surface

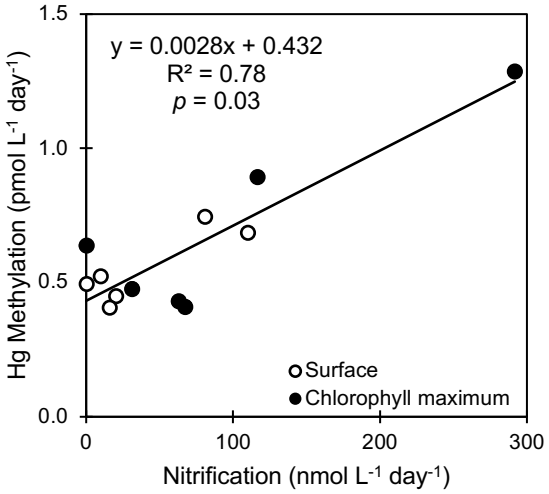

Figure 3.2. Relationship between potential Hg methylation and nitrification rates in the Western Tropical North Atlantic Ocean ($p = 0.03$). Surface samples have a least squares regression of $y = 0.0026x + 0.4492$ ($R^2 = 0.74$), and chlorophyll maximum samples have a least squares regression of $y = 0.0029x + 0.4144$ ($R^2 = 0.77$). Similar slopes of surface and chlorophyll maximum samples suggest that the relationships are similar throughout the water column.

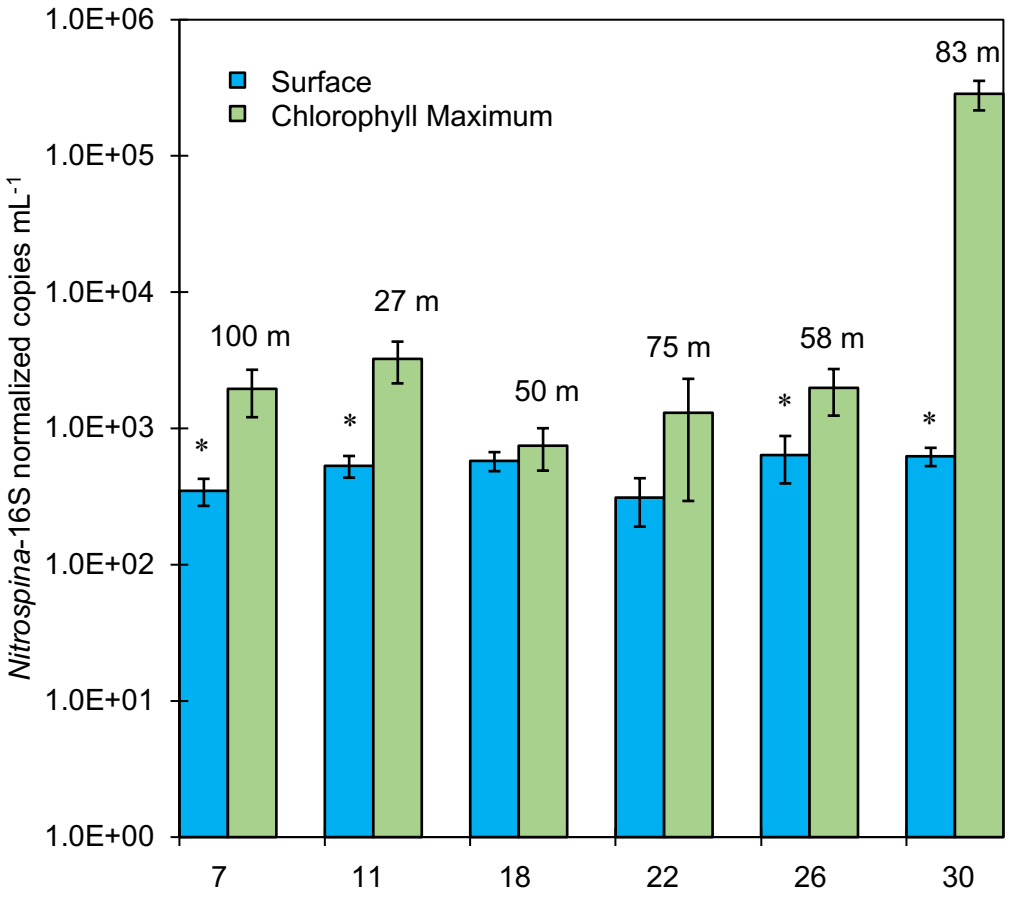

Figure 3.3. Relative expression of *Nitrospina*-16S for all stations at surface and chlorophyll maxima on a log scale with standard deviation. Gene copy numbers were normalized to the RNA extracted from each sample. Surface depth ranged from 3.6 to 5.9 m below the sea surface. Highest normalized copies were found in chlorophyll maximum samples from station 30, where highest Hg methylation and nitrification rates were found. *Denotes difference ($p < 0.05$) between surface and deep chlorophyll maximum samples at a given station.

Table 3.3. Potential Hg methylation and nitrification rates (mean ± standard error; n = 3, except n = 1 for Hg methylation at station 11 surface and nitrification at station 30 surface). ND = not detected.

Station	Date	Depth	Hg Methylation rate (pmol L^{-1} day^{-1})	Nitrification rate (nmol L^{-1} day^{-1})
7	6/18/19	3.6	0.52 ± 0.14	9.8 ± 10
		100	0.43 ± 0.07	63 ± 9
11	6/21/19	3.7	0.45	20 ± 17
		25	0.41 ± 0.04	67 ± 20
18	6/27/19	5.4	0.49 ± 0.06	ND
		50	0.64 ± 0.11	ND
22	6/30/19	5.9	0.41 ± 0.02	16 ± 17
		74	0.48 ± 0.11	31 ± 10
26	7/2/19	5.7	0.69 ± 0.26	110 ± 87
		58	0.89 ± 0.31	117 ± 60
30	7/5/19	5.3	0.74 ± 0.29	81
		83	1.29 ± 0.49	292 ± 100

ocean near the Amazon River plume and oxic waters underlying the plume. These findings support previous molecular work (Tada et al. 2020; Gilmour et al. 1992; Gionfriddo et al. 2016) suggesting that Hg methylation may often be associated with nitrification in the oxic surface ocean.

Since methylation rate is likely substrate limited, and Hg concentration in our incubations was elevated by an order of magnitude above ambient (Villar et al. 2020; Whalin et al. 2007; Lehnherr et al. 2011), actual *in situ* production of MeHg is estimated at 36–90 Mmol of MeHg $year^{-1}$. Based on the relationship in Figure 3.2 and an estimated range of surface-water nitrification rates (0 to 97 nmol L^{-1} day^{-1}) in the Atlantic, Pacific, and Indian Oceans (Ward and Zafiriou 1988; Newell et al. 2011; Grundle et al. 2013), a *gross potential* production of 360–900 Mmol of MeHg $year^{-1}$ is predicted in the open ocean. This flux is about 2- to 5-fold greater than annual Hg loadings to the surface ocean from external sources (e.g., river discharges and atmospheric deposition; ~20 Mmol $year^{-1}$) and net estimated MeHg production in the ocean (1−10 Mmol $year^{-1}$) based on mass balances (Hammerschmidt and Bowman, 2012; Mason et al., 2012).

The positive *y*-intercept of the relationship between MeHg production and nitrification (Figure 3.2) suggests MeHg production from additional processes, such as sulfate- and iron-reduction or abiotic processes. The 2- to 5-fold difference between gross MeHg production estimates based on our measurements and net MeHg production from mass balance is likely due in part to similarly high demethylation rates in the open ocean (Villar et al. 2020; Munson et al. 2018), which is consistent with the high turnover rates implied by our data.

Both potential nitrification and Hg methylation rates were positively correlated

across all stations and depths (Spearman's rho = 0.58 to 0.87) with several pigment concentrations (normalized to total chlorophyll *a*) associated with *Prochlorococcus* and eukaryotic picophytoplankton (Jeffrey et al. 2012). These pigments include divinyl chlorophyll *b*, chlorophyll *b*, and but-fucoxanthin, but these correlations were largely driven by data from the chlorophyll maxima of Stations 26 and 30 (Figure 3.4; Figure 3.5). These stations were located in the northern and western reaches of the Amazon River plume, more than 1300–1700 km from the mouth of the river (Figure 3.1). Here, the plume is diluted by mixing with seawater and is more transparent, alleviating light limitation. High rates of primary production and nitrogen fixation have been measured previously in this area of the Amazon River plume (Carpenter et al. 1999; Subramaniam et al. 2008; Montoya et al. 2019). Normalized concentrations of divinyl chlorophyll *b* and total chlorophyll *b*, diagnostic of pico-eukaryotes, were elevated at the chlorophyll maxima at these stations (Table 3.3; Figure 3.4; Figure 3.5). Since correlations between pigments and nitrification or Hg methylation rates were driven by two data points from Stations 26 and 30 (Figure 3.4; Figure 3.5), and since phytoplankton can outcompete nitrifiers for dissolved inorganic N, we interpret these relationships with pigments to likely be coincidental and do not appear to provide an alternative explanation for the relationship between nitrification and Hg methylation (Table 3.4; Lomas and Lipschultz 2006).

Several studies suggest that particles include suboxic microhabitats, where hotspots of both nitrite oxidation and Hg methylation might co-occur within an otherwise oxic water column (Chakraborty et al., 2021; Medeiros et al., 2015; Zhang et al., 2019). However, nitrification and Hg methylation rates were not correlated with turbidity,

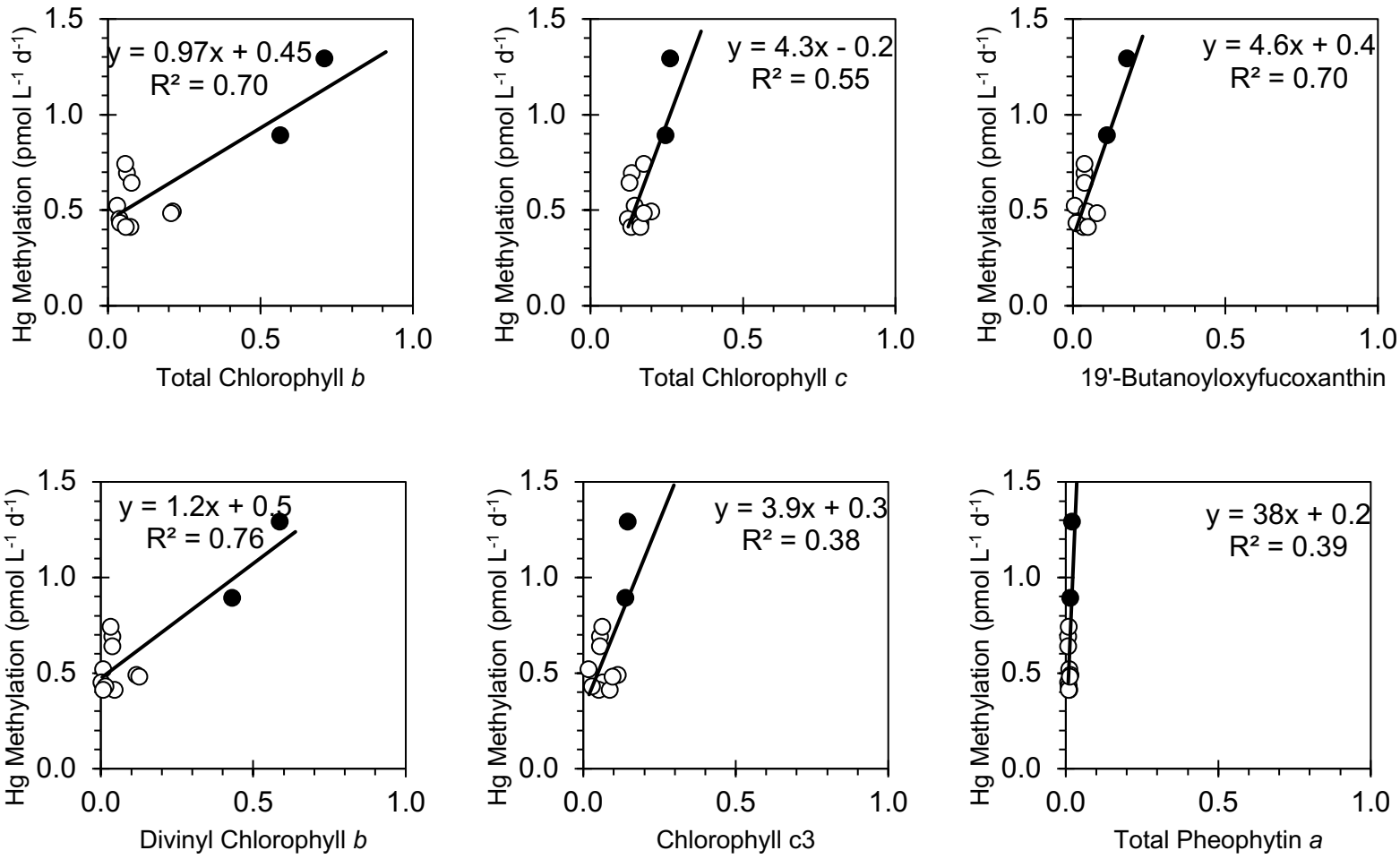

Figure 3.4. Linear regressions between Hg methylation rates and phytoplankton pigment concentrations (normalized). Black circles are from the chlorophyll maxima at stations 26 and 30, which appear to drive the linear relationships. Pigment data were normalized to total chlorophyll *a* for each station and depth.

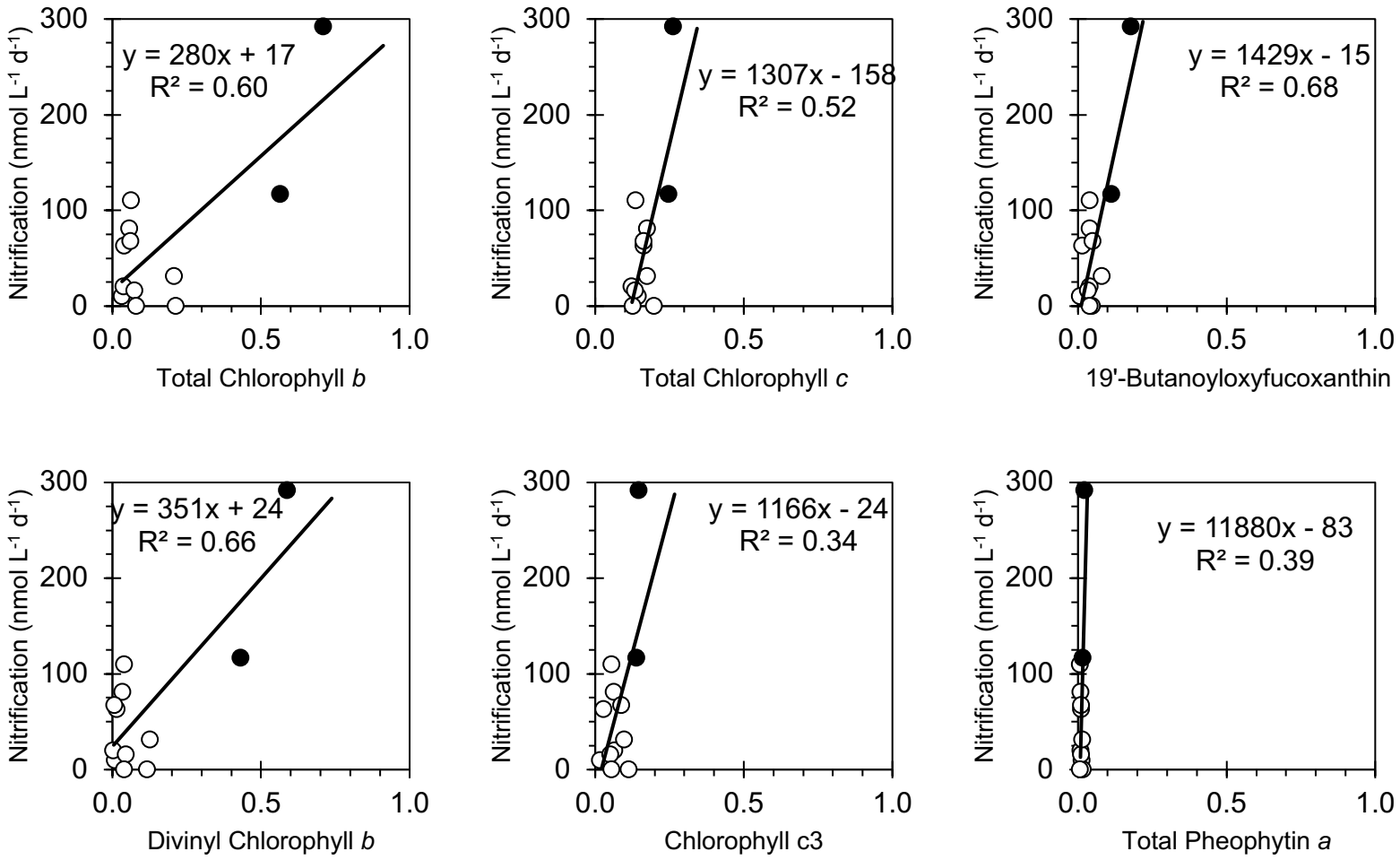

Figure 3.5. Linear regressions between nitrification rates and phytoplankton pigment concentrations (normalized). Black circles are from stations 26 and 30, which appear to drive the linear relationships. Pigment data were normalized to total chlorophyll *a* for each station and depth.

implying that loading of terrigenous particulates and organic matter from the Amazon River were not the driving factor for either pathway.

While some *Nitrospina* are microaerophilic, and all previously known pathways of Hg methylation are anaerobic, the lack of correlation with beam attenuation as a proxy for turbidity (Spearman's rho = −0.02, $p = 0.95$) is consistent with an aerobic pathway. Previous studies have also found filtered seawater (0.45 μm) can have methylation rates 1.4x higher than unfiltered samples (Munson et al., 2018).

Coupling of microbial Hg methylation and nitrification provides a mechanistic explanation for MeHg production in oxic waters, as well as MeHg distributions and bioaccumulation in marine systems. In addition to providing novel, process-based data, these results can also be viewed in the context of a changing marine MeHg cycle as a result of anthropogenic environmental stressors. Increased reactive N loading to the ocean is already causing coastal eutrophication and leading to increasing hypoxic zones worldwide (Falkowski et al., 2011; Peña et al., 2010). Human activities have also tripled Hg inputs to the surface ocean since industrialization (Lamborg et al., 2014). The combination of increasing substrates for nitrification and Hg methylation, development of hypoxic zones, and overall conditions favorable for Hg methylation may lead to greater MeHg bioaccumulation in seafood and, thus, human health risks.

Table 3.4. Pigment data normalized to total chlorophyll *a* concentration for that station and depth.

Station	Depth (m)	Total Chlorophyll *a* (mg m^{-3})	Total Chlorophyll *b*	Total Chlorophyll *c*	19'-Butanoyloxyfucoxanthin	Divinyl Chlorophyll *b*	Chlorophyll c3	Total Pheophytin *a*
7	3.6	1.212	0.032	0.146	0.008	0.009	0.019	0.012
	31	0.984	0.042	0.166	0.014	0.016	0.030	0.011
11	3.7	0.226	0.040	0.124	0.040	0.004	0.066	0.009
	25	0.456	0.061	0.164	0.050	0.009	0.090	0.011
18	5.4	0.549	0.215	0.200	0.047	0.118	0.115	0.016
	50	0.124	0.081	0.129	0.040	0.040	0.056	0.008
22	5.9	0.170	0.076	0.135	0.035	0.047	0.053	0.012
	74	0.335	0.209	0.176	0.081	0.128	0.099	0.015
26	5.7	0.124	0.065	0.137	0.040	0.040	0.056	0.008
	58	0.609	0.567	0.248	0.113	0.432	0.140	0.016
30	5.3	0.203	0.059	0.177	0.039	0.034	0.064	0.010
	83	0.925	0.711	0.263	0.178	0.588	0.147	0.023

3.5 References

Bowman, K.L., Hammerschmidt, C.R., 2011. Extraction of monomethylmercury from seawater for low-femtomolar determination. Limnology and Oceanography: Methods 9, 121–128. https://doi.org/10.4319/lom.2011.9.121

Bowman, K.L., Hammerschmidt, C.R., Lamborg, C.H., Swarr, G., 2015. Mercury in the North Atlantic Ocean: The U.S. GEOTRACES zonal and meridional sections. Deep-Sea Research Part II: Topical Studies in Oceanography 116, 251–261. https://doi.org/10.1016/j.dsr2.2014.07.004

Bristow, L.A., Sarode, N., Cartee, J., Caro-Quintero, A., Thamdrup, B., Stewart, F.J., 2015. Biogeochemical and metagenomic analysis of nitrite accumulation in the Gulf of Mexico hypoxic zone. Limnology and Oceanography 60, 1733–1750. https://doi.org/10.1002/lno.10130

Carpenter, E.J., Montoya, J.P., Burns, J., Mulholland, M.R., Subramaniam, A., Capone, D.G., 1999. Extensive bloom of a N 2-fixing diatom/cyanobacterial association in the tropical Atlantic, Source: Marine Ecology Progress Series.

Chakraborty, S., Andersen, K.H., Visser, A.W., Inomura, K., Follows, M.J., Riemann, L., 2021. Quantifying nitrogen fixation by heterotrophic bacteria in sinking marine particles. Nature Communications 12. https://doi.org/10.1038/s41467-021-23875-6

Clark, D.R., Rees, A.P., Joint, I., 2008. Clark, Darren R., Andrew P. Rees, and Ian Joint. Ammonium regeneration and nitrification rates in the oligotrophic Atlantic Ocean: Implications for new production estimates. Limnol. Oceanogr. 53, 52–62.

Falkowski, P.G., Algeo, T., Codispoti, L., Deutsch, C., Emerson, S., Hales, B., Huey, R.B., Jenkins, W.J., Kump, R., Levin, L.A., Lyons, T.W., Nelson, N.B., Schofield, O.S., Summons, R., Talley, L.D., Thomas, E., Whitney, F., Pilcher, C.B., 2011. Ocean deoxygenation: Past, present, and future. Geophysical Research Letters 92, 409–420. https://doi.org/10.1029/2008GL034185

Gilmour, C.C., Elias, D.A., Kucken, A.M., Brown, S.D., Palumbo, A. v., Schadt, C.W., Wall, J.D., 2011. Sulfate-reducing bacterium Desulfovibrio desulfuricans ND132 as a model for understanding bacterial mercury methylation. Applied and Environmental Microbiology 77, 3938–3951. https://doi.org/10.1128/AEM.02993-10

Gilmour, C.C., Henry, E.A., Mitchell, R., 1992. Sulfate stimulation of mercury methylation in freshwater sediments. Environmental Science & Technology 26, 2281–2287. https://doi.org/10.1021/es00035a029

Gionfriddo, C.M., Tate, M.T., Wick, R.R., Schultz, M.B., Zemla, A., Thelen, M.P., Schofield, R., Krabbenhoft, D.P., Holt, K.E., Moreau, J.W., 2016. Microbial mercury methylation in Antarctic sea ice. Nature Microbiology 1. https://doi.org/10.1038/nmicrobiol.2016.127

Grundle, D.S., Juniper, S.K., Giesbrecht, K.E., 2013. Euphotic zone nitrification in the NE subarctic Pacific: Implications for measurements of new production. Marine Chemistry 155, 113–123. https://doi.org/10.1016/j.marchem.2013.06.004

Hammerschmidt, C.R., Bowman, K.L., 2012. Vertical methylmercury distribution in the subtropical North Pacific Ocean. Marine Chemistry 132–133, 77–82. https://doi.org/10.1016/j.marchem.2012.02.005

Hampel, J.J., McCarthy, M.J., Aalto, S.L., Newell, S.E., 2020. Hurricane Disturbance Stimulated Nitrification and Altered Ammonia Oxidizer Community Structure in Lake Okeechobee and St. Lucie Estuary (Florida). Frontiers in Microbiology 11. https://doi.org/10.3389/fmicb.2020.01541

Hampel, J.J., McCarthy, M.J., Gardner, W.S., Zhang, L., Xu, H., Zhu, G., Newell, S.E., 2018. Nitrification and ammonium dynamics in Taihu Lake, China: Seasonal competition for ammonium between nitrifiers and cyanobacteria. Biogeosciences 15, 733–748. https://doi.org/10.5194/bg-15-733-2018

Heiss, E.M., Fulweiler, R.W., 2016. Coastal water column ammonium and nitrite oxidation are decoupled in summer. Estuarine, Coastal and Shelf Science 178, 110–119. https://doi.org/10.1016/j.ecss.2016.06.002

Hintelmann, H., Evans, R.D., 1997. Application of stable isotopes in environmental tracer studies - Measurement of monomethylmercury (CH3Hg+) by isotope dilution ICP-MS and detection of species transformation. Fresenius J Anal Chem 358, 378–385.

Hintelmann, H., Evans, R.D., Villeneuve, J.Y., 1995. Measurement of mercury methylation in sediments by using enriched stable mercury isotopes combined with methylmercury determination by gas chromatography–inductively coupled plasma mass spectrometry. Journal of Analytical Atomic Spectrometry 10, 619–624. https://doi.org/10.1039/JA9951000619

Hintelmann, H., Keppel-jones, K., Douglas Evans, R., 2000. Constants of mercury methylation and demethylation rates in sediments and comparison of tracer and ambient mercury availability, Environmental Toxicology and Chemistry.

Hou, L., Xie, X., Wan, X., Kao, S.J., Jiao, N., Zhang, Y., 2018. Niche differentiation of ammonia and nitrite oxidizers along a salinity gradient from the Pearl River estuary to the South China Sea. Biogeosciences 15, 5169–5187. https://doi.org/10.5194/bg-15-5169-2018

Jeffrey, S.W., Wright, S.W., Zapata, M., 2012. Microalgal classes and their signature pigments, in: Phytoplankton Pigments. Cambridge University Press, pp. 3–77. https://doi.org/10.1017/cbo9780511732263.004

Lamborg, C.H., Hammerschmidt, C.R., Bowman, K.L., Swarr, G.J., Munson, K.M., Ohnemus, D.C., Lam, P.J., Heimbürger, L.E., Rijkenberg, M.J.A., Saito, M.A., 2014. A global ocean inventory of anthropogenic mercury based on water column measurements. Nature 512, 65–68. https://doi.org/10.1038/nature13563

Lehnherr, I., st. Louis, V.L., Hintelmann, H., Kirk, J.L., 2011. Methylation of inorganic mercury in polar marine waters. Nature Geoscience 4, 298–302. https://doi.org/10.1038/ngeo1134

Lomas, M.W., Lipschultz, F., 2006. Lomas, Michael W., and Fredric Lipschultz. Forming the primary nitrite maximum: Nitrifiers or phytoplankton? Limnol. Oceanogr., 51(5), 2006, 2453–2467, Limnol. Oceanogr.

Mason, R.P., Choi, A.L., Fitzgerald, W.F., Hammerschmidt, C.R., Lamborg, C.H., Soerensen, A.L., Sunderland, E.M., 2012. Mercury biogeochemical cycling in the ocean and policy implications. Environmental Research 119, 101–117. https://doi.org/10.1016/j.envres.2012.03.013

Mason, R.P., Sullivan, K.A., 1999. The distribution and speciation of mercury in the South and equatorial Atlantic. Deep-Sea Research II 46, 937–956.

McIlvin, M.R., Altabet, M.A., 2005. Chemical Conversion of Nitrate and Nitrite to Nitrous Oxide for Nitrogen and Oxygen Isotopic Analysis in Freshwater and Seawater. Analytical Chemistry 77, 5589–5595. https://doi.org/10.1021/AC050528S

Medeiros, P.M., Seidel, M., Ward, N.D., Carpenter, E.J., Gomes, H.R., Niggemann, J., Krusche, A. v., Richey, J.E., Yager, P.L., Dittmar, T., 2015. Fate of the Amazon River dissolved organic matter in the tropical Atlantic Ocean. Global Biogeochemical Cycles 29, 677–690. https://doi.org/10.1002/2015GB005115

Mincer, T.J., Church, M.J., Taylor, L.T., Preston, C., Karl, D.M., DeLong, E.F., 2007. Quantitative distribution of presumptive archaeal and bacterial nitrifiers in Monterey Bay and the North Pacific Subtropical Gyre. Environmental Microbiology 9, 1162–1175. https://doi.org/10.1111/j.1462-2920.2007.01239.x

Monperrus, M., Tessier, E., Amouroux, D., Leynaert, A., Huonnic, P., Donard, O.F.X., 2007. Mercury methylation, demethylation and reduction rates in coastal and marine surface waters of the Mediterranean Sea. Marine Chemistry 107, 49–63. https://doi.org/10.1016/j.marchem.2007.01.018

Montoya, J.P., Landrum, J.P., Weber, S.C., 2019. Amazon River influence on nitrogen fixation in the western tropical North Atlantic. THE SEA: THE CURRENT AND FUTURE OCEAN Journal of Marine Research 77, 191–213.

Munson, K.M., Babi, D., Lamborg, C.H., 2014. Determination of monomethylmercury from seawater with ascorbic acid-assisted direct ethylation. Limnology and Oceanography: Methods 12, 1–9. https://doi.org/10.4319/lom.2014.12.1

Munson, K.M., Lamborg, C.H., Boiteau, R.M., Saito, M.A., 2018. Dynamic mercury methylation and demethylation in oligotrophic marine water. Biogeosciences 15, 6451–6460. https://doi.org/10.5194/bg-15-6451-2018

Newell, S.E., Babbin, A.R., Jayakumar, A., Ward, B.B., 2011. Ammonia oxidation rates and nitrification in the Arabian Sea. Global Biogeochemical Cycles 25. https://doi.org/10.1029/2010GB003940

Newell, S.E., Fawcett, S.E., Ward, B.B., 2013. Depth distribution of ammonia oxidation rates and ammonia-oxidizer community composition in the Sargasso Sea. Limnology and Oceanography 58, 1491–1500. https://doi.org/10.4319/lo.2013.58.4.1491

Newell, S.E., McCarthy, M.J., Gardner, W.S., Fulweiler, R.W., 2016. Sediment Nitrogen Fixation: a Call for Re-evaluating Coastal N Budgets. Estuaries and Coasts 39, 1626–1638. https://doi.org/10.1007/s12237-016-0116-y

Ortiz, V.L., Mason, R.P., Evan Ward, J., 2015. An examination of the factors influencing mercury and methylmercury particulate distributions, methylation and demethylation rates in laboratory-generated marine snow. Marine Chemistry 177, 753–762. https://doi.org/10.1016/j.marchem.2015.07.006

Parks, J.M., Johs, A., Podar, M., Bridou, R., Hurt, R.A., Smith, S.D., Tomanicek, S.J., Qian, Y., Brown, S.D., Brandt, C.C., Palumbo, A. v, Smith, J.C., Wall, J.D., Elias, D.A., Liang, L., 2013. The Genetic Basis for Bacterial Mercury Methylation. Science (1979) 339, 1332–1335.

Peña, M.A., Peña, P., Katsev, S., Oguz, T., Gilbert, D., 2010. Modeling dissolved oxygen dynamics and hypoxia, Biogeosciences.

Santoro, A.E., Casciotti, K.L., Francis, C.A., 2010. Activity, abundance and diversity of nitrifying archaea and bacteria in the central California Current. Environmental Microbiology 12, 1989–2006. https://doi.org/10.1111/j.1462-2920.2010.02205.x

Subramaniam, A., Yager, P.L., Carpenter, E.J., Mahaffey, C., Björkman, K., Cooley, S., Kustka, A.B., Montoya, J.P., Sañudo-Wilhelmy, S.A., Shipe, R., Capone, D.G., 2008. Amazon River enhances diazotrophy and carbon sequestration in the tropical North Atlantic Ocean. PNAS 105, 10460–10465. https://doi.org/10.1073pnas.0710279105

Tada, Y., Marumoto, K., Takeuchi, A., 2020. Nitrospina-Like Bacteria Are Potential Mercury Methylators in the Mesopelagic Zone in the East China Sea. Frontiers in Microbiology 11. https://doi.org/10.3389/fmicb.2020.01369

Tolar, B.B., Wallsgrove, N.J., Popp, B.N., Hollibaugh, J.T., 2017. Oxidation of urea-derived nitrogen by thaumarchaeota-dominated marine nitrifying communities. Environmental Microbiology 19, 4838–4850. https://doi.org/10.1111/1462-2920.13457

Villar, E., Cabrol, L., Heimbürger-Boavida, L.E., 2020. Widespread microbial mercury methylation genes in the global ocean. Environmental Microbiology Reports 12, 277–287. https://doi.org/10.1111/1758-2229.12829

Ward, B.B., Zafiriout, O.C., 1988. Nitrification and nitric oxide in the oxygen minimum of the eastern tropical North Pacific. Deep-Sea Research 35, 1127–1142.

Whalin, L., Kim, E.H., Mason, R., 2007. Factors influencing the oxidation, reduction, methylation and demethylation of mercury species in coastal waters. Marine Chemistry 107, 278–294. https://doi.org/10.1016/j.marchem.2007.04.002

Zhang, L., Wu, S., Zhao, L., Lu, X., Pierce, E.M., Gu, B., 2019. Mercury Sorption and Desorption on Organo-Mineral Particulates as a Source for Microbial Methylation. Environmental Science and Technology 53, 2426–2433. https://doi.org/10.1021/acs.est.8b06020

Chapter 4: GEOTRACES: GP15 PACIFIC OCEAN TRANSECT

Lindsay D. Starr, Yipeng He, Carl Lamborg, Robert P. Mason, Chad R. Hammerschmidt

4.1 Abstract

Methylmercury (MeHg) is a bioaccumulative neurotoxin that can concentrate to potentially harmful levels in higher levels of marine food webs. Formation of MeHg in the ocean is poorly understood, in part due to lack of knowledge of its mechanisms of formation and distribution in ocean basins. To better understand Hg partitioning and distributions in the Pacific Ocean, multiple Hg species were measured along a meridional section from Alaska to Tahiti in 2018. We quantified filtered total Hg (HgT) and MeHg, as well as HgT and MeHg associated with suspended particles, in high-resolution vertical profiles along the meridional transect of 152° W, which included the Alaskan shelf, North Pacific gyre, and the Loihi seamount. Filtered HgT concentrations were elevated below 1000 m near the Loihi Seamount, with an average concentration of 1.45 pM, possibly indicating enrichment from hydrothermal venting. Filtered MeHg concentrations ranged from 0.01 to 0.61 pM, with lower concentrations south of the equator. Total Hg in suspended particles was greatest in the upper 1000 m near the Alaskan Shelf and decreased in concentration southward (ranging from 0.10 to 1.77 pM). Suspended particle MeHg was greatest in the surface ocean in the upper 300 m near the Intertropical Convergence Zone (ITCZ), with concentrations ranging from 0.005 to 0.020 pM across the section. For both HgT and MeHg, particle-associated concentrations appear to be

related to organic fraction, and concentrations decreased southward. In general, all measured Hg species had greater concentrations in the northern than southern Pacific Ocean, consistent with prior measurements. Results from this expedition provide useful information regarding HgT and MeHg in the North and South Pacific Ocean, but additional Hg speciation data is needed for water masses south of Tahiti and the Southern Ocean.

4.2 Introduction

Mercury (Hg) is an environmental contaminant from natural and anthropogenic sources (Fitzgerald et al., 2007). Methylmercury (MeHg), more specifically monomethyl mercury (MMHg), bioaccumulates in food webs and is neurotoxic to humans (Dórea, 2008; Mason et al., 2012). Sources of MeHg in the ocean are thought to be largely internal, deriving from production of Hg^{2+} in continental margin sediments, hydrothermal vent plumes, and microbial activity in oxic and anoxic regions of the water column (Hammerschmidt & Fitzgerald, 2006; Lamborg et al., 2006; Lehnherr et al., 2011; Monperrus et al., 2007). Current estimates for the amount of anthropogenic Hg in the upper ocean (<1,000 m) from Zhang et al. (2014) vary from 50 to 200 Mmol, comprising a larger percentage of HgT in shallower water. The amount of anthropogenic Hg is expected to double in the ocean within the next few decades, due to release of industrial Hg (Sunderland et al., 2009; Mason et al., 2012). The sinking and subsequent remineralization of particles from the surface ocean serves as the “biological pump” to the deep ocean (de La Rocha and Passow, 2007), which moves anthropogenic Hg from surface to deep waters. Thus, it is important to document Hg distribution and quantify the

relative impacts of internal vs. new, anthropogenic sources over time, as well as establish sensitivity of Hg distribution in changing environmental conditions.

Total dissolved Hg (HgT) in the marine water column is comprised of four main species: Hg^{2+}, Hg^{0}, MMHg, and dimethylmercury (DMHg; MeHg = MMHg + DMHg). The majority of Hg in marine systems is inorganic (Hg^{2+}) and is often complexed with organic ligands (Fitzgerald et al., 2007). In the North Pacific Ocean, Sunderland et al. (2009) noted that HgT concentrations varied meridionally and reflect circulation of water masses, such as North Pacific Intermediate Water (NPIW) and Pacific Subarctic Water (PSW). Total dissolved Hg profiles in the central Pacific Ocean are distinctly different than measurements from the North and South Pacific gyres in the intermediate waters (Munson et al., 2015). Deep waters in the Pacific Ocean, the oldest water in the ocean, have higher Hg concentrations than surface waters (Munson et al., 2015; Bowman et al., 2016), because they have accumulated Hg over time as a consequence of the biological. However, some deep water masses in the Pacific are "newer" (such as Circumpolar Deep Water), having formed within the last 100 years from sinking, cold, dense water around Antarctica, so it has generally lower Hg concentrations (Bowman et al., 2016).

As noted above, MeHg in the water column is thought to be produced from microbial methylation of inorganic Hg^{2+} to either MMHg or DMHg (Blum et al., 2013; Mason & Fitzgerald, 1990). Dissolved MMHg and DMHg comprise 15% and 7%, respectively, of total Hg in seawater (Munson et al., 2015), but contributions vary spatially and perhaps temporally. Maximum concentrations of MMHg in the open ocean are typically found at depths of net remineralization (150–1000 m; Sunderland et al., 2009). Concentration, and presumably production, of MeHg is higher in low-oxygen

thermocline seawater, coincident with increased heterotrophic microbial respiration associated with sinking organic matter (Bowman et al., 2020; Hammerschmidt & Bowman, 2012). In the North and Equatorial Pacific Ocean, MeHg in the water column has a nutrient-like profile, with very low concentrations in the surface ocean, and higher concentrations in intermediate waters, supporting the interpretation that MeHg distribution is microbially driven (Blum et al., 2013).

Previous work described the distribution of HgT and MeHg in the upper 1000 m in the North Pacific Ocean (Sunderland et al., 2009) and full depth profiles in the tropical North and South Pacific Ocean (Munson et al., 2015). However, deep water profiles along the transect in the North and South Pacific Ocean outside of the tropics remain uncharacterized. In the Pacific Ocean, dissolved HgT and MeHg were reported from the CLIVAR (cruise P16N; Sunderland et al., 2009) cruise along 150˚W in the upper 1000 m, and Hammerschmidt and Bowman (2012) measured dissolved and particulate HgT and MeHg at the SAFe (Sampling and Analysis of Fe), site in the North Pacific (140°W, 30°N). Both cruises noted a strong influence of the NPIW on MeHg concentrations for depths of ~300 to 700 m. Measurements from SAFe specifically found that particulate MeHg was enriched from the NPIW, which moves water from the western to the eastern Pacific at these depths (Talley, 1992). In the North Pacific, Sunderland et al. (2009) measured HgT and MeHg in unfiltered seawater from the Gulf of Alaska to Hawaii along a transect following 152°W and found a positive relationship between MeHg and organic carbon remineralization. Another cruise (Metzyme; Munson et al., 2015) started south of Hawaii (20°N) in the North Pacific and cruised southwest to 20˚S, measuring dissolved and particulate HgT and MeHg. A general decline in particulate MeHg concentrations

was noted moving south (Munson et al., 2015). Equatorial Pacific measurements were initially made by Mason and Fitzgerald (1990), and again by Bowman et al. (2016); the latter study measured both dissolved and particulate HgT and MeHg concentrations and showed a decrease in HgT and MeHg, which were determined using 'clean lab' techniques.

The GP15 transect spans CLIVAR and Metzyme, and also shared crossover stations with the Equatorial Pacific GP16 GEOTRACES cruise (Figure 4.1; Mason and Fitzgerald, 1990; Sunderland et al., 2009; Munson et al., 2015; Bowman et al., 2016). The GP15 cruise was used to characterize the distribution of Hg species in the Pacific Ocean to better constrain potential sources of HgT and MeHg, and also to better understand Hg cycling in the meridional (152° W) Pacific Ocean. HgT and MeHg concentrations were measured in suspended particles and in the dissolved fraction. The cruise traveled from Alaska to Tahiti and sampled from the Alaskan Shelf, NPIW, Loihi seamount, and Antarctic bottom water (Figure 4.1).

4.3 Methods

4.3.1 Sample collection

Seawater was sampled between September and December 2018 during the U.S. GEOTRACES Meridional Pacific section (GP15) aboard the *R/V Roger Revelle*. The section began on the shelf of the Gulf of Alaska before following along 152°W to Papeete, Tahiti (Figure 4.1). Water was sampled from four shelf stations and 19 full depth stations using 12-L, Teflon-coated Go-Flo bottles attached with a plastic-coated hydrowire (Cutter & Bruland, 2012). Immediately after recovery, water samples were

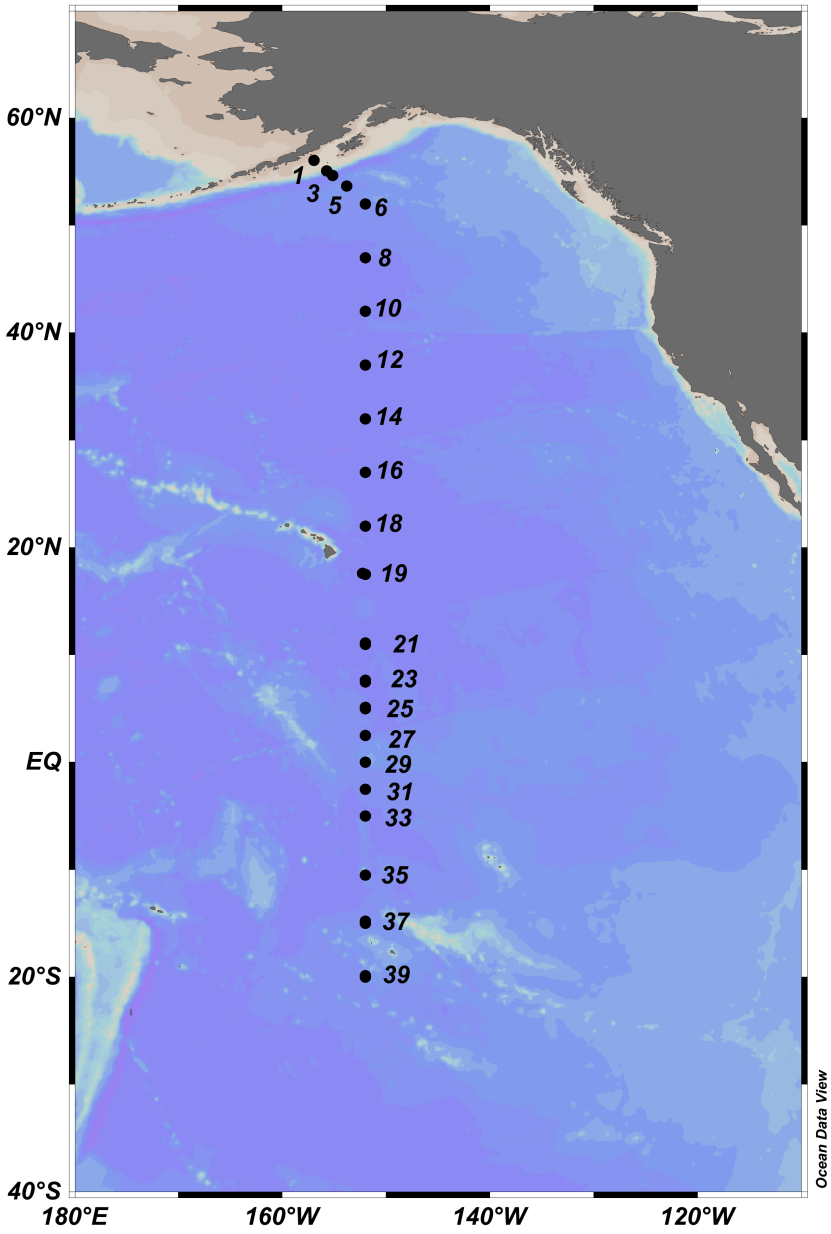

Figure 4.1 Cruise track for GEOTRACES GP15 sampling stations in the Meridional Pacific Ocean. All stations displayed were sampled from surface to full depth.

transferred to a trace-metal clean laboratory van, filtered (0.2 μm Pall AcroPak-200), and transferred to 250 mL glass sample bottles (Lamborg et al., 2012). Sample bottles were acid-cleaned before collection and analyzed in a clean lab at Wright State University (Hammerschmidt et al., 2011).

Suspended particle (1–51 μm) samples were collected onto 142 mm Whatman QMA filters from 16 depths at 13 stations with McLane *in situ* pumps (Bishop et al., 2012). Two 13 mm diameter filter subsamples were collected from the whole filter using an acid-cleaned acrylic "punch" and dried under HEPA-filtered air before cold-storage and shipment to Wright State University for analysis of HgT and MeHg (Bowman et al., 2015a). The total volume of seawater represented by the subsamples varied between 2 and 110 L, where it was assumed, there was uniform flow through the filter.

4.3.2 Dissolved Total Hg Analysis

HgT samples were shipped to Wright State University and digested via oxidation with bromine monochloride (BrCl; 1% by volume; Bloom & Crecelius, 1983) for at least 12 hours. Samples were pre-reduced with NH_2OH to remove volatile halogens. Samples were further reduced with $SnCl_2$ to convert Hg^{2+} to Hg^0, then purged with Hg-free N_2 in a custom sparger, where evolved Hg^0 was quantified by dual Au-amalgamation cold vapor atomic fluorescence spectrometry (CVAFS; Bloom & Fitzgerald, 1988; Fitzgerald &Gill, 1979). Total Hg in seawater was calibrated with aqueous Hg^{2+} standards traceable to US National Institute of Standards and Technology (NIST). A seawater standard reference BCR–579 (Total Mercury in Coastal Seawater, European Commission) averaged 9.7 ±

1.0 pM (n = 16; two outliers removed), which was within the certified range of 9.5 ± 2.5 pmol kg^{-1}. The method detection limit for HgT was 0.01 pM.

4.3.3 Dissolved MeHg

After collection, all seawater samples were preserved and acidified to 0.5% with sulfuric acid (H_2SO_4; trace metal grade) and stored double-bagged in a cold room (4 °C). All seawater samples were shipped to University of Connecticut for MeHg analysis. Prior to analysis, the samples were further digested overnight in 1% H_2SO_4 (trace metal grade) and neutralized with 8 N potassium hydroxide (KOH) to pH 4.9. Then, 60 µL of 25% ascorbic acid and 225 µL of 2 M acetate buffer were added to each sample and ethylated using 30 µL of 1% sodium tetraethyl borate (NaTEB) before analysis under a Tekran 2700 Automated Methylmercury Analysis System against a standard curve (operation recovery = 103 ± 7%; Bowman et al., 2015; Munson et al., 2014).

4.3.4 Particulate MeHg and HgT

Particulate MeHg and HgT were leached from filter punches with high-purity 2 M HNO_3 for 4 hours in a 60 °C water bath (Bowman et al., 2015). MeHg was quantified by flow-injection GC-CVAFS (Tseng et al., 2005), and analyses were calibrated with MMHg standards, which were calibrated versus digestates of TORT-3 (lobster hepatopancreas, National Research Council of Canada). For particulate HgT, 2 mL aliquots of the same filter digestate were oxidized with BrCl for 12-72 hours. Samples were neutralized with NH_2OH, reduced with $SnCl_2$, and analyzed with CVAFS, which was calibrated with Hg^{2+} standards traceable to the US NIST (Bloom & Fitzgerald,

1988). The estimated detection limits for MeHg particulate ($MeHg_{Part}$) and HgT particulate (HgT_{part}) were 0.002 and 0.02 pM, respectively. Small volumes and low sample concentrations did not permit duplicate analyses for $MeHg_{part}$.

4.5 Results and Discussion

4.5.1 Physical oceanography of the section

The cruise transect covered a large portion (9,000 km) of the Pacific Ocean and included sampling of multiple water masses. Deep and bottom water masses sampled included Pacific Deep Water (PDW) and Lower Circumpolar Deep Water (LCDW; Figure 4.2). The deep water masses from the Indian, Pacific, and Atlantic Oceans mix within the Antarctic Circumpolar Current (ACC). This mixture of deep-water masses is referred to as Circumpolar Deep Water (CDW), which is down-welled when converging with the ACC and spreads north into the Pacific Ocean (Falkowski et al., 2011; Kawabe & Fujio, 2010). The CDW is divided into two layers: (1) the Lower CDW (LCDW) has greater dissolved oxygen concentrations due to the mixing of North Atlantic Deep Water (NADW) and is found at depths of >4000 m south of the equator; and (2) the Upper CDW (UCDW) is composed of Indian Ocean deep water and PDW (Falkowski et al., 2011) and found at 2000 to 4000 m depth south of the equator. The UCDW flows into the Pacific basin via internal upwelling and diffusion, becoming PDW as it moves north. PDW is the dominant water mass in the Pacific Ocean at depths from 2000 to 5000 m (Lawrence et al., 2022).

NPIW is formed in the western North Pacific Ocean from the deep shelf water of the Sea of Okhotsk mixing with Oyashio and Kuroshio water

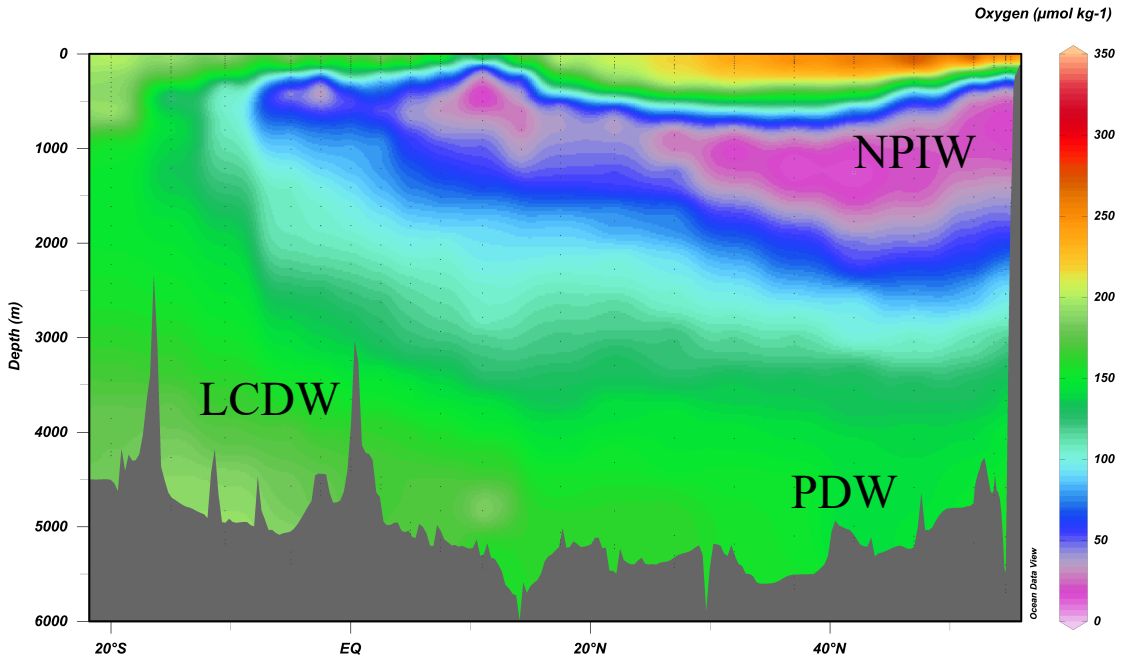

Figure 4.2. Oxygen concentrations used to determine water masses: North Pacific Intermediate Water (NPIW), Pacific Deep Water (PDW), and Lower Circumpolar Deep Water (LCDW).

(Talley, 1997; You et al., 2003). This water mass is defined as underlying the subtropical gyre from 25° to 40°N at a depth of ~300 to 800 m, with salinity of 34.0–34.4 and σ_θ of 26.5 to 27.4 (You et al., 2003). Water from the Sea of Okhotsk is rich with organic carbon and trace metals (Hernes & Benner, 2002; Nishioka et al., 2007) and was previously identified as having distinctly high MeHg concentrations (Hammerschmidt and Bowman, 2012).

Pacific Subarctic Upper Water (PSUW) near 50°N, at a depth of 200 m, is a water mass from cold subpolar surface water subducting under, and carried east, along the Subarctic Front, until reaching the west coast of North America (Talley, 1992; Falkowski et al., 2011). This water is indicated by a decrease in temperature and salinity. The fresher, colder water north of 40°N is from precipitation along coastal mountain ranges bordering the Alaska Gyre, where precipitation exceeds evaporation (Brown et al., 2010). Freshwater from regional glaciers, run-off, and rivers such as the Copper River, continue to add fresh water to the upper 50 m (Musgrave et al., 1992).

4.5.2 Filtered HgT

Filtered HgT samples from the Pacific GP15 cruise ranged from 0.10 to 2.82 pM and averaged 0.98 ± 0.38 pM (n = 466). Filtered HgT displayed nutrient-type vertical distributions along the transect, from scavenging at the surface, remineralization in low-oxygen (less than 50 μmol kg^{-1}) thermocline waters, and accumulation in deep water (Figure 4.3). These results agree with previous measurements in the North and Central Pacific Ocean (Sunderland et al., 2009; Hammerschmidt and Bowman, 2012; Munson et al., 2015). At the SAFe site in the North Pacific Ocean, HgT ranged from 0.25 to 1.5 pM,

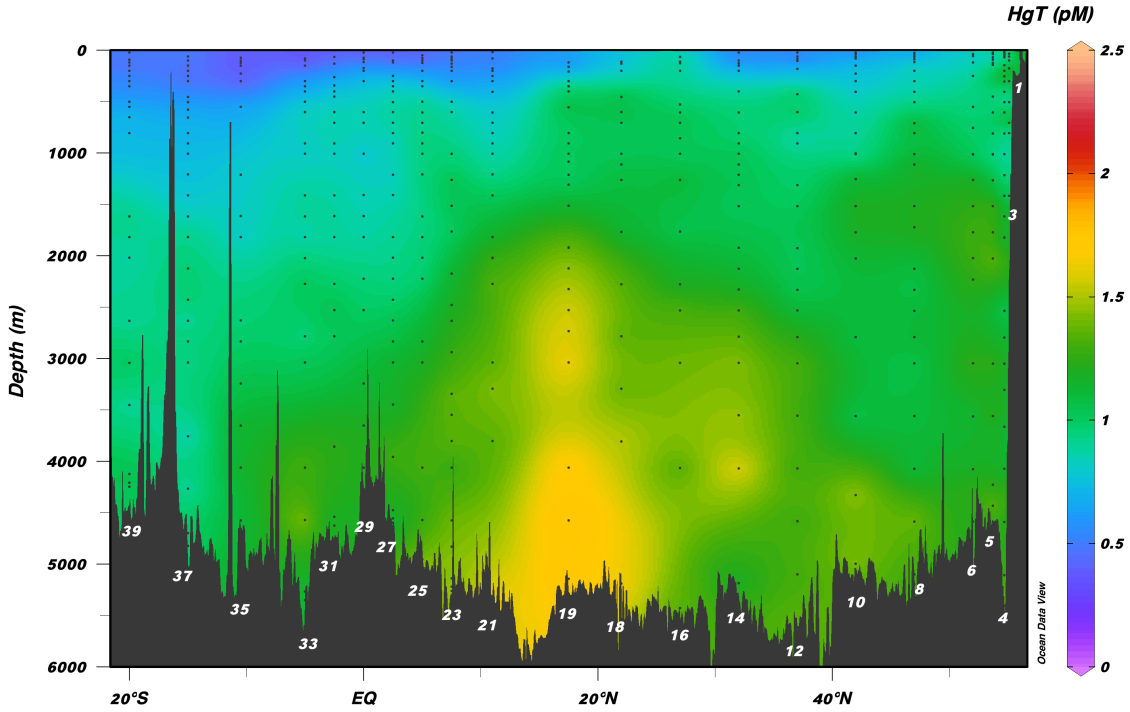

Figure 4.3. Distribution of dissolved HgT; black dots are sampling depths, with station numbers in white at the bottom. Lower HgT concentrations were observed in surface waters, increasing with depth. The highest concentrations were detected below 4000 m at station 19, near the Loihi Seamount.

similar to results from Sunderland et al. (2009; 0.50 to 2.39 pM) and Munson et al. (2015; 0.05 to 2.39 pM). The upper 20 to 1000 m of sea water for this transect, excluding the Alaskan Shelf (stations 1, 3, 4, and 5), had a mean HgT of 0.73 ± 0.29 pM. Higher than average concentrations were observed at the Alaska shelf stations (1, 3, 4, and 5; 20 to 1000 m; station 2 not sampled), with an average concentration of 1.01 ± 0.66 pM, and at stations containing NPIW (12, 14, and 16, depth 300–700 m), with an average concentration of 1.03 ± 0.13 pM (Figure 4.3). The highest concentrations (1.48 ± 0.32 pM, n = 15), however, were found near 20°N at depths greater than 1000 m near the Loihi Seamount.

Station 14 (152°W, 32°N) was the closest to SAFe in the oligotrophic northeast Pacific Ocean, previously occupied as part of GEOTRACES intercalibration activities, and where Hammerschmidt and Bowman (2012) previously analyzed seawater for dissolved HgT and MeHg (Figure 4.4). Both stations exhibited low HgT concentrations in surface waters, with concentrations increasing with depth. The depth profile at Station 14 had surface (<150 m) HgT concentrations averaging 0.39 ± 0.16 pM, similar to those reported by Hammerschmidt and Bowman (2012; 0.40 pM). Concentrations increased with depth to ~1 pM in the NPIW from 200 to 600 m and then into bottom waters (Figure 4.5). Sunderland et al. (2009) measured HgT at a nearby station (152°W 29°N) and reported concentrations in the NPIW near 2 pM. This higher concentration could be due to anthropogenic sources of Hg from the western Pacific Ocean, but without additional information, it is difficult to explain this difference.

A crossover station with a previous cruise in the eastern tropical South Pacific Ocean (GEOTRACES GP16) occurred at station 39 (10°S, 152°W;

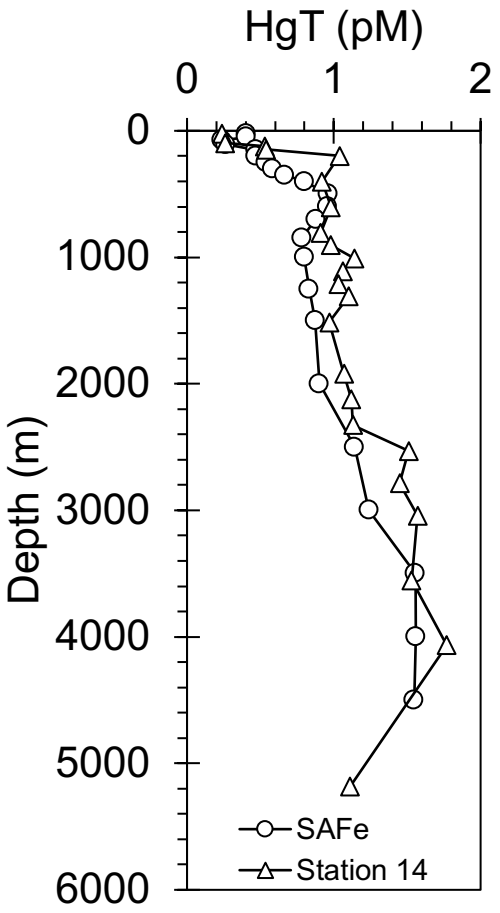

Figure 4.4. HgT concentration profile at Station 14, located near the SAFe site, plotted with HgT concentrations measured at SAFe by Hammerschimdt and Bowman (2012).

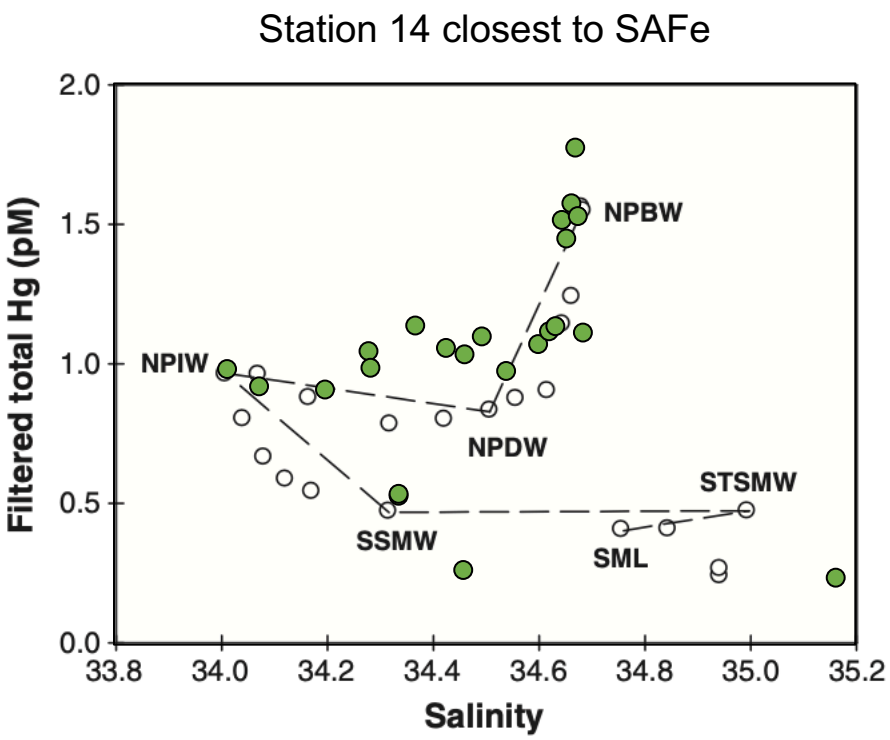

Figure 4.5. Scatter plot of salinity and filtered HgT for station 14, located closest to the SAFe site. The white circles are from Hammerschmidt and Bowman (2012), the green circles are from this study. See text for abbreviations.

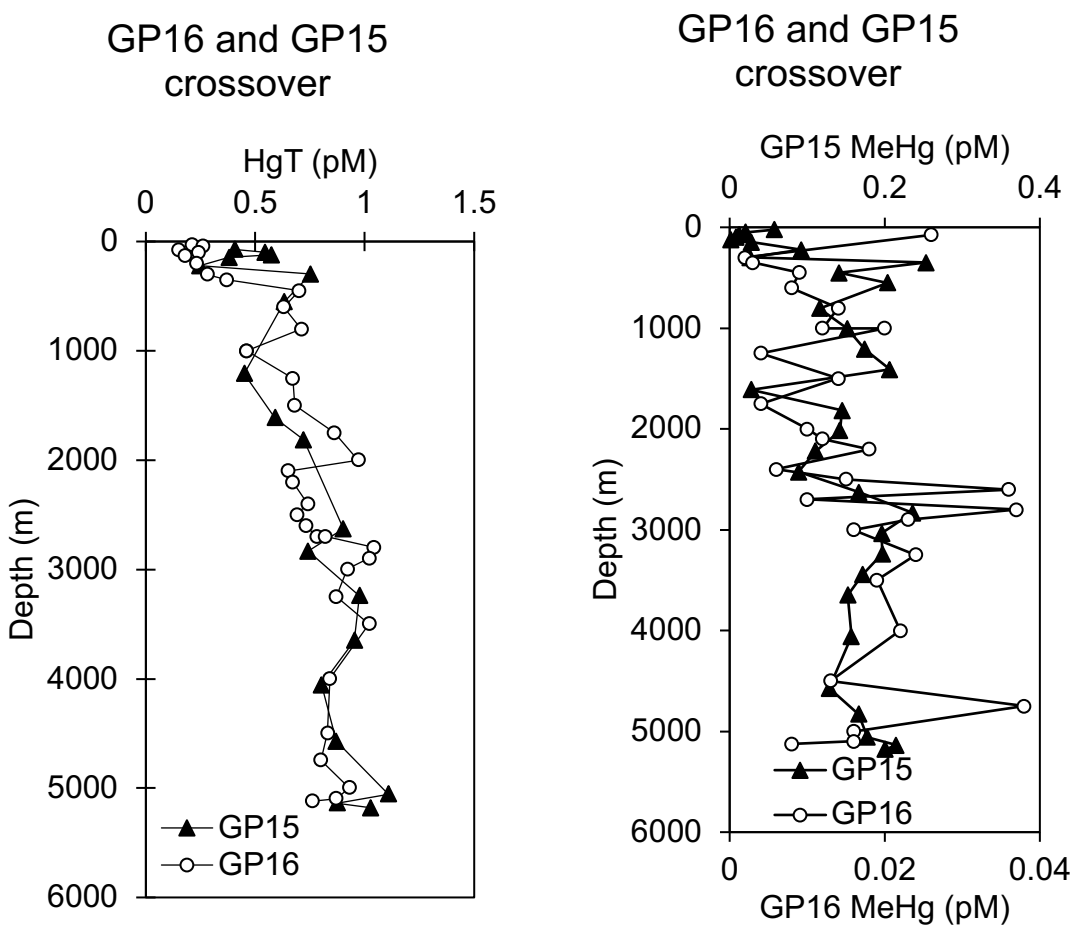

Figure 4.6. Cross over station with GP16 (Bowman et al., 2016). HgT concentrations from GP15 were higher in the surface ocean compared to GP16, but below a depth of 500 m, concentrations were similar. MeHg concentrations from GP16 were lower than during GP15 (note that the two cruises are plotted on different x axes).

Bowman et al., 2016). The previous cruise measured dissolved HgT and MeHg from the surface ocean to a depth of 5000 m. Total dissolved Hg for GP16 in surface water (< 500m) had a mean of 0.29 ± 0.17 pM (n = 9) compared to GP15, where mean HgT was higher ($p < 0.01$, t-test) at 0.51 ± 0.16 pM (n = 8; Figure 4.6). This higher HgT concentration in surface waters could be due to greater anthropogenic Hg emissions north of the equator from the Eastern hemisphere relative to the tropical South Pacific transect of GP16. HgT concentrations for both GP15 and GP16 increased from 500 m to 5000 m, and average HgT concentrations were similar for GP15 (0.90 ± 0.18 pM, n = 13) and GP16 (0.79 ± 0.15 pM, n = 26). Both profiles were similar in shape and not different from each other ($p > 0.56$, t-test). This lack of change in the deep ocean is expected, since the PDW is the oldest deep ocean water and has not been in contact with the atmosphere for about 1,500 years.

As noted, deep water below 2500 m contained higher concentrations of dissolved HgT than water shallower than 2500 m. Lamborg et al. (2014) observed a ratio of filtered HgT to remineralized phosphate (P_{remin}, calculated from Apparent Oxygen Utilization divided by 170; Sarmiento and Anderson, 1994) of 1.02 ± 0.03 pmol μmol^{-1} at depths in water masses that lack anthropogenic CO_2. This ratio arises from remineralization of sinking particles (the "biological carbon pump"; de La Rocha and Passow, 2007) moving Hg and P from surface to deep waters, adding to pre-formed Hg, and P and can act as a benchmark to compare water masses to identify anthropogenic Hg. In this study, deep water concentrations of filtered HgT from >2500 m were generally at or below the 1.02 pmol μmol^{-1} background value (Figure 4.7). Further work is needed in the future to

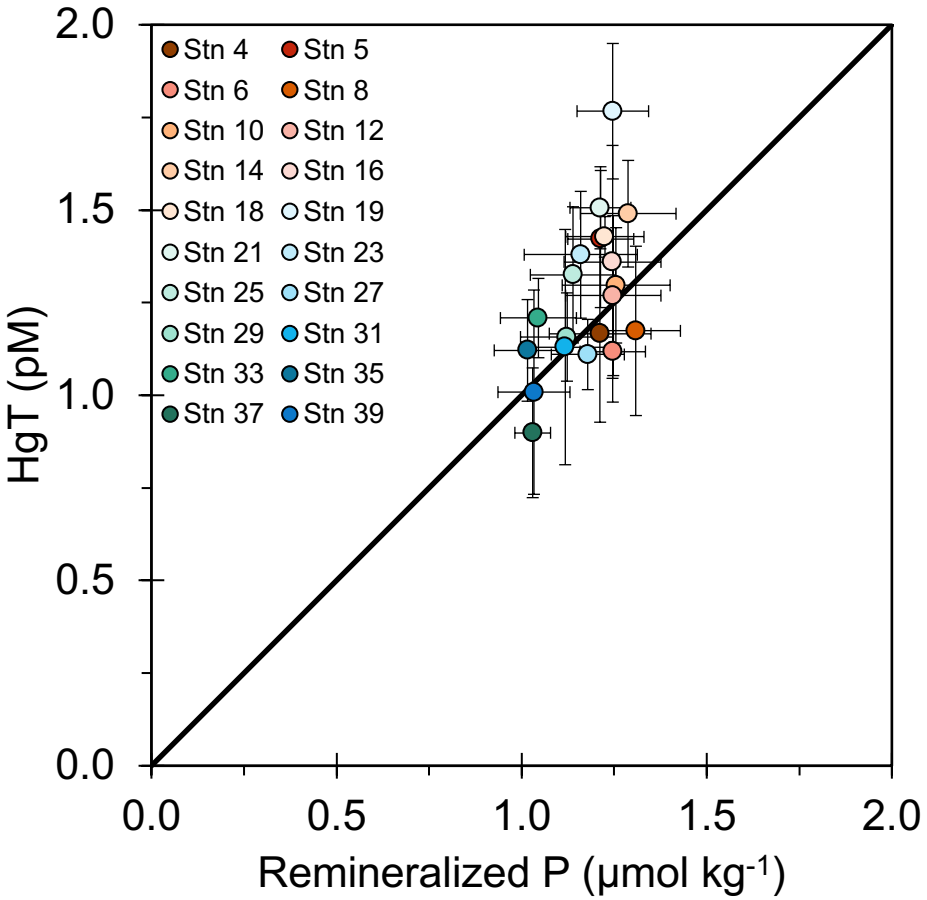

Figure 4.7. Remineralized P vs. dissolved HgT for all stations at depths below 1000 m. The solid line is the 1:1 ratio of dissolved HgT and remineralized P. Stations with values above the line are considered to be anthropogenically influenced (Lamborg et al., 2014).

explore whether these new, lower deep-water values require a re-analysis of "background" Hg:P_{remin} ratios.

At Station 19, HgT concentrations at depths greater than 1000 m were higher than at any other station (1.48 ± 0.32, n = 16, $p < 0.01$), and at depths greater than 2500 m, the HgT:P_{remin} ratio was still above 1.02 (1.25 ± 0.23 pmol μmol^{-1}; n = 5). This higher ratio suggests that the Loihi Seamount is a source of mantle plume Hg and illustrates that naturally elevated Hg:P_{remin} ratios can occur when Hg is supplied internally. This conclusion is supported by a correlation between HgT and ^{3}He:^{4}He ratios, which are indicative of Hg supplied from submarine volcanism (Jenkins et al., 2020). HgT and $\partial^{3}He$ concentrations at Station 19 had a positive linear relationship (Figure 4.8; $R^2 = 0.50$; $p < 0.01$; Jenkins et al., 2020). Hydrothermal vents are heterogeneous, and there can be large variations in vent fluid composition (Chmiel et al., 2021), as observed on GEOTRACES cruises in the North Atlantic and Eastern Tropical Pacific Oceans, which were influenced by hydrothermal vent fluid (Bowman et al., 2015, 2016). Samples collected from GEOTRACES North Atlantic showed dissolved HgT concentrations 10x higher than surrounding stations and increased concentrations of Hg^0 and MMHg (Bowman et al., 2015), in contrast to GEOTRACES Eastern Tropical Pacific (GP16), where vent fluid was not enriched with dissolved HgT, but particulate HgT was increased at surrounding stations (Bowman et al., 2016).

4.5.3 Dissolved MeHg

Across all stations and depths, MeHg exhibited a log-normal distribution with geometric mean of 0.028 + 0.050 − 0.018 pM (Figure 4.9; n = 822) and ranged from

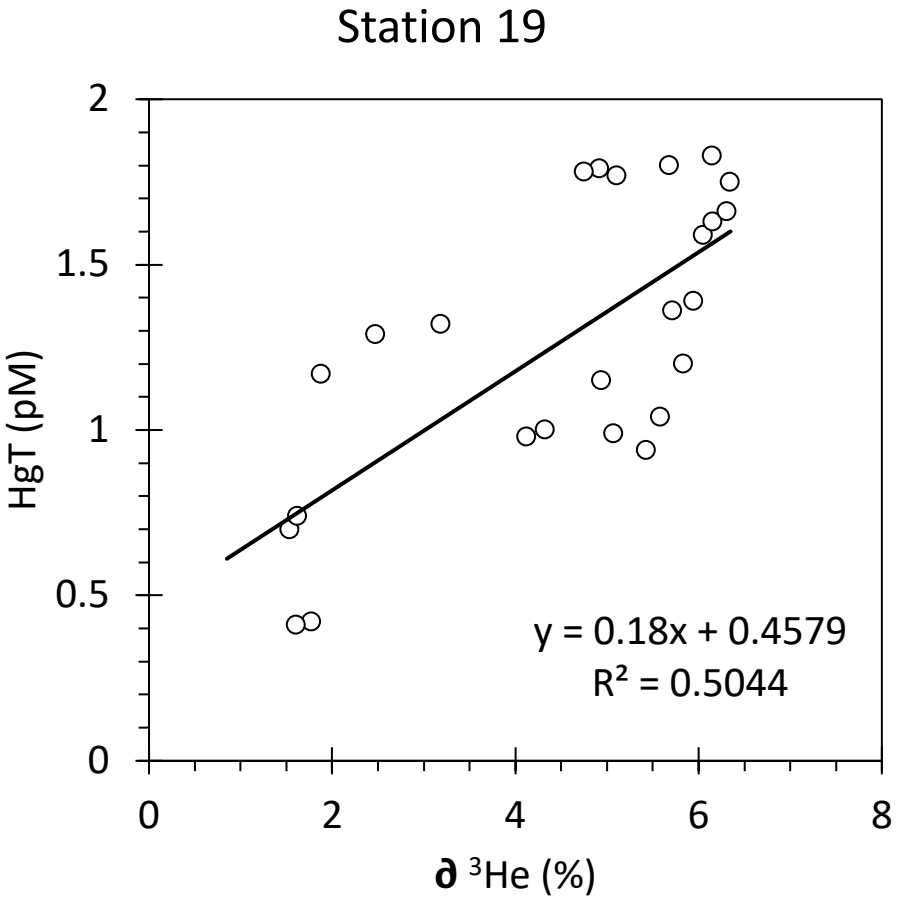

Figure 4.8. ∂^{3}He vs. dissolved HgT concentrations below 1000 m at Station 19 near the Loihi Seamount (Jenkins et al., 2020). **∂**^{3}He is a known hydrothermal plume gas. A positive linear correlation was observed ($p < 0.01$), suggesting that the Loihi Seamount is a strong source of HgT.

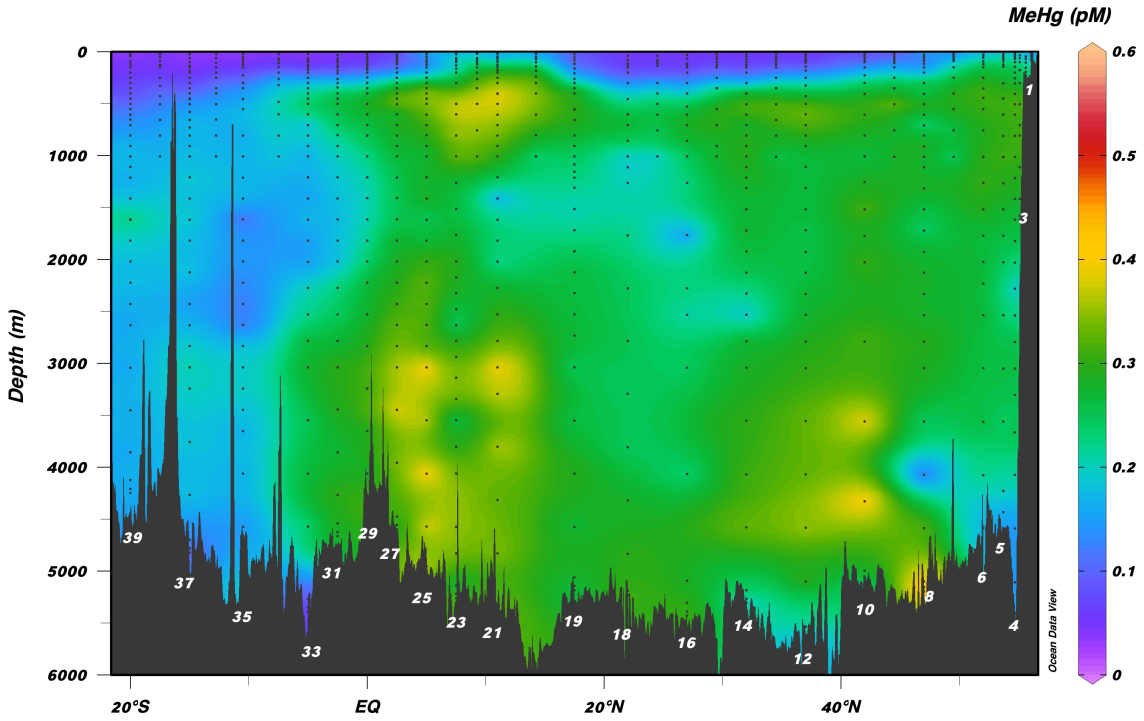

Figure 4.9. Distribution of dissolved MeHg along the cross-section of the cruise track. Lower concentrations were observed in the surface ocean, increasing with depth, although a wedge of lower concentrations was measured in South Pacific waters in the LCDW. Highest concentrations were observed in the deep ocean on either side of the Loihi Seamount.

below detection to 0.61 pM. MeHg represented 22 ± 12% of HgT (n = 453). The mean %MeHg was similar to those reported for other studies in the North and East Pacific Ocean (14 ± 7 %, Sunderland et al., 2009; 14 ± 4 %, Munson et al., 2015; 19 ± 16 %, Bowman et al., 2016). Surface dissolved MeHg was lowest in the upper 500 m (mean = 0.25 ± 0.01 pM; n = 349) compared to water deeper than 500 m (mean = 0.19 ± 0.01 pM; n = 454).

The depth profiles from this transect represent total MeHg, which combines MMHg and DMHg. Previous cruises in the Pacific Ocean measured MeHg as MMHg and DMHg separately (Bowman et al., 2016; Munson et al., 2015), and Sunderland et al. (2009) measured total MeHg in unfiltered seawater. All profiles measured before this study show low concentrations in the surface ocean, increasing in the production zone. Concentrations increase in deep water from organic matter remineralization and the biological pump (Lam et al., 2011). A crossover station (152°W, 10°S) with a previous GEOTRACES cruise (GP16) in the South Pacific Ocean (Bowman et al., 2016) had an overall lower MeHg profile concentration than GP15. Depth profiles from GP16 and GP15 have the same general trend, with low concentrations in the surface ocean, increasing with depth. MeHg concentrations for 17° to 8 °N, from depths 200 to 1000 m, averaged 0.06 ± 0.04 pM (Munson et al., 2015), whereas the mean MeHg concentration for the same latitudes and depths from GP15 were 0.35 ± 0.12 pM. Similar differences for those latitudes were apparent for intermediate and deep water; 0.15 ± 0.04 pM and 0.13 ± 0.03 pM, respectively (this study), and from Munson et al. (2015); 0.24 ± 0.07 pM and 0.33 ± 0.07 pM, respectively. While MeHg concentrations from Munson et al. (2015) were closer to measurements from GP15, they were still lower overall. Kim et al. (2016)

measured MeHg in the western Pacific Ocean from the surface to 500 m and reported MeHg concentrations in the aphotic zone (below 1,000 m) ranging from 0.03 to 0.91 pM.

4.5.4 Particulate HgT

Mean HgT_{part} exhibited a log-normal distribution with a mean of 0.083 (+ 0.178 − 0.057) pM (n = 176) and ranged from 0.01 to 1.77 pM (Figure 4.10). HgT_{part} concentrations were greatest off the shelf of Alaska and had a mean of 0.23 pM (n = 11). Generally, concentrations were elevated in surface water and decreased with depth. Circumpolar water below 1000 m from stations 25 to 39 had the lowest concentrations of HgT_{part} (mean = 0.04 ± 0.01 pM; n = 36).

The highest concentrations of HgT_{part} were found in the PSUW at station 1, where fluvial inputs from regional glaciers and local rivers are a source of particles to the North Pacific Ocean (Lawrence et al., 2022). The concentration of opal was highest for suspended particulate matter (SPM) in the upper 400 m of the North Pacific Ocean, indicating glacial outwash (Jenckes et al., 2022). A comparison of HgT_{part} to HgT + HgT_{part} showed a higher ratio (29 ± 4 %, n = 20) in the upper 400 m of seawater from the PSUW (55°N) to 35°N, compared to the ratio for the whole transect (13 ± 1 %, n = 126), suggesting that detrital material was delivering more HgT_{part} than HgT to the PSUW (Lamborg et al., 2016; Liu et al., 2022).

Partitioning between dissolved and particulate Hg exerts a primary control on the residence time of Hg in the ocean (Lamborg et al., 2016). A particle's affinity for Hg is measured by the partition coefficient (K_d). For the GP15 transect, the mean log K_d was 7.08 ± 0.50 (n = 103). Log K_d from the equatorial Pacific Ocean from GP16 had a mean

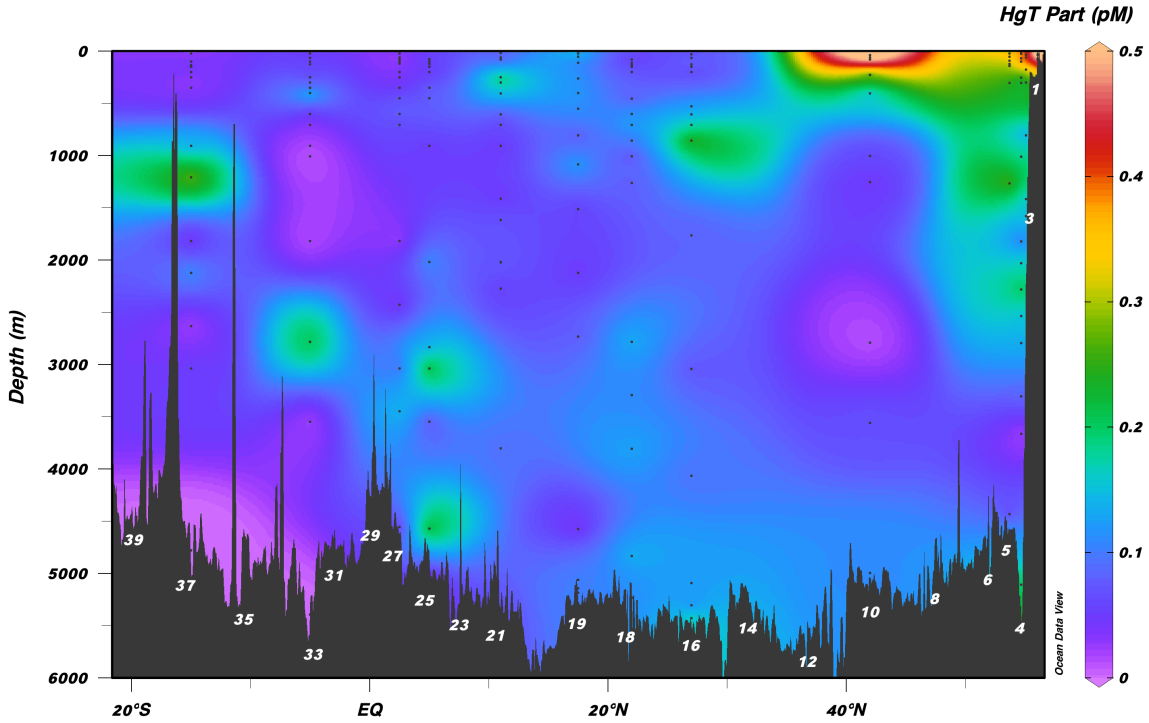

Figure 4.10. Distribution of particulate HgT along the cross-section of the GP15 cruise track. Concentrations were highest off the coast of Alaska, where the Copper River flows into the Gulf of Alaska. The lowest concentrations were found in the South Pacific Ocean in oligotrophic waters of the LCDW.

of 7.11 ± 0.38 and was considered high compared to the North Atlantic (6.52 ± 0.32) and Arctic Oceans (6.74 ± 0.53; Agather et al., 2019; Bowman et al., 2016; Cui et al., 2021). Particulate Hg concentrations are a small percentage (<15%) of total Hg in seawater and facilitate the slow downward flux of Hg to the seafloor (Lamborg et al., 2016). The sinking and subsequent remineralization of particles from the surface ocean serves as the "biological pump" to the deep ocean, which moves organic matter (including anthropogenic Hg) from surface to deep waters. Particulate HgT was generally highest within the upper 50 m of the water column, consistent with higher particle abundance in surface waters (Munson et al., 2015; Sunderland et al., 2009). Upwelling in the Pacific Ocean near the equator can export Hg from the surface mixed layer to intermediate waters by particle transport and remineralization (Bowman et al., 2016; Munson et al., 2015). Hg particles have been studied in the Pacific Ocean (Bowman et al., 2016; Hammerschmidt & Bowman, 2012a; Munson et al., 2015); however, early measurements of Hg distributions in the Pacific Ocean did not distinguish between dissolved and particulate Hg (Laurier et al., 2004; Mason & Fitzgerald, 1990; Sunderland et al., 2009), so there is not a long record of particulate Hg concentrations in the Pacific Ocean.

4.5.5 Particulate MeHg

$MeHg_{Part}$ exhibited a log-normal distribution with a mean of 1.225 (+ 2.333 − 0.803) fM (n = 180) across the entire transect (Figure 4.11). Concentrations ranged from below detection to 20 fM, with peak concentrations found near the ITCZ at stations 21 and 23 in surface water <100 m (11 ± 5 fM, n = 3). Elevated

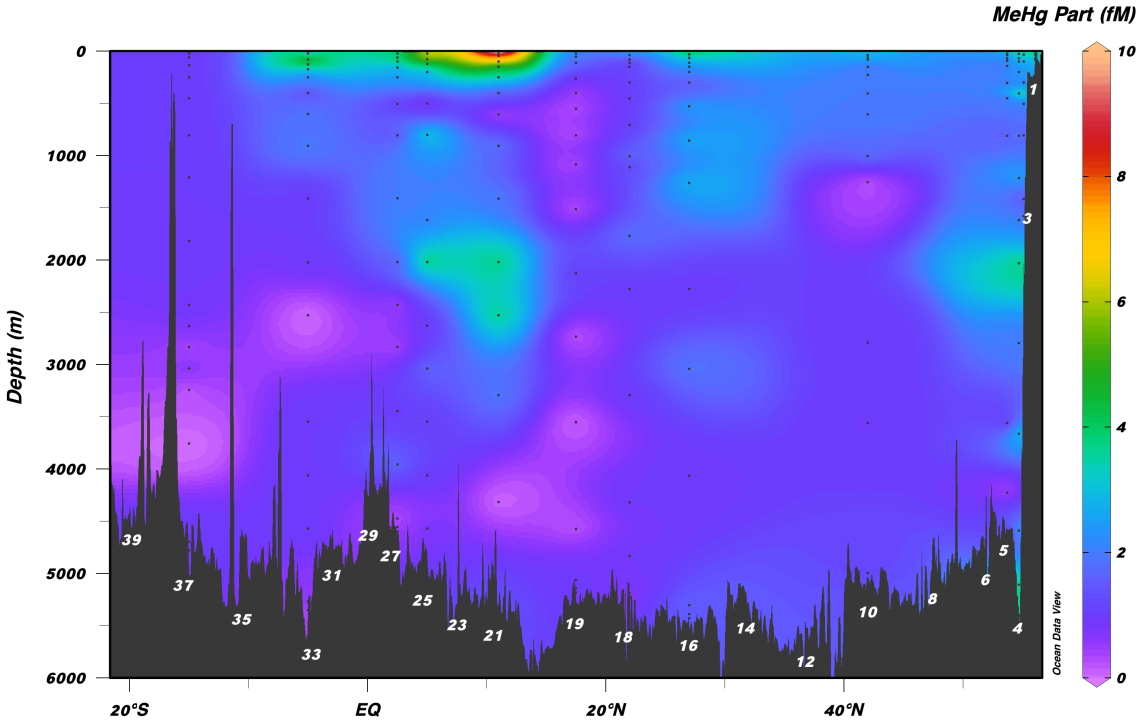

Figure 4.11. Distribution of particulate MeHg along the cross-section of the cruise track. Highest concentrations were observed in the upper 300 m of seawater near the ITCZ. Lowest concentrations were observed in the deep ocean and South Pacific waters.

$MeHg_{Part}$ concentrations of 4.0 ± 2.7 fM (n = 10) were also found on the Alaskan shelf and upper 100 m of stations 4 and 5. Deep waters >1000 m had lower concentrations (1.3 ± 0.1 fM, n= 93) and were lower compared to the upper <1000 m (2.5 ± 0.3 fM, n = 87; ANOVA, $p < 0.01$). A wedge of low $MgHg_{part}$ (not detected to 6 fM) from depths greater than 200 m was present from Stations 19 to 37. This water is from the Southern Ocean (CDW), which is the most oligotrophic ocean water.

An area of higher $MeHg_{part}$ surface concentrations were found near the ITCZ, an area of converging trade winds and high precipitation, which leads to higher particulate deposition (Seo et al., 2021). These particulates can help fuel Hg methylation, and increased MeHg concentrations were observed for both particulate and dissolved MeHg at Stations 21–25 in the upper 500 m.

4.6 Conclusion

Four species of Hg were analyzed along a meridional transect at 152°W in the Pacific Ocean from 56°N to 20°S. Total Hg concentrations from this cruise compared well to HgT concentrations measured in the Pacific Ocean by Sunderland et al. (2009), Munson et al. (2015), and Bowman et al. (2016). Total Hg concentrations were greatest near the Loihi Seamount below 1000 m. MeHg measured on this cruise was higher than previously measured in the Pacific Ocean (Bowman et al., 2016), but were similar to concentrations measured reported by Munson et al. (2015). HgT_{part} was highest at station 1 from regional glacial and local river output, and concentrations decreased toward the south. $MeHg_{Part}$ was highest at the ITCZ and, similar to HgT_{part}, decreased toward the south. Overall, depth and latitudinal patterns observed for the three species of Hg agreed

well with previous measurements, and dissolved MeHg measurements from GP15 had higher concentrations than those from previous measurements in the Pacific Ocean.

4.7 References

Agather, A. M., Bowman, K. L., Lamborg, C. H., & Hammerschmidt, C. R. (2019). Distribution of mercury species in the Western Arctic Ocean (U.S. GEOTRACES GN01). *Marine Chemistry*, *216*. https://doi.org/10.1016/j.marchem.2019.103686

Bishop, J. K. B., Lam, P. J., & Wood, T. J. (2012). Getting good particles: Accurate sampling of particles by large volume in-situ filtration. *Limnology and Oceanography: Methods*, *10*(SEPTEMBER), 681–710. https://doi.org/10.4319/lom.2012.10.681

Bloom, N., & Fitzgerald, W. F. (1988). Determination of volatile mercury species at the picogram level by low-temperature gas chromatography with cold-vapor atomic fluorescence detection. *Analytica Chimica Acta*, *208*, 151–161. https://doi.org/https://doi.org/10.1016/S0003-2670(00)80743-6

Bloom, N. S., & Crecelius, E. A. (1983). Determination of mercury in seawater at sub-nanogram per liter levels. *Marine Chemistry*, *14*(1), 49–59. https://doi.org/https://doi.org/10.1016/0304-4203(83)90069-5

Blum, J. D., Popp, B. N., Drazen, J. C., Anela Choy, C., & Johnson, M. W. (2013). Methylmercury production below the mixed layer in the North Pacific Ocean. *Nature Geoscience*, *6*(10), 879–884. https://doi.org/10.1038/ngeo1918

Bowman, K. L., Hammerschmidt, C. R., Lamborg, C. H., & Swarr, G. (2015a). Mercury in the North Atlantic Ocean: The U.S. GEOTRACES zonal and meridional sections. *Deep-Sea Research Part II: Topical Studies in Oceanography*, *116*, 251–261. https://doi.org/10.1016/j.dsr2.2014.07.004

Bowman, K. L., Hammerschmidt, C. R., Lamborg, C. H., & Swarr, G. (2015b). Mercury in the North Atlantic Ocean: The U.S. GEOTRACES zonal and meridional sections. *Deep-Sea Research Part II: Topical Studies in Oceanography*, *116*, 251–261. https://doi.org/10.1016/j.dsr2.2014.07.004

Bowman, K. L., Hammerschmidt, C. R., Lamborg, C. H., Swarr, G. J., & Agather, A. M. (2016). Distribution of mercury species across a zonal section of the eastern tropical South Pacific Ocean (U.S. GEOTRACES GP16). *Marine Chemistry*, *186*, 156–166. https://doi.org/10.1016/j.marchem.2016.09.005

Bowman, K. L., Collins, R. E., Agather, A. M., Lamborg, C. H., Hammerschmidt, C. R., Kaul, D., et al. (2020). Distribution of mercury-cycling genes in the Arctic and equatorial Pacific Oceans and their relationship to mercury speciation. *Limnology and Oceanography*, *65*(S1), S310–S320. https://doi.org/10.1002/lno.11310

Brown, M. T., Lippiatt, S. M., & Bruland, K. W. (2010). Dissolved aluminum, particulate aluminum, and silicic acid in northern Gulf of Alaska coastal waters: Glacial/riverine inputs and extreme reactivity. *Marine Chemistry*, *122*(1–4), 160–175. https://doi.org/10.1016/j.marchem.2010.04.002

Chmiel, R., Lanning, N., Laubach, A., Lee, J.-M., Fitzsimmons, J., Hatta, M., et al. (n.d.). Major processes of the dissolved cobalt cycle in the North and equatorial Pacific Ocean. https://doi.org/10.5194/bg-2021-305

Cui, X., Lamborg, C. H., Hammerschmidt, C. R., Xiang, Y., & Lam, P. J. (2021). The Effect of Particle Composition and Concentration on the Partitioning Coefficient for Mercury in Three Ocean Basins. *Frontiers in Environmental Chemistry*, *2*. https://doi.org/10.3389/fenvc.2021.660267

Cutter, G. A., & Bruland, K. W. (2012). Rapid and noncontaminating sampling system for trace elements in global ocean surveys. *Limnology and Oceanography: Methods*, *10*(JUNE), 425–436. https://doi.org/10.4319/lom.2012.10.425

Dórea, J. G. (2008). Persistent, bioaccumulative and toxic substances in fish: Human health considerations. *Science of the Total Environment*, *400*(1–3), 93–114. https://doi.org/10.1016/j.scitotenv.2008.06.017

Falkowski, P. G., Algeo, T., Codispoti, L., Deutsch, C., Emerson, S., Hales, B., et al. (2011). Ocean deoxygenation: Past, present, and future. *Geophysical Research Letters*, *92*, 409–420. https://doi.org/10.1029/2008GL034185

Fitzgerald, W. F., & Gill, G. A. (1979). Subnanogram Determination of Mercury by Two-Stage Gold Amalgamation and Gas Phase Detection Applied to Atmospheric Analysis. *Transform Techniques in Chemistry*, *51*(11), 59. Retrieved from https://pubs.acs.org/sharingguidelines

Hammerschmidt, C. R., & Bowman, K. L. (2012a). Vertical methylmercury distribution in the subtropical North Pacific Ocean. *Marine Chemistry*, *132–133*, 77–82. https://doi.org/10.1016/j.marchem.2012.02.005

Hammerschmidt, C. R., & Bowman, K. L. (2012b). Vertical methylmercury distribution in the subtropical North Pacific Ocean. *Marine Chemistry*, *132–133*, 77–82. https://doi.org/10.1016/j.marchem.2012.02.005

Hammerschmidt, C. R., & Fitzgerald, W. F. (2006). Methylmercury cycling in sediments on the continental shelf of southern New England. *Geochimica et Cosmochimica Acta*, *70*(4), 918–930. https://doi.org/10.1016/j.gca.2005.10.020

Hammerschmidt, C. R., Bowman, K. L., Tabatchnick, M. D., & Lamborg, C. H. (2011). Storage bottle material and cleaning for determination of total mercury in seawater. *Limnology and Oceanography: Methods*, *9*(OCTOBER), 426–431. https://doi.org/10.4319/lom.2011.9.426

Hernes, P. J., & Benner, R. (2002). Transport and diagenesis of dissolved and particulate terrigenous organic matter in the North Pacific Ocean. *Deep-Sea Research I*, *49*, 2119–2132.

Jenckes, J., Ibarra, D. E., & Munk, L. A. (2022). Concentration-Discharge Patterns Across the Gulf of Alaska Reveal Geomorphological and Glacierization Controls on Stream Water Solute Generation and Export. *Geophysical Research Letters*, *49*(1). https://doi.org/10.1029/2021GL095152

Jenkins, W. J., Hatta, M., Fitzsimmons, J. N., Schlitzer, R., Lanning, N. T., Shiller, A., et al. (2020). An intermediate-depth source of hydrothermal 3He and dissolved iron in the North Pacific. *Earth and Planetary Science Letters*, *539*. https://doi.org/10.1016/j.epsl.2020.116223

Kawabe, M., & Fujio, S. (2010). Pacific Ocean circulation based on observation. *Journal of Oceanography*, *66*, 389.

Kim, H., Rhee, T. S., Hahm, D., Hwang, C. Y., Yang, J., & Han, S. (2016). Contrasting distributions of dissolved gaseous mercury concentration and evasion in the North Pacific Subarctic Gyre and the Subarctic Front. *Deep-Sea Research Part I: Oceanographic Research Papers*, *110*, 90–98. https://doi.org/10.1016/j.dsr.2016.02.001

de La Rocha, C. L., & Passow, U. (2007). Factors influencing the sinking of POC and the efficiency of the biological carbon pump. *Deep-Sea Research Part II: Topical*

Studies in Oceanography, *54*(5–7), 639–658. https://doi.org/10.1016/j.dsr2.2007.01.004

Lam, P. J., Doney, S. C., & Bishop, J. K. B. (2011). The dynamic ocean biological pump: Insights from a global compilation of particulate organic carbon, CaCO 3, and opal concentration profiles from the mesopelagic. *Global Biogeochemical Cycles*, *25*(3). https://doi.org/10.1029/2010GB003868

Lamborg, C. H., von Damm, K. L., Fitzgerald, W. F., Hammerschmidt, C. R., & Zierenberg, R. (2006). Mercury and monomethylmercury in fluids from Sea Cliff submarine hydrothermal field, Gorda Ridge. *Geophysical Research Letters*, *33*(17). https://doi.org/10.1029/2006GL026321

Lamborg, C. H., Hammerschmidt, C. R., Gill, G. A., Mason, R. P., & Gichuki, S. (2012). An intercomparison of procedures for the determination of total mercury in seawater and recommendations regarding mercury speciation during GEOTRACES cruises. *Limnology and Oceanography: Methods*, *10*(FEBRAURY), 90–100. https://doi.org/10.4319/lom.2012.10.90

Lamborg, C. H., Hammerschmidt, C. R., & Bowman, K. L. (2016). An examination of the role of particles in oceanic mercury cycling. *Philosophical Transactions of the Royal Society A: Mathematical, Physical and Engineering Sciences*, *374*(2081). https://doi.org/10.1098/rsta.2015.0297

Laurier, F. J. G., Mason, R. P., Gill, G. A., & Whalin, L. (2004). Mercury distributions in the North Pacific Ocean - 20 Years of observations. *Marine Chemistry*, *90*(1-4 SPEC. ISS.), 3–19. https://doi.org/10.1016/j.marchem.2004.02.025

Lawrence, R. M., Shrikumar, A., le Roy, E., Swift, J., Lam, P. J., & Casciotti, K. L. (2022). Water mass analysis of the 2018 GEOTRACES Pacific Meridional Transect (GP15). *Global Biogeochemical Cycles*. https://doi.org/10.1002/essoar.10510438.1

Lehnherr, I., st. Louis, V. L., Hintelmann, H., & Kirk, J. L. (2011). Methylation of inorganic mercury in polar marine waters. *Nature Geoscience*, *4*(5), 298–302. https://doi.org/10.1038/ngeo1134

Liu, C., Huo, D., Liu, Z., Wang, X., Guan, C., Qi, J., & Wang, F. (2022). Turbulent Mixing in the Barrier Layer of the Equatorial Pacific Ocean. *Geophysical Research Letters*, *49*(5). https://doi.org/10.1029/2021GL097690

Mason, R P, & Fitzgerald, W. F. (1990). Alkylmercury species in the equatorial Pacific. *Letters to Nature*, *347*, 457–459.

Mason, R. P., Choi, A. L., Fitzgerald, W. F., Hammerschmidt, C. R., Lamborg, C. H., Soerensen, A. L., & Sunderland, E. M. (2012). Mercury biogeochemical cycling in the ocean and policy implications. *Environmental Research*, *119*, 101–117. https://doi.org/10.1016/j.envres.2012.03.013

Mason, Robert P., Choi, A. L., Fitzgerald, W. F., Hammerschmidt, C. R., Lamborg, C. H., Soerensen, A. L., & Sunderland, E. M. (2012). Mercury biogeochemical cycling in the ocean and policy implications. *Environmental Research*, *119*, 101–117. https://doi.org/10.1016/j.envres.2012.03.013

Monperrus, M., Tessier, E., Amouroux, D., Leynaert, A., Huonnic, P., & Donard, O. F. X. (2007). Mercury methylation, demethylation and reduction rates in coastal and marine surface waters of the Mediterranean Sea. *Marine Chemistry*, *107*(1), 49–63. https://doi.org/10.1016/j.marchem.2007.01.018

Munson, K. M., Babi, D., & Lamborg, C. H. (2014). Determination of monomethylmercury from seawater with ascorbic acid-assisted direct ethylation. *Limnology and Oceanography: Methods*, *12*(1 JAN), 1–9. https://doi.org/10.4319/lom.2014.12.1

Munson, K. M., Lamborg, C. H., Swarr, G. J., & Saito, M. A. (2015). Mercury species concentrations and fluxes in the Central Tropical Pacific Ocean. *Global Biogeochemical Cycles*, *29*(5), 656–676. https://doi.org/10.1002/2015GB005120

Musgrave, D. L., Weingartner, T. J., & Royer, T. C. (1992). Circulation and hydrography in the northwestern Gulf of Alaska. *Deep Sea Research Part A. Oceanographic Research Papers*, *39*(9), 1499–1519. https://doi.org/https://doi.org/10.1016/0198-0149(92)90044-T

Nishioka, J., Ono, T., Saito, H., Nakatsuka, T., Takeda, S., Yoshimura, T., et al. (2007). Importance of iron supply to the western subarctic Pacific Ocean. *Journal of Geophysical Research*.

Sarmiento, J. G., & Anderson, L. A. (1994). Redfield ratios of remineralization determined by nutrient data analysis. *Global Biogeochemical Cycles*, *8*(1), 65–80.

Seo, I., Kim, M. G., Yoo, C. M., & Hyeong, K. (2021). Geochemically Defined Mean Position of the Intertropical Convergence Zone in the Central Pacific. *Geophysical Research Letters*, *48*(19). https://doi.org/10.1029/2021GL094432

Sunderland, E. M., Krabbenhoft, D. P., Moreau, J. W., Strode, S. A., & Landing, W. M. (2009). Mercury sources, distribution, and bioavailability in the North Pacific Ocean: Insights from data and models. *Global Biogeochemical Cycles*, *23*(2). https://doi.org/10.1029/2008GB003425

Talley, L. D. (1992). Distribution and formation of North Pacific Intermediate Water. *Journal of Physical Oceanography*, *23*, 517–537.

Talley, L. D. (1997). North Pacific Intermediate Water Transports in the Mixed Water Region. *Journal of Physical Oceanography*, *27*, 1795–1803.

Tseng, C. M., Hammerschmidt, C. R., & Fitzgerald, W. F. (2005). Determination of methylmercury in environmental matrixes by on-line flow injection and atomic fluorescence spectrometry. *Analytical Chemistry*, *76*(23), 7131–7136. https://doi.org/10.1021/ac049118e

You, Y., Suginohara, N., Fukasawa, M., Yoritaka, H., Mizuno, K., Kashino, Y., & Hartoyo, D. (2003). Transport of North Pacific intermediate water across Japanese WOCE sections. *Journal of Geophysical Research: Oceans*, *108*(6). https://doi.org/10.1029/2002jc001662

Chapter 5: CONCLUSION

The overarching theme of this dissertation was to address knowledge gaps in Hg methylation in oxic waters, such as Lake Erie and the Tropical North Atlantic Ocean, as well as distribution of total Hg and MeHg in Lake Erie and the Pacific Ocean. I focused on addressing those research gaps in the field with analyses of water column dissolved and particulate HgT and MeHg concentrations and Hg methylation rates. These results have contributed to the understanding of Hg methylation in oxic waters, as well as identifying patterns of HgT and MeHg in the Pacific Ocean.

I examined concentrations and fluxes of HgT and MeHg from near the Detroit and Maumee River mouths, which discharge into the western basin of Lake Erie, and the Sandusky Bay connection to the central basin of Lake Erie. Average HgT concentrations were similar near the Detroit River mouth (5.4 ± 0.8 pM) and Sandusky Bay connection (5.3 ± 0.9 pM) and less than near the Maumee River mouth (11.6 ± 2.8 pM). Similarly, MeHg was lower at the Detroit (0.38 ± 0.25 pM) and Sandusky River Bay connection (0.24 ± 0.13 pM) than at the Maumee River mouth (0.63 ± 0.46 pM; $p = 0.03$). The mean fraction of total Hg as MeHg in water was comparable among the rivers (~5%), suggesting similar biogeochemical cycling. Estimated river fluxes of MeHg were much greater from the Detroit River (9.5 kg yr^{-1}) than from either the Maumee (0.78 kg yr^{-1}) or Sandusky River Bay connection (0.03 kg yr^{-1}), as expected since the Detroit River

accounts for about 95% of total water discharge into Lake Erie. The highest potential for Hg methylation was found in the Central Basin (0.66 ± 0.03 day^{-1}), followed by the Sandusky Bay connection (0.33 ± 0.01 day^{-1}), the Detroit (0.09 ± 0.01 day^{-1}), Maumee (0.03 ± 0.01 day^{-1}) river mouths. Annually, *in situ* production was an order of magnitude lower than river supply. These results suggest that the Detroit River is the major source of MeHg from the upper Great Lakes basin to western Lake Erie and that much of the MeHg in river water may be derived from *in situ* transformations, especially for the Central Basin and Sandusky Bay. Overall, however, Hg concentrations and fluxes observed in this study were orders of magnitude less than those reported in previous decades, which may be a positive result of the Ohio Clean Air and Water Act of 2004.

Potential MeHg production rates in Western Tropical North Atlantic Ocean surface waters, within and near the Amazon River plume, were correlated positively and strongly to nitrification rates and *Nitrospina*-specific 16S gene expression. Potential Hg methylation and nitrification rates were highest at the most saline and least turbid stations, indicating that sediment particles and nutrient-rich, riverine discharges from the Amazon River were not the primary factors promoting either process. These novel results in oxic seawater provide further evidence that Hg methylation may be linked to abundant, nitrifying microbes and may help explain marine MeHg distributions.

To better understand Hg partitioning and distributions in the Pacific Ocean, multiple Hg species were measured during a meridional section from Alaska to Tahiti in 2018. We quantified filtered total Hg (HgT) and MeHg, as well as HgT and MeHg associated with suspended particles in high-resolution vertical profiles along the meridional transect of 152° W, which included the Alaskan shelf, North Pacific gyre, and

the Loihi seamount. Filtered HgT concentrations were elevated below 1000 m near the Loihi Seamount, with an average concentration of 1.45 pM, possibly indicating enrichment from hydrothermal venting. Filtered MeHg concentrations ranged from 0.01 to 0.61 pM, with lower concentrations south of the equator. Total Hg in suspended particles was greatest in the upper 1000 m near the Alaskan Shelf and decreased in concentration southward (ranging from 0.10 to 1.77 pM). Suspended particle MeHg was greatest in the surface ocean in the upper 300 m near the ITCZ and equator, with concentrations ranging from 0.005 to 0.020 pM across the section. For both HgT and MeHg, particle-associated concentrations appear to be related to organic particles, and concentrations generally decreased southward. All measured Hg species had greater concentrations in the northern Pacific Ocean, compared to southern sites, consistent with prior measurements. Results from this expedition provided useful information regarding potential sources and sinks of HgT and MeHg in the North Pacific Ocean, but additional Hg speciation data is needed for water masses south of Tahiti and the Southern Ocean.

5.1 Future Directions

The combination of increasing substrates for nitrification and Hg methylation, development of hypoxic zones, and overall conditions favorable for Hg methylation may lead to greater MeHg bioaccumulation in seafood and, thus, human health risks. Streets et al. (2018) reported that global Hg emissions for developing nations are trending up, while developed nations are maintaining their current levels. The general increase in Hg emissions will add additional Hg to the oceans and freshwater aquatic systems. The additional Hg in these aquatic environments may bioaccumulate in aquatic organisms,

representing increased human health risks.

To mitigate Hg pollution in the environment, monitoring of Hg regulations needs to occur. Such monitoring has occurred in the Great Lakes region with the implementation of Areas of Concern (AOC). Rivers feeding into the Great Lakes have been monitored, and risk assessments have been conducted for their Hg pollution into the Great Lakes. The work presented in this dissertation demonstrates the importance of monitoring Hg in aquatic environments, as well as the significance of long term studies, especially in aquatic systems with large human influences and valuable ecosystem services. A long term study by Blanchfield et al. (2021) demonstrated the significance of long term Hg monitoring in the Experimental Great Lakes region of Canada and showed that, once additions of Hg to the lake ceased, the rate of increase Hg lowered over time. This evidence can be applied globally; i.e., as Hg deposition decreases, the rate Hg accumulation in fish will also decrease.

The above studies have improved our understanding of Hg methylation and distribution in marine and freshwater systems, but some major knowledge gaps remain, especially regarding the connection between biotic Hg methylation and *Nitrospina*. Recent work by Villar et al. (2020) and Tada et al. (2020) showed that the putative *hgc* gene homologue in *Nitrospina* is widespread in our oceans and may be methylating Hg. While the work in this dissertation demonstrated that Hg methylation and nitrification are co-occurring in space and time, and *Nitrospina* are active, we do not know if *Nitrospina* is methylating Hg. Future work needs to study *Nitrospina* in culture to observe if it actually methylates Hg.

Recent Hg research in the Great Lakes has focused on modeling Hg concentrations in sediment and biota (Lepak et al., 2015; Ogorek et al., 2021). While modeling and Hg concentrations in sediment and biota are important, they do not represent the full cycle of Hg in the Great Lakes. In addition to modeling overall trends of Hg in the Great Lakes region, more work needs to be conducted on water column Hg cycling Lake Erie, specifically in the hypoxic area of the central basin. The western basin experiences annual harmful algal blooms (HABs) from excess nitrogen and phosphorus from the watershed, resulting in high biomass and subsequent central basin hypoxia (Wynne et al., 2021). Hg methylation can occur in anaerobic conditions in the water column and sediment, thus becoming a large source of MeHg to Lake Erie (Gilmour et al., 1992; Graham et al., 2012; Kerin et al., 2006). No recently published research has measured Hg concentrations during and after HABs in the western and central basins of Lake Erie. The work described here from the western and central basins of Lake Erie showed the importance of water column Hg from riverine inputs to the western basin, suggesting that further research should aim to further constrain these riverine inputs. This work could be paired with work from other Great Lakes to complete the Hg cycle for sources and fluxes of Hg.

While Hg concentrations in sediment have been measured regularly in the Great Lakes (Ogorek et al., 2021), direct measurements of sediment-water fluxes of HgT and MeHg need to be conducted as well. Measuring MeHg fluxes directly allows potential rate calculations to be made over a set time period and for determining spatial and temporal patterns of directional Hg fluxes (i.e., influx vs. efflux). Lastly, I found significant flux of Hg from three river mouths into the western basin of Lake Erie during

the late summer/early fall, but measurements from the water column throughout the year should also be made. Winter sampling under ice is of particular importance because Hg has been shown to accumulate under ice (Agather et al., 2019).

The overarching theme of this dissertation was to address knowledge gaps in Hg methylation in oxic waters, such as Lake Erie and the Tropical North Pacific Ocean, as well as distribution of total Hg and MeHg in Lake Erie and the Pacific Ocean. More work still needs to be done in these varying environments to complete the understanding of the cycling of Hg. The work done on this dissertation created a foundation for future work in these varying environments.

5.2 References

Agather, A. M., Bowman, K. L., Lamborg, C. H., & Hammerschmidt, C. R. (2019). Distribution of mercury species in the Western Arctic Ocean (U.S. GEOTRACES GN01). *Marine Chemistry*, *216*. https://doi.org/10.1016/j.marchem.2019.103686

Gilmour, C. C., Henry, E. A., & Mitchell, R. (1992). Sulfate stimulation of mercury methylation in freshwater sediments. *Environmental Science & Technology*, *26*(11), 2281–2287. https://doi.org/10.1021/es00035a029

Graham, A. M., Aiken, G. R., & Gilmour, C. C. (2012). Dissolved organic matter enhances microbial mercury methylation under sulfidic conditions. *Environmental Science and Technology*, *46*(5), 2715–2723. https://doi.org/10.1021/es203658f

Kerin, E. J., Gilmour, C. C., Roden, E., Suzuki, M. T., Coates, J. D., & Mason, R. P. (2006). Mercury methylation by dissimilatory iron-reducing bacteria. *Applied and Environmental Microbiology*, *72*(12), 7919–7921. https://doi.org/10.1128/AEM.01602-06

Lepak, R. F., Yin, R., Krabbenhoft, D. P., Ogorek, J. M., Dewild, J. F., Holsen, T. M., & Hurley, J. P. (2015). Use of Stable Isotope Signatures to Determine Mercury Sources in the Great Lakes. *Environmental Science and Technology Letters*, *2*(12), 335–341. https://doi.org/10.1021/acs.estlett.5b00277

Ogorek, J. M., Lepak, R. F., Hoffman, J. C., DeWild, J. F., Rosera, T. J., Tate, M. T., et al. (2021). Enhanced Susceptibility of Methylmercury Bioaccumulation into Seston of the Laurentian Great Lakes. *Environmental Science and Technology*, *55*(18), 12714–12723. https://doi.org/10.1021/acs.est.1c02319

Ogorek, J. M., Lepak, R. F., Hoffman, J. C., DeWild, J. F., Tate, M. T., Hurley, J. P., & Krabbenhoft, D. P. (n.d.). Enhanced susceptibility of methylmercury bioaccumulation into seston of the Laurentian Great Lakes 4 5. https://doi.org/10.5066/P9GEIVXD

Tada, Y., Marumoto, K., & Takeuchi, A. (2020). Nitrospina-Like Bacteria Are Potential Mercury Methylators in the Mesopelagic Zone in the East China Sea. *Frontiers in Microbiology*, *11*. https://doi.org/10.3389/fmicb.2020.01369

Villar, E., Cabrol, L., & Heimbürger-Boavida, L. E. (2020). Widespread microbial mercury methylation genes in the global ocean. *Environmental Microbiology Reports*, *12*(3), 277–287. https://doi.org/10.1111/1758-2229.12829

Wynne, T. T., Stumpf, R. P., Litaker, R. W., & Hood, R. R. (2021). Cyanobacterial bloom phenology in Saginaw Bay from MODIS and a comparative look with western Lake Erie. *Harmful Algae*, *103*, 101999.